ANL-75-60

Part I

ANL-75-60

Part I

RADIOLOGICAL AND ENVIRONMENTAL RESEARCH DIVISION ANNUAL REPORT

Fundamental Molecular Physics and Chemistry

July 1974—June 1975

U of C-AUA-USERDA

ARGONNE NATIONAL LABORATORY, ARGONNE, ILLINOIS

Prepared for the U. S. ENERGY RESEARCH AND DEVELOPMENT ADMINISTRATION under Contract W-31-109-Eng-38

Printed in the United States of America
Available from
National Technical Information Service
U. S. Department of Commerce
5285 Port Royal Road
Springfield, Virginia 22161
Price: Printed Copy $7.00; Microfiche $2.25

Distribution Category:
Biology and Medicine (UC-48)

ANL-75-60
Part I

ARGONNE NATIONAL LABORATORY
9700 South Cass Avenue
Argonne, Illinois 60439

RADIOLOGICAL AND ENVIRONMENTAL RESEARCH DIVISION ANNUAL REPORT

Fundamental Molecular Physics and Chemistry

July 1974 through June 1975

R. E. Rowland, Division Director
Mitio Inokuti, Section Head

Preceding Report: 75-3, Part I, July 1973–June 1974

FOREWORD

The Fundamental Molecular Physics and Chemistry Section has continued to work vigorously in three scientific fields: electron collisions with molecules, photoabsorption and photoionization, and pertinent theories. The papers in the present report are ordered according to the subjects treated. Papers 1–13 deal with photoabsorption, photoionization, and closely related topics. Papers 14–19 concern slow-electron collisions, papers 20–22 secondary-electron spectra, papers 23–30 theories chiefly related to the transfer of radiation energy to matter, and papers 31–37 other theoretical problems. Paper 38 describes a data-processing technique. Our major accomplishments are summarized below.

The determination of the optical oscillator-strength distribution has been extended both to a wider energy range and to additional molecular species. In particular, a number of molecular species of atmospheric interest have been investigated (papers 1–4). A new versatile analyzer for ejected electrons (described in paper 13) represents a notable enhancement of our capabilities. Experiments on slow-electron collisions with molecules have uncovered threshold effects (paper 14) and the systematics of resonances in many examples (papers 15–18).

A theory of molecular photoionization has been successfully developed; its initial application to K-shell ionization led to the discovery of new phenomena specific to molecules (papers 8–11). A semi-empirical theory of the ejection of secondary electrons by charged-particle impact has been extended to numerous molecules (papers 20–22). Much effort has been devoted to theories of electron degradation and ionization yields in macroscopic volumes of gases (papers 26–30). These theories link secondary-electron and other cross sections to radiological physics. Finally, some progress is being made in theoretical spectroscopy of highly stripped ions — a subject of importance to controlled thermonuclear research (papers 31–33).

We are pleased to report having played major roles in two meetings. First, at the Twenty-Third Annual Meeting of the Radiation Research Society,

May 1975, Miami Beach, Professor U. Fano gave a plenary lecture entitled "Platzman's Analysis of the Delivery of Radiation Energy of Molecules." He outlined the work of the late Robert L. Platzman and collaborators (including some of us) over many years, explained its significance to radiation research, and stressed the merit of the approach, which underlies much of our Section's activities. Following the lecture, a symposium, which we organized, treated mechanisms of energy transfer from electrons to matter and pointed out their consequences in chemistry and biology. Second, the Section presented three lectures at the Symposium on the Distribution of Secondary Electrons from Ionizing Collisions, December 1974, London, Ontario, Canada. The symposium reviewed current knowledge of secondary electron spectra and some of its radiological applications. A full record of the symposium has appeared in Radiat. Res. 64, 1–204 (1975).

In accordance with the broadened mission of ERDA, the Section has been renamed, and its goal has been expanded to include chemical physics pertinent to non-nuclear energy technology and its environmental implications. Although our program was previously conceived to elucidate elementary mechanisms of radiation, some of our capabilities may be devoted also to basic problems in non-nuclear applications. For instance, our photoabsorption studies have already focussed on atmospheric species.

TABLE OF CONTENTS

Fundamental Molecular Physics and Chemistry

APPARENT OSCILLATOR STRENGTHS FOR MOLECULAR OXYGEN, DERIVED FROM ELECTRON ENERGY-LOSS MEASUREMENTS*

R. H. Huebner, R. J. Celotta,† S. R. Mielczarek,† and C. E. Kuyatt†

Oscillator strengths for O_2 (Figure 1) from 6 to 14 eV are derived from the energy-loss spectrum of 100-eV incident electrons. Integrated f values for the Schumann-Runge bands (Figure 2) and continuum (Table 1), which span four orders of magnitude in intensity, agree well with high-resolution photoabsorption measurements. Vibrational structure superimposed on the Schumann-Runge continuum, previously assigned to the $(3s\sigma_g)^3\Pi_g$ Rydberg state, contributes less than 0.5% to the total oscillator strength determined for that region (see Table 2). These data also yield f values for discrete bands in the region between 9.5 and 14.0 eV, where line saturation problems complicate oscillator strength analysis of the optical data. An oscillator-strength sum of 0.198 is obtained for all transitions below the ionization potential at 12.07 eV.

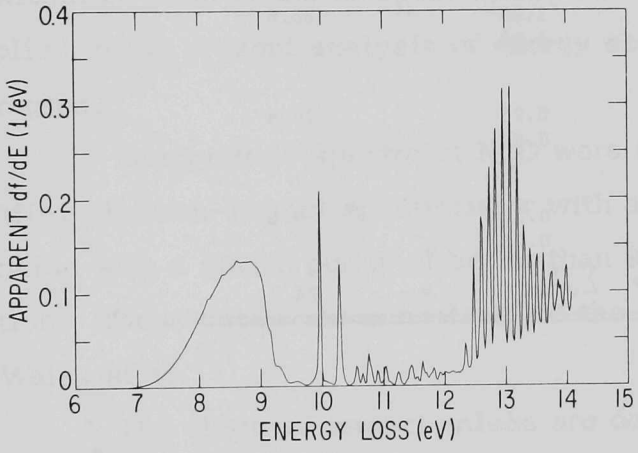

FIG. 1.--Apparent oscillator-strength distribution for O_2 as derived from the electron energy-loss spectrum for 100-eV incident electrons scattered at zero andle.
(ANL Neg. 149-6516)

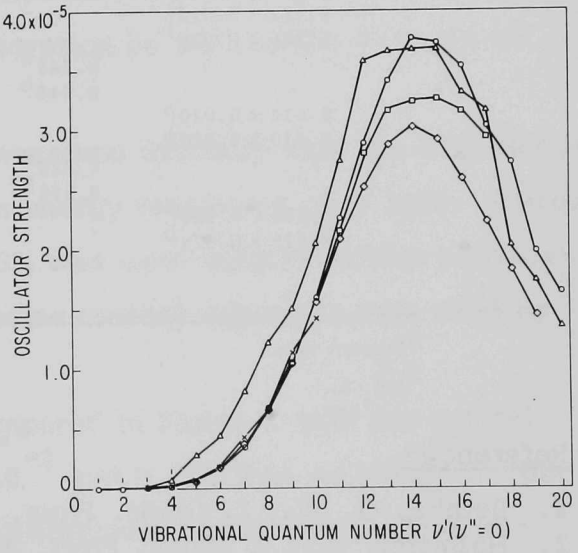

FIG. 2.--Comparison of discrete oscillator-strength values for the Schumann-Runge bands: circle, present results; square, Ref. 1; X, Ref. 2; diamond, Ref. 3; triangle, Ref. 4.
(ANL Neg. 149-6514)

---

*Summary of a paper published in J. Chem. Phys. 63, 241 (1975).

†National Bureau of Standards, Washington, D.C. 20234.

TABLE 1. Values of f_{cont} for the Schumann-Runge Continuum

	Watanabe, Inn, and Zelikoff[a]	Metzger and Cook[b]	Goldstein and Mastrup[c]
E_1, eV	7.067	7.079	7.048
E_2, eV	9.670	9.187	9.744
f (optical)	0.161	0.142	0.156
f (electron impact)	0.162	0.156	0.162

[a]Ref. 5; [b]Ref. 6; [c]Ref. 7.

TABLE 2. Comparison of the Energies and Intensities Measured for the $^3\Pi_g$ Rydberg State of Oxygen

v'	Energy, eV	Spacing, eV	Rel. Intensity	$10^5 \times$ apparent f value
0	8.138 ± 0.010[a]		0.71	18.2
	8.145 ± 0.020[b]		0.73	
		0.234[a]		
		0.222[b]		
1	8.372 ± 0.010[a]		1.00	25.6
	8.366 ± 0.020[b]		1.00	
		0.242[a]		
		0.244[b]		
2	8.614 ± 0.010[a]		0.75	20.8
	8.610 ± 0.020[b]		0.80	
		0.226[a]		
		0.215[b]		
3	8.840 ± 0.010[a]		0.32	9.6
	8.825 ± 0.020[b]		0.25	
			$\sum_{v'} f_{v'0}$ =	74.2

[a]Present work.

[b]Ref. 8.

References

1. Bethke, G. W., J. Chem. Phys. 31, 669 (1959).
2. Halmann, M., J. Chem. Phys. 44, 2406 (1966).
3. Ackerman, M., F. Biaume, and G. Kockarts, Planet. Space Sci. 18, 1639 (1970).
4. Farmer, A. J. D., W. Fabian, B. R. Lewis, K. H. Lokan, and G. N. Haddad, J. Quant. Spectrosc. Radiat. Transfer 8, 1739 (1968).
5. Watanabe, K., E. C. Y. Inn, and M. Zelikoff, J. Chem. Phys. 21, 1026 (1953).
6. Metzger, P. H. and G. R. Cook, J. Quant. Spectrosc. Radiat. Transfer 4, 107 (1964).
7. Goldstein, R. and F. N. Mastrup, J. Opt. Soc. Am. 56, 765 (1966).
8. Cartwright, D. C., W. J. Hunt, W. Williams, S. Trajmar, and W. A. Goddard, III, Phys. Rev. A 8, 2436 (1973).

APPARENT OSCILLATOR STRENGTHS FOR NITROUS OXIDE*

R. H. Huebner, R. J. Celotta,† S. R. Mielczarek,† and C. E. Kuyatt†

Several energy-loss studies[1-4] of N_2O have been made, but very little oscillator-strength information has been extracted from such measurements. The f values for seven Rydberg transitions were obtained by Weiss et al.,[2] but they did not extend their analysis to transitions below 13.5 eV. No other electron energy-loss data have been used to derive oscillator strengths for this molecule. We have successfully determined oscillator-strength distribution from high-quality electron energy-loss spectra for a number of molecules in previous work from spectra obtained for 100-eV incident electrons scattered within 20 mrad of the incident direction. The same technique[5] has been applied in the present analysis of energy absorption by N_2O in the 4- to 14-eV region.

Energy-loss spectra of N_2O were measured digitally with the NBS Model AN-1 electron-impact spectrometer with an energy resolution of 42 meV. Nitrous oxide with a stated purity of better than 98% was used without further purification. These data were normalized to the same optical value[6] as was used by Weiss et al.[2]

The electron-impact values are compared in Figure 1 with the optical data.[7-9] Integrated f values of 1.44×10^{-3} and 0.352 that we obtain for the bands at 6.83 and 9.64 eV are in excellent agreement with optical measurements.[7,8] Our value of 2.85×10^{-2} for the structured band at 8.52 eV is considerably higher than the optical values reported by Zelikoff et al.[7] and Rabalais et al.,[8] and may be indicative of line saturation problems in their work. Oscillator strengths derived from the electron impact measurements

---

*Summary of a paper presented at the IXth Int. Conf. on the Physics of Electronic and Atomic Collisions, Seattle, July 1975. A full account of the work has appeared in J. Chem. Phys. 63, 4490 (1975).

† National Bureau of Standards, Washington, D.C. 20234.

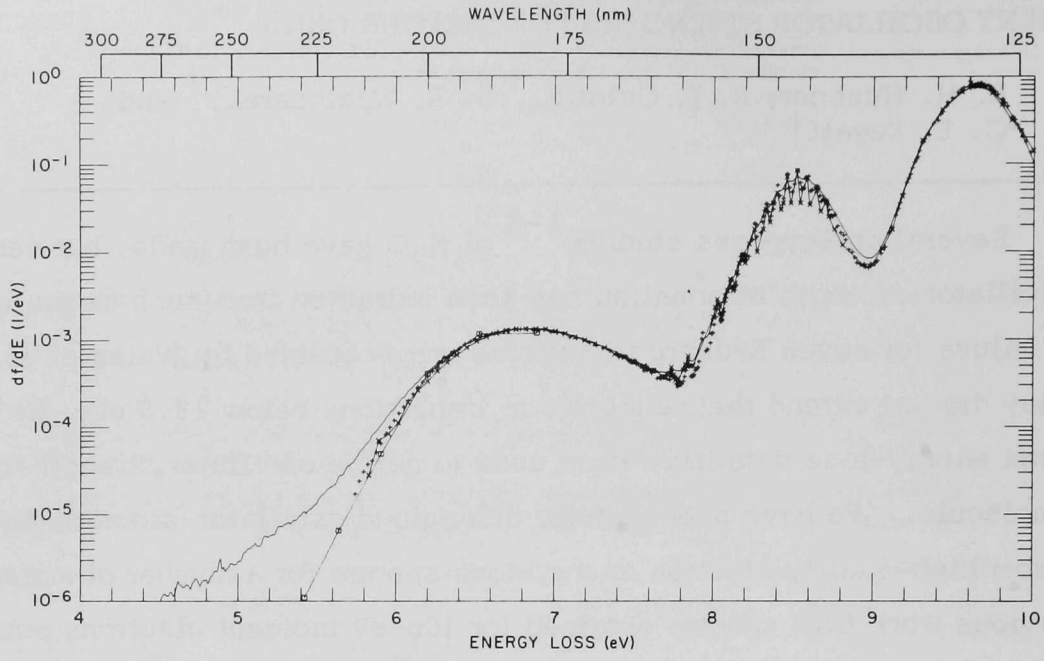

FIG. 1.--Comparison of optical and electron-impact oscillator strengths in the 4- to 10-eV region; +, Ref. 7; x, Ref. 8; square, Ref. 9; solid line, present results. (ANL Neg. 149-6752)

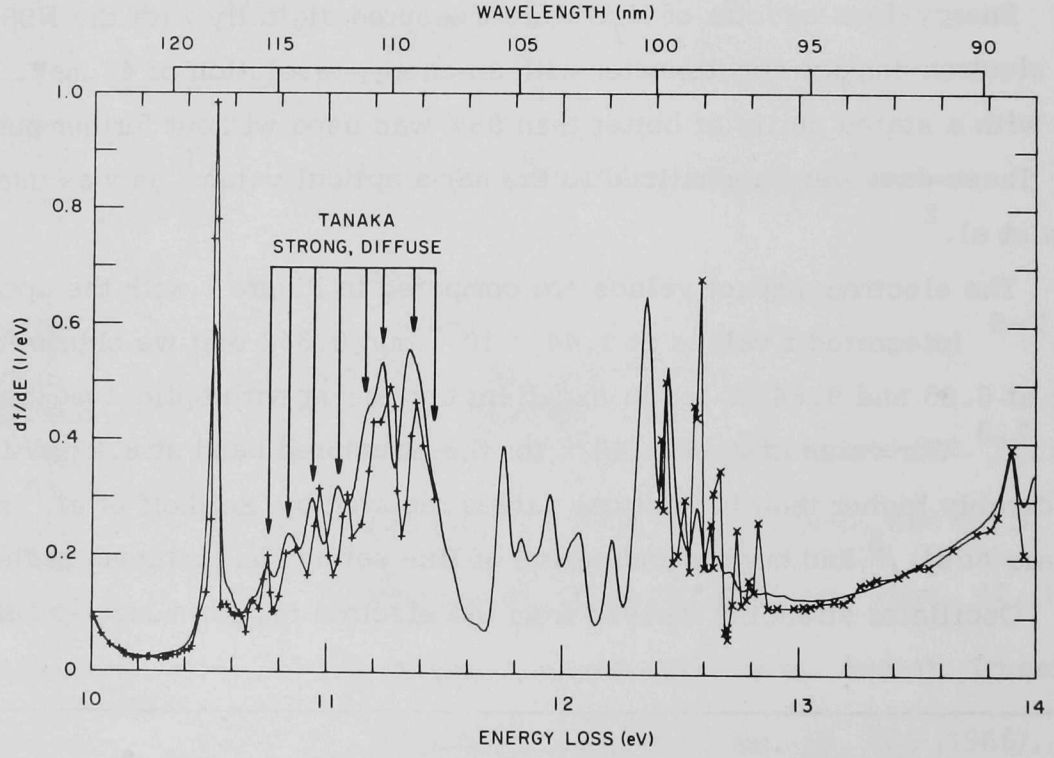

FIG. 2.--Comparison of optical and electron-impact oscillator strengths in the 10- to 14-eV region; +, Ref. 7; x, Ref. 6; solid line, present results. (ANL Neg. 149-6753)

below 5.6 eV, although small, are greater than those observed optically. The enhanced intensity we observe in this region is probably associated with the weak transition reported recently by Hall et al.[4] at low impact energies. The energy absorption region between 10 and 14 eV is shown in Figure 2.

In the region between 11.5 and 12.4 eV, no optical values are available for comparison. From the data in Figure 2 we have determined integrated values of the oscillator strength for small energy-loss intervals in the 10- to 14-eV region. These values, presented in Table 1, were obtained by numerical integration of the data between the tabulated energy limits E_1 and E_2. Direct comparison of intensities with the optical measurements is complicated owing to the large difference in energy resolution achieved with the two techniques. However, above 10.8 eV the centers of the absorption maxima reported by Zelikoff et al.[7] appear to be displaced to higher energies by about 30 meV. Our peak positions are closer to the energies of the strong diffuse progression

TABLE 1. Oscillator Strength for Transitions in N_2O from 10 to 14 eV

E_m, eV	E_1, eV	E_2, eV	f value	Identification
continuum	10.23	10.36	4.56×10^{-3}	
10.52	10.36	10.56	4.21×10^{-2}	Ry 3pπ, 3pσ ($^2\Pi$ core)
10.59 sh	10.56	10.64	1.00×10^{-2}	Tanaka weak band 1
10.68 sh	10.64	10.71	8.40×10^{-3}	Tanaka weak band 2
10.75	10.71	10.78	1.17×10^{-2}	Tanaka strong band 3
10.84	10.78	10.89	2.34×10^{-2}	Tanaka strong band 3
10.94	10.89	10.99	2.56×10^{-2}	Tanaka strong band 3
11.05	10.99	11.09	2.85×10^{-2}	Tanaka strong band 3
11.24	11.09	11.29	8.48×10^{-2}	Ry 3dπ ($^2\Pi$ core)
(11.19 sh)				Tanaka strong band 3
11.35	11.29	11.67	1.10×10^{-1}	Ry 4sσ ($^2\Pi$ core)
(others)				Ry 3d? ($^2\Pi$ core)
11.75	11.67	11.80	31.0×10^{-2}	Ry 4pπ, 4pσ ($^2\Pi$ core)
11.83	11.80	11.86	1.28×10^{-2}	Ry 4d? ($^2\Pi$ core)
11.95	11.86	12.00	3.30×10^{-2}	Ry 4dπ ($^2\Pi$ core)
(11.89 sh)				
12.07	12.00	12.14	2.60×10^{-2}	Ry 5sσ ($^2\Pi$ core)
(12.04 sh)				
12.21	12.14	12.26	1.85×10^{-2}	Ry 5pπ, 5pσ ($^2\Pi$ core)
12.36	12.26	12.41	5.99×10^{-2}	Ry 3sσ ($^2\Sigma^+$ core)
12.45	12.41	12.53	4.20×10^{-2}	Ry 6pπ, 6pσ ($^2\Pi$ core)
12.57	12.53	12.62	2.10×10^{-2}	Ry 7pπ, 7pσ ($^2\Pi$ core)
12.65	12.62	12.69	1.33×10^{-2}	Ry 8pπ, 8pσ ($^2\Pi$ core)
12.71	12.69	12.76	1.14×10^{-2}	Ry 9pπ, 9pσ ($^2\Pi$ core)
12.79	12.76	12.83	1.01×10^{-2}	
12.86	12.83	12.90	9.77×10^{-3}	
continuum	12.90	13.80	1.57×10^{-1}	Portion of $^2\Pi$ ionization cont.
13.90	13.80	13.95	4.89×10^{-2}	Ry 3pσ ($^2\Sigma^+$ core)
14.00	13.95	14.09	4.39×10^{-2}	Ry 3pπ ($^2\Sigma^+$ core)

reported in the high-resolution work of Tanaka et al.[10] Examination of the irregular intensity variation in the npπ and npσ Rydberg series converging to the $^2\Pi$-ion limit suggests considerable interchannel interaction with the nsσ series ($^2\Sigma^+$ ion core).

References

1. Lassettre, E. N., A. Skerbele, M. A. Dillon, and K. J. Ross, J. Chem. Phys. 48, 5066 (1968).
2. Weiss, M. J., S. R. Mielczarek, and C. E. Kuyatt, J. Chem. Phys. 54, 1412 (1971).
3. Foo, V. U., C. E. Brion, and J. B. Hasted, Proc. Roy. Soc. London A322, 535 (1971).
4. Hall, R. I., A. Chutjian, and S. Trajmar, J. Phys. B 6, L365 (1973).
5. Huebner, R. H., R. J. Celotta, S. R. Mielczarek, and C. E. Kuyatt, J. Chem. Phys. 59, 5434 (1973); J. Chem. Phys. 63, 2411 (1975).
6. Cook, G. R., P. H. Metzger, and M. Ogawa, J. Opt. Soc. Am. 58, 129 (1968).
7. Zelikoff, M., K. Watanabe, and E. C. Y. Inn, J. Chem. Phys. 21, 1643 (1953).
8. Rabalais, J. W., J. M. McDonald, V. Scherr, and S. P. McGlynn, Chem. Rev. 71, 73 (1971).
9. Bates, D. R. and P. B. Hayes, Planet. Space. Sci. 15, 189 (1967).
10. Tanaka, Y., A. S. Jursa, and F. J. LeBlanc, J. Chem. Phys. 32, 1205 (1960).

PRELIMINARY REPORT ON ELECTRON ENERGY-LOSS MEASUREMENTS FOR $CClF_3$, CCl_2F_2, and CCl_3F

D. L. Bushnell, Jr.,* R. H. Huebner, R. J. Celotta,† and S. R. Mielczarek†

Currently, nation-wide research efforts are devoted to studying the possible ozone (O_3) depletion in the stratosphere by the chemical action of chlorine atoms released from CCl_2F_2 or CCl_3F upon absorption of ultraviolet radiation. Since electron-impact data taken in the forward scattering direction can be used to derive oscillator strengths and thus to yield apparent photoabsorption cross sections, we have carried out such an analysis for CCl_2F_2, CCl_3F, and $CClF_3$. We obtain oscillator-strength distributions between 5 and 20 eV and compare these to available photoabsorption data. Certain photoabsorption values agree very well with this electron-impact data, but other optical studies deviate in some spectral regions by as much as a factor of 5. Also, the electron energy-loss spectrum reveals electronic transitions previously undetected by photoabsorption.

Introduction

Ultraviolet radiation from the sun can be deleterious to many life processes, yet the solar spectrum is such that only wavelengths from 150 nm (8.26 eV) to the visible cutoff have enough intensity to be of concern.[1] Indeed, it is known that human DNA (molecules basic to all life processes) absorbs heavily in this region of the uv spectrum.

This energy-absorbing ability of molecular oxygen, O_2, exhibited in the Schuman-Runge continuum, provides for a screening effect of this uv radiation up to 200 nm (6.2 eV). The much less abundant, but nevertheless strongly absorbing ozone (O_3), filters out the rest of this harmful ultraviolet up to about 300 nm (4.1 eV).

An equilibrium concentration of ozone is maintained in the stratosphere by a natural balance between many chemical reactions that both generate and destroy ozone. The important Chapman reactions[2] describe the production of

*Undergraduate research participant from the University of Illinois, Urbana, Ill., sponsored by the Center for Educational Affairs, Argonne National Laboratory.

†National Bureau of Standards, Washington, D.C. 20234.

ozone by photodissociation of O_2 and subsequent combination of oxygen atoms with oxygen molecules in a three-body reaction yielding O_3. Photodecomposition of N_2O is the major natural source of nitric oxides that limit present ozone concentration in the stratosphere.[3] This occurs through a catalytic sequence of reactions resulting in a net destruction of ozone. Recent concern[4] has been generated over a newly discovered mechanism of ozone destruction by the chlorofluoromethanes. It has been found that chlorine atoms photodissociated from these molecules can react catalytically to destroy ozone in a reaction sequence similar to those identified for the nitric oxides. Details of this subject have been reviewed by Rowland and Molina.[5]

The current environmental importance of understanding the excitation properties of halocarbons 11 (CCl_3F) and 12 (CCl_2F_2) has prompted our analysis of them by electron-collision techniques. Electron energy-loss spectra for CCl_3F, CCl_2F_2, and $CClF_3$ were obtained digitally with the National Bureau of Standards Model AN-1 electron spectrometer for 100-eV incident electrons scattered within an acceptance angle of 20 mrad about the incident direction.

The spectrum thus obtained shows the intensity of electrons scattered vs. the amount of energy lost.

Our particular study concerned the following:

1) Analysis of the electron energy-loss spectra to obtain differential oscillator strengths and photoabsorption cross sections for a wide range of energy loss (5 to 20 eV);

2) comparison of this information to corresponding photoabsorption measurements;

3) identification and assignment of certain electronic transitions; and

4) determination of reliable oscillator-strength distributions for CCl_3F, CCl_2F_2, and $CClF_3$.

An important aspect of this study has been to provide new information[6] pertinent to the problem of ozone depletion by halocarbons 11 and 12. These molecules, $CFCl_3$ and CF_2Cl_2, are more commonly known by their Dupont copyrighted tradenames, Freon 11 and Freon 12.

The available photoabsorption data for halocarbons 11, 12, and 13 are very sparse. For each molecule there exist two independent photoabsorption studies below 10 eV.[5,7] That of Rowland and Molina[5] covers only the limited energy region of 5.7 to 6.7 eV. Above approximately 10 eV only the optical measurements of Gilbert et al.[8] are available. For CCl_2F_2, unpublished measurements of Person, Fowler, and Nicole[9] of this laboratory are available.

Experimental Results

Energy-loss spectra for CCl_3F, CCl_2F_2, and $CClF_3$ obtained with 100 eV incident electrons and zero scattering angle are presented in Figures 1, 2, and 3, respectively. Spectra recorded at energy losses below 5 eV displayed a flat constant background with no additional structure due to electronic transitions. These spectra were converted to apparent oscillator-strength distribution by the procedure discussed in detail previously.[10,11]

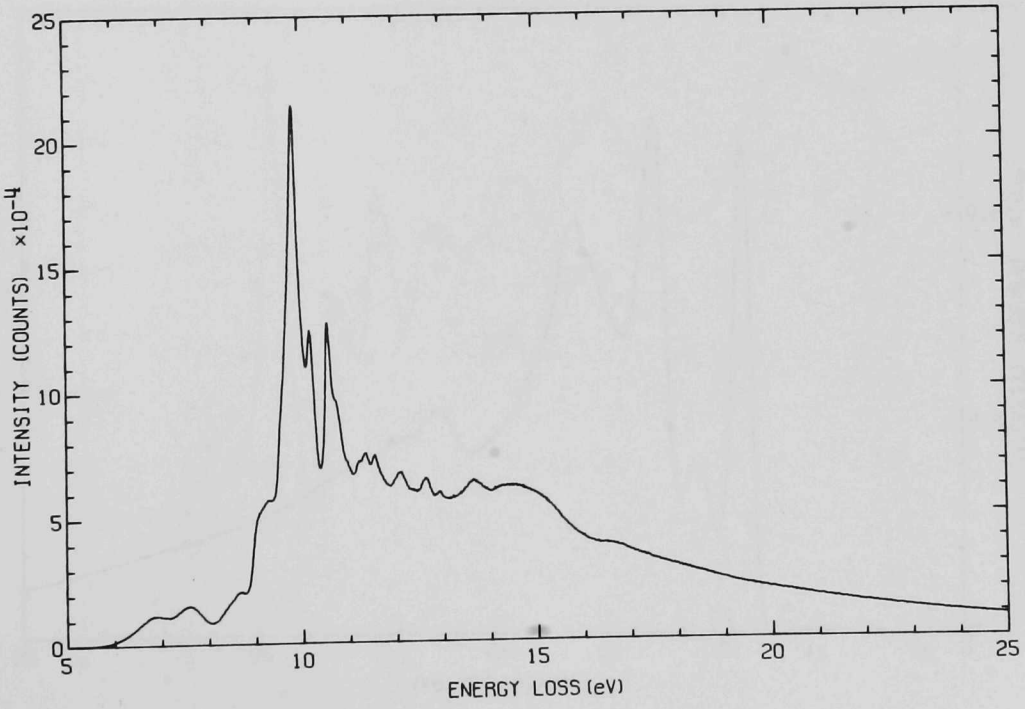

FIG. 1.--Energy-loss spectrum of halocarbon 11 ($CFCl_3$)

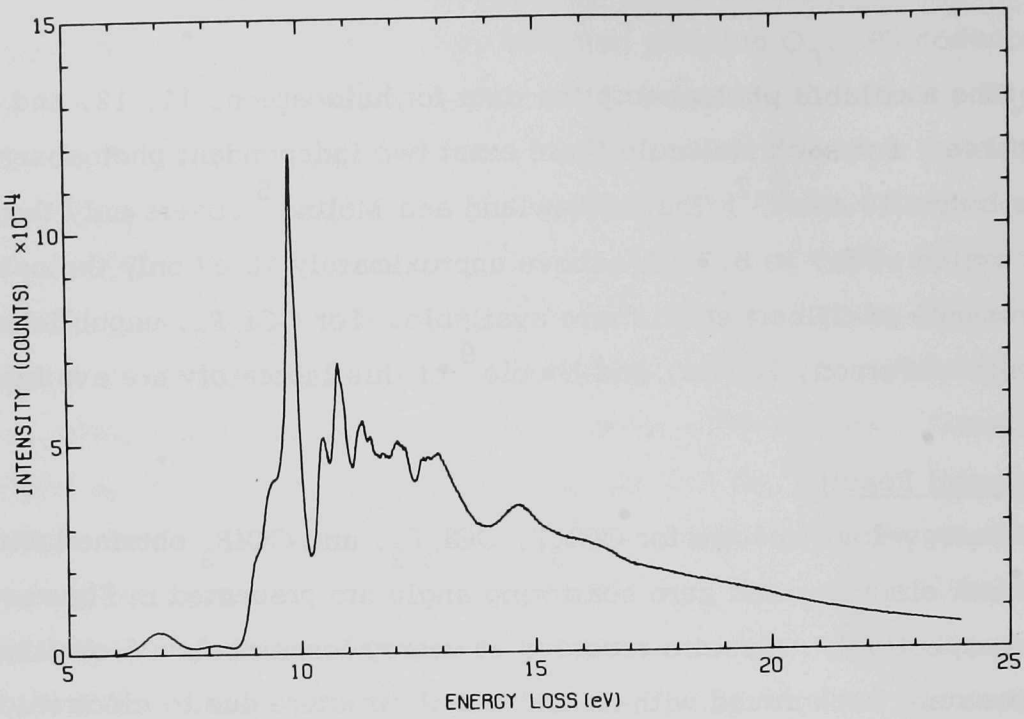

FIG. 2.--Energy-loss spectrum of halocarbon 12 (CF_2Cl_2)

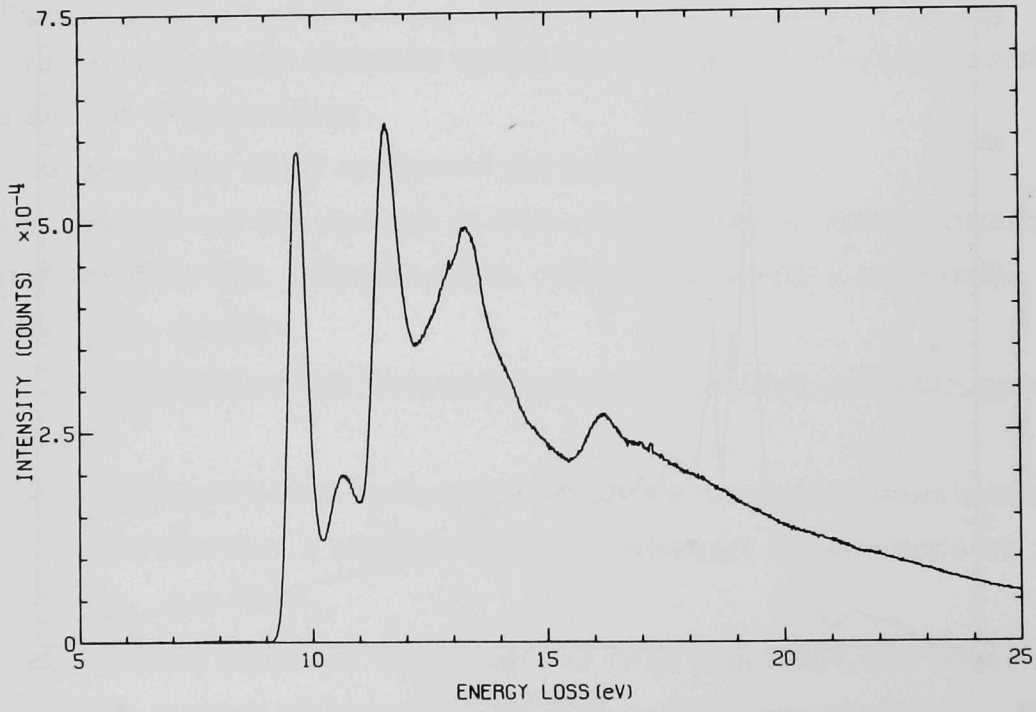

FIG. 3.--Energy-loss spectrum of halocarbon 13 (CF_3Cl)

Halocarbon 12 (CCl_2F_2)

The data for CCl_2F_2 were normalized at 12.22 eV to df/dE = 0.732 eV^{-1} taken from the very recent measurements of Person et al.[9] This normalization yields agreement to within ± 5% with their spectral measurements from 12.0 to 14.5 eV. The apparent oscillator-strength distribution is compared in Figure 4 with values extracted from the photoabsorption measurements of Doucet et al.[7] and Gilbert et al.[8] The agreement is relatively good up to 11.3 eV, where the data from Gilbert et al[8] drop significantly, relative to the electron-energy loss (EEL) values. At 12.1 eV the EEL values are larger by nearly a factor of 1.5, and near the 13.0-eV peak the EEL measurements are still a factor of 1.4 greater than the optical values of Gilbert et al.[8]

One possible explanation for the disagreement between the optical and the EEL values in the region above 11.4 eV is that for photon energies greater than about 11.8 eV, the LiF absorption cell windows used by Gilbert et al.[8]

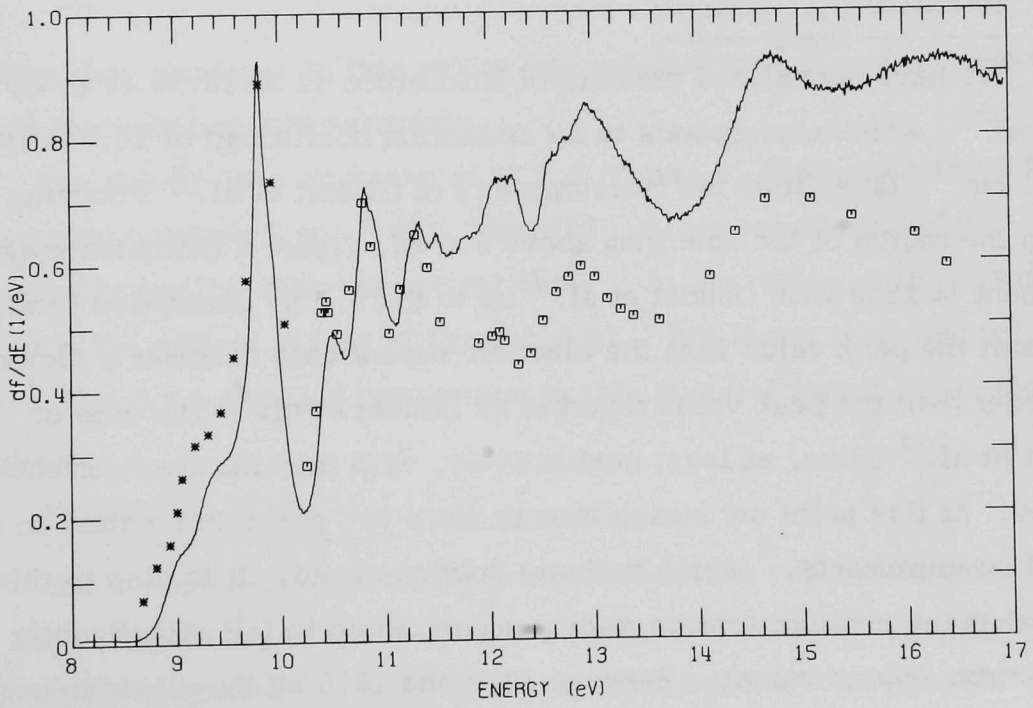

FIG. 4.--Comparison of oscillator strengths for halocarbon 12 in the region 8 to 17 eV. Solid line, electron-impact results from present work; stars, optical values of Ref. 7; squares, optical values of Ref. 8.

become opaque. To obtain values at higher photon energies one must change over to "windowless" operation, which can cause serious difficulties, such as inaccurate pressure determinations, resulting in a decrease in the accuracy of the photoabsorption measurements. Since our present results agree closely with those of Person et al.[9] between 12.0 and 14.5 eV, we suspect that the measurements of Gilbert et al.[8] at energies above 11.8 eV are subject to some large undetermined error. It is also interesting to note that Figure 4 reveals indications of three absorption bands at 10.9, 11.5, and 11.8 eV not observed by Gilbert et al.[8]

The region of the spectrum that is pertinent to the ozone problem lies below 8.5 eV, and the region of 5.6 to 6.9 eV (2200 Å → 1800 Å) is of primary importance. For CCl_2F_2, two broad peaks are observed between 5.5 and 8.5 eV. Both of them are likely to be caused by transitions that result in the ejection of a chlorine atom. Our f values are larger by a factor of 4 at 7.0 eV and a factor of 5 at 8.2 eV than those of Doucet et al.[7] This disagreement is further discussed elsewhere in this report.[6]

Halocarbon 11 (CCl_3F)

We have normalized the data of halocarbon 11 at 10.76 eV to df/dE = 0.906 eV^{-1}, which corresponds to an extinction coefficient of 26,000 liter mol^{-1} cm^{-1}, taken from the measurements of Gilbert et al.[8] Focusing attention on the region of the spectrum above 8.0 eV, Figure 5 indicates reasonable agreement (± 15%) with Doucet et al.[7] up to the 9.8 eV absorption band. At this point the peak value from the electron-impact data becomes a factor of 1.5 larger than the peak value reported by Doucet et al.[7] The data of Gilbert et al.[8] agree, at least qualitatively, with the EEL measurements up to 11.4 eV. At this point our measurements show two peaks in contrast to the optical measurements,[8] which indicate only one band. It is also in this region that the photoabsorption measurements begin to fall significantly below the electron-impact values. Between 12.0 and 13.0 eV the electron-impact measurements are nearly a factor of 2 larger than the photoabsorption values of Gilbert et al.[8] As previously discussed, it is likely that the "windowless"

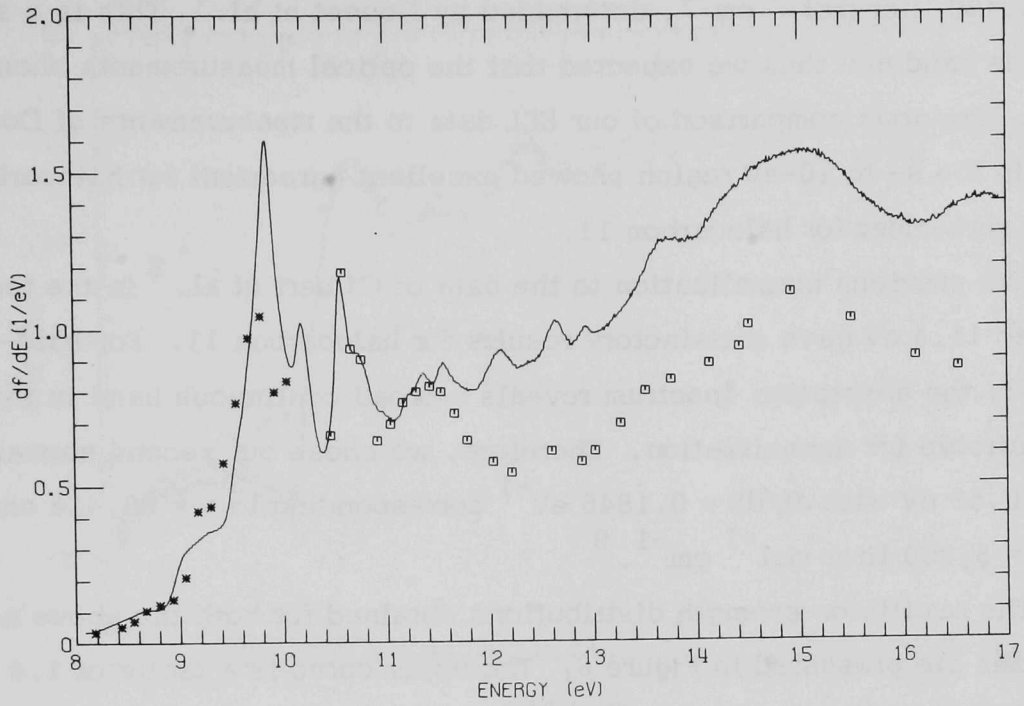

FIG. 5.--Comparison of oscillator strengths for halocarbon 11 in the region 8 to 17 eV. Solid line, electron-impact results from present work; stars, optical values of Ref. 7; squares, optical values of Ref. 8.

operation they employed in this region has resulted in a decreased accuracy of their photoabsorption measurements.

The energy-loss spectrum of CCl_3F (Figure 1) shows two broad bands in the region between 5 and 8 eV. The df/dE values we obtain below 7.7 eV are generally smaller than the optical data.[7] In the region of the 6.7-eV absorption the optical values of Doucet et al.[7] are larger than ours by roughly a factor of 1.7. A detailed comparison in this spectral region is presented elsewhere.

Halocarbon 13 ($CClF_3$)

The normalization for $CClF_3$ is somewhat less reliable than for the two other molecules owing to the large uncertainty in the limited optical data[7,8] available for comparison. Two different normalizations were chosen. Initially we selected a normalization value at 9.63 eV of df/dE = 0.5639 eV^{-1}, corresponding to a wave number ν = 77,670 cm^{-1}, and molar-extinction coefficient

ϵ_{10} = 16,190 liter mol^{-1} cm^{-1}, determined by Doucet et al.[7] This is a strong absorption band and thus we expected that the optical measurements should be reliable. Previous comparison of our EEL data to the measurements of Doucet et al.[7] in the 9- to 10-eV region showed excellent agreement for halocarbon 12, but poor agreement for halocarbon 11.

Our previous normalization to the data of Gilbert et al.[8] in the region of 10.4 to 11.4 eV gave satisfactory results for halocarbon 11. For halocarbon 13, the absorption spectrum reveals a broad continuous band in this region suitable for normalization. Therefore, we chose our second normalization at 10.59 eV with df/dE = 0.1846 eV^{-1} corresponding to ν = 85,414 cm^{-1} and ϵ_{10} = 5,300 liter mol^{-1} cm^{-1}.[8]

The oscillator-strength distributions obtained for both the above normalizations are presented in Figure 6. The upper curve is a factor of 1.4 greater than the lower curve at all energies, with the distribution normalized at 9.63 eV being the largest. Unlike halocarbons 11 and 12, this molecule displays only one weak continuous absorption band below 9.0 eV. The photoabsorption measurements[7] indicate a single absorption shoulder in this region, but at an energy near 8.9 eV. This is nearly one eV higher in energy than the weak absorption band at 8.1 eV observed in our spectrum. Once again, above 11.5 eV, the "windowless" measurements of Gilbert et al.[8] drop considerably below the electron-impact values. In this region of the peak at 13.4 eV, the electron-impact values are larger than the optical values[8] by nearly a factor of 1.4 or more.

Discussion

Assignments of the observed excitations in the halocarbon spectra are particularly complicated because of the many possible excited states available which may be superimposed on dissociation or ionization continua. For each of the halocarbons studied here, it is reasonable to assume that most of the low-energy transitions arise from excitation of the chlorine lone-pair electrons. Some specific assignments have been attempted by Doucet et al.,[7] but these can only be regarded as tentative. Nevertheless, it does appear that most of

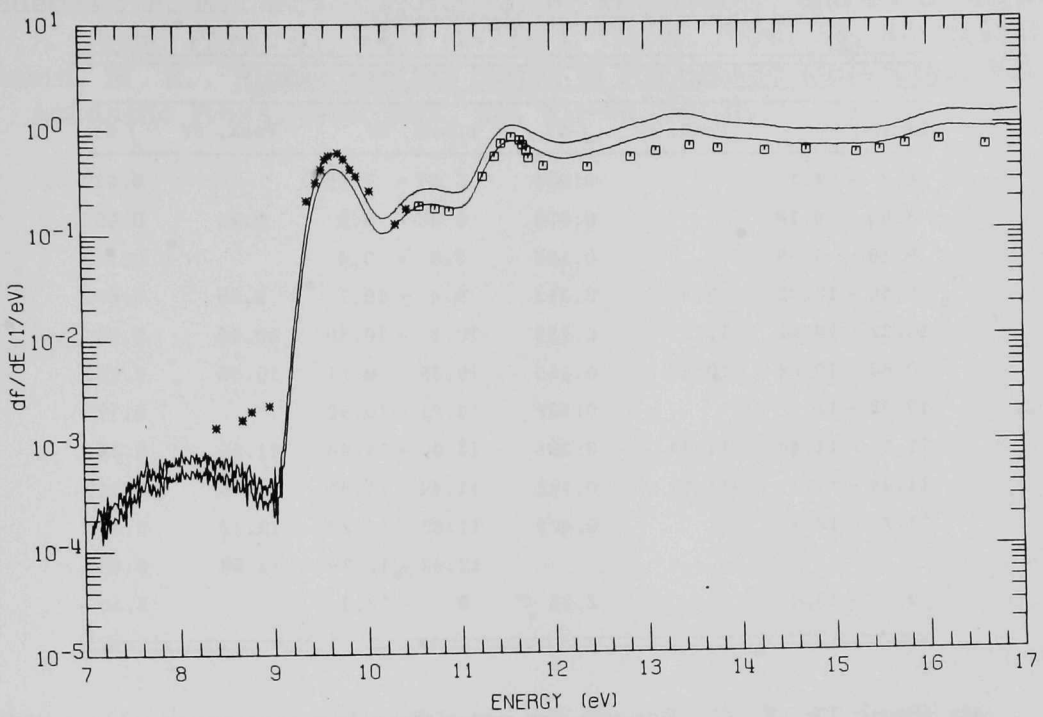

FIG. 6.--Comparison of oscillator strengths for halocarbon 13 in the region 7 to 17 eV (note logarithmic scale). Upper solid line, present results normalized at 9.63 eV; lower solid line, present results normalized at 10.59 eV; stars, optical values of Ref. 7; squares, optical values of Ref. 8.

the sharp structure in this region can be correlated with Rydberg transitions predicted by the empirical rules proposed by Robin.[12] By combining this observation with the more reliable oscillator strengths obtained in this work, we hope to improve the assignment of transitions for these molecules. Integrated oscillator strengths for the similar bands in CCl_2F_2 and CCl_3F are given in Table 1. For halocarbon 11, CCl_3F, there are 12 lone-pair chlorine electrons. For halocarbon 12, CCl_2F_2, there are only 8 chlorine lone-pair electrons. If we assume that below 13 eV nearly all of the oscillator strength comes from transitions between the chlorine lone-pair orbitals and Rydberg orbitals, then we might expect a ratio of 3:2 for the oscillator strength sum. Indeed, the ratio lies between 1.5 and 1.6, which does tend to indicate that the excitations below 13.0 eV for these two molecules are mainly due to transitions from Cl molecular orbitals. We are in the process of applying similar considerations to the individual absorption bands.

TABLE 1. Integrated Oscillator Strengths for Specified Energy Bands Derived from Electron Energy-Loss Measurements

CCl_2F_2			CCl_3F		
Limits, eV	Peak, eV	$\int df$	Limits, eV	Peak, eV	$\int df$
6.4 - 7.1		0.008	5.51 - 7.08		0.020
8.51 - 9.18		0.050	8.05 - 8.8	8.71	0.055
9.18 - 9.58		0.120	8.8 - 9.4		0.167
9.58 - 10.22	9.8	0.313	9.4 - 10.1	9.86	0.673
10.22 - 10.62	10.5	0.153	10.1 - 10.39	10.18	0.241
10.62 - 10.88	10.82	0.155	10.39 - 10.71	10.56	0.292
10.88 - 11.1		0.127	10.71 - 10.92		0.176
11.1 - 11.44	11.34	0.206	11.0 - 11.44	11.36	0.346
11.44 - 11.7	11.50	0.162	11.44 - 11.83	11.55	0.328
11.7 - 12.4		0.479	11.83 - 12.27	12.12	0.387
			12.27 - 12.79	12.64	0.492
0 - 13.0		2.23	0 - 13.0		3.50

We thank Dr. J. C. Person for providing his measurements on CCl_2F_2 prior to publication, and for frequent helpful discussions.

References

1. Tousey, R. The Middle Ultraviolet: Its Science and Technology, A.E.S. Green, Ed., John Wiley & Sons, Inc., New York, pp. 1–39 (1966).
2. Chapman, S., Q. J. R. Meteorol. Soc. 3, 103 (1930).
3. Bates, D. R. and P. B. Hayes, Planet. Space Sci. 15, 189 (1967).
4. Fluorocarbons — Impact on Health and Environment, Hearings before the Subcommittee on Public Health and Environment of the Committee on Interstate and Foreign Commerce, House of Representatives, Ninety-Third Congress, Second Session on H.R. 17577 and H.R. 17545, Dec 11–12, 1974, Ser. No. 93-110, U.S. Government Printing Office, Washington, D.C. (1975).
5. Rowland, R. S. and M. J. Molina, Rev. Geophys. Space Phys. 13, 1 (1975).
6. Huebner, R. H., D. L. Bushnell, Jr., R. J. Celotta, S. R. Mielczarek, and C. E. Kuyatt, this report, paper 4.
7. Doucet, J., P. Sauvageau, and C. Sandorfy, J. Chem. Phys. 58, 3708 (1973).
8. Gilbert, R., P. Sauvageau, and C. Sandorfy, J. Chem. Phys. 60, 4820 (1974).
9. Person, J. C., D. E. Fowler, and P. P. Nicole, this report, paper 6.
10. Huebner, R. H. and R. J. Celotta, Argonne National Laboratory Radiological and Environmental Research Division Annual Report, July 1971–June 1972, ANL-7960, Part I, p. 49.

11. Huebner, R. H., R. J. Celotta, S. R. Mielczarek, and C. E. Kuyatt, J. Chem. Phys. 59, 5434 (1973); J. Chem. Phys. 63, 241 (1975).
12. Robin, M. B., Higher Excited States of Polyatomic Molecules, Vol. 1, Academic Press, New York, pp. 51–68 (1974).

ULTRAVIOLET PHOTOABSORPTION BY HALOCARBONS 11 AND 12 FROM ELECTRON-IMPACT MEASUREMENTS*

R. H. Huebner, D. L. Bushnell, Jr.,† R. J. Celotta,‡
S. R. Mielczarek,‡ and C. E. Kuyatt‡

It is a matter of widespread concern[1] that chlorine atoms released by photolysis of the chlorofluoromethanes reaching the stratosphere may deplete the ozone layer. The magnitude and time scale predicted for this effect depend on large-scale models that require data on the primary processes involved. Ultraviolet photoabsorption is the first step in the sequence of events, and therefore, accurate absorption cross sections of halocarbons 11 and 12 ($CFCl_3$ and CF_2Cl_2) are of considerable interest. However, previous optical determinations[2,3] between 200 and 120 nm (i.e., 6.2 and 10.33 eV) are not in agreement. Recently we have used electron-impact measurements to derive reliable oscillator-strength distributions for a number of molecules.[4,5] Our studies have exhibited excellent agreement (i.e., better than ± 15%) between electron impact and optical values in the energy-loss region below 15 eV ($\lambda > 80$ nm).

Electron energy-loss spectra were measured digitally for $CFCl_3$ and CF_2Cl_2 with the NBS Model AN-1 electron-impact spectrometer[5] for 100-eV electrons scattered within 20 mrad of the incident direction. Sample gases obtained commercially were used without further purification. Analysis by gas chromatography indicated a purity greater than 99.8% with the only identifiable impurity being 0.1% CF_2ClH in CF_2Cl_2. Oscillator-strength distributions were derived by a procedure[5] that accounts for the finite angular acceptance of the spectrometer. For halocarbon 12, the relative distribution was normalized at an energy of 12.22 eV to a value of $df/dE = 0.732\ eV^{-1}$

---

*Summary of a paper published in Nature 257, 376 (1975).

†Undergraduate Research Participant from the Physics Department, University of Illinois, Urbana, Ill., sponsored by the Center for Educational Affairs, Argonne National Laboratory.

‡National Bureau of Standards, Washington, D.C. 20234.

from unpublished measurements of J. C. Person and co-workers. Our normalized values agree within ± 5% of the measurements of Person et al. but are nearly a factor of 1.4 higher than those of Gilbert et al.[6] between 12 and 15 eV. However, between 10.4 and 11.4 eV our values are close to those of Gilbert et al.[6] In fact, the disagreement occurs mainly in the spectral region where they operate with a windowless absorption cell. Thus, we suspect some undetermined error in their measurements in the windowless region.

For halocarbon 11, only the data of Gilbert et al.[6] are available for normalization. We have normalized our halocarbon 11 data at 10.76 eV to $df/dE = 0.906\ eV^{-1}$, corresponding to their molar extinction coefficient of 26,000 liter $mole^{-1}$ cm^{-1} measured at 115.2 nm. This gives good agreement with their values below 11.4 eV, but again our values are nearly twice as large in the windowless region. A more detailed analysis of this vacuum ultraviolet region is given elsewhere in this report.[7]

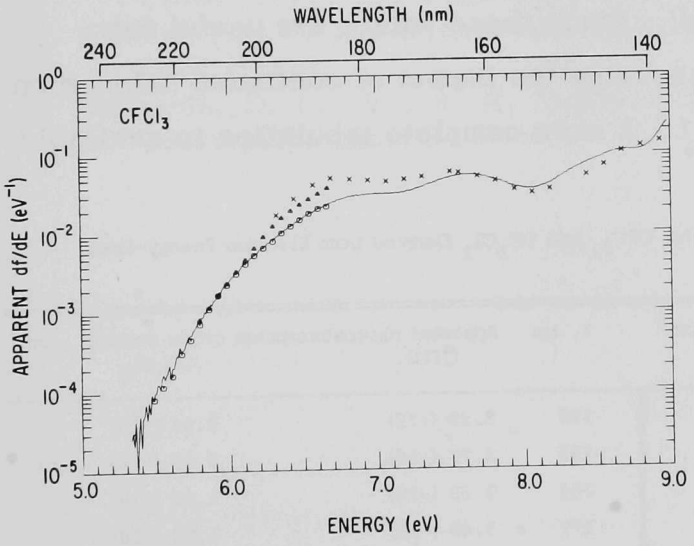

FIG. 1.--Comparison of oscillator strengths for halocarbon 11 ($CFCl_3$) in the ultraviolet absorption region: solid line, present electron-impact results; x, optical values of Ref. 2; triangles, optical values of Ref. 2 as quoted by Ref. 3; open circles, optical values of Ref. 3.
(ANL Neg. 149-75-111)

Our results relevant to the ozone depletion problem are shown in Figures 1 and 2. Our electron-impact data are compared with the photoabsorption measurements of Doucet et al.[2] and the very recent work of Rowland and Molina.[3] Our measurements for halocarbons 11 and 12 characterize energy absorption in the so-called "window" region of the solar radiation flux.[3] These values extend from the Hartley band of O_3 (maximum at 4.9 eV or 255 nm) to the Schumann-Runge continuum of O_2 (8.5 eV or 146 nm maximum). We confirm

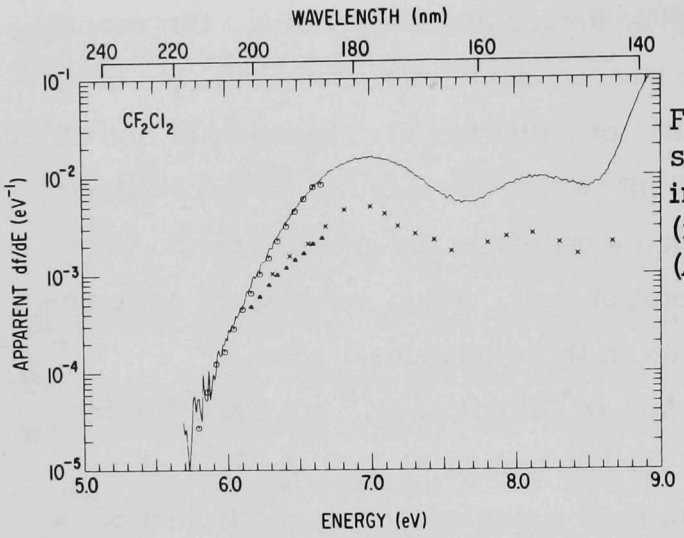

FIG. 2.--Comparison of oscillator strengths for halocarbon 12 (CF_2Cl_2) in the ultraviolet absorption region (identifications same as for Fig. 1). (ANL Neg. 149-75-112)

the recent measurements of Rowland and Molina[3] for both halocarbons and disagree with earlier measurements[2] by as much as a factor of two for $CFCl_3$ and a factor of four for CF_2Cl_2. Also, our results differ from those of Doucet et al.[2] at higher energies for both halocarbons. Apparent photoabsorption cross sections can be calculated from the present results by multiplying by the factor 1.0975×10^{-16} $cm^2 \cdot eV$. Since these values are useful for atmospheric model calculations assessing the impact of continued halocarbon releases, they are given in Table 1. A more complete tabulation is available upon request.

TABLE 1. Apparent Photoabsorption Cross Sections for $CFCl_3$ and CF_2Cl_2 Derived from Electron Energy-Loss Measurements

λ, nm	Apparent photoabsorption cross section, cm^2		λ, nm	Apparent photoabsorption cross section, cm^2	
	$CFCl_3$	CF_2Cl_2		$CFCl_3$	CF_2Cl_2
225	1.11 (-20)[a]	—	188	2.29 (-18)	8.42 (-19)
221	2.20 (-20)	—	185	2.77 (-18)	1.15 (-18)
218	4.55 (-20)	1.97 (-21)	182	3.23 (-18)	1.49 (-18)
214	9.77 (-20)	4.50 (-21)	177	3.49 (-18)	1.76 (-18)
210	1.64 (-19)	1.08 (-20)	172	3.68 (-18)	1.39 (-18)
207	2.90 (-19)	2.63 (-20)	168	4.75 (-18)	8.91 (-19)
203	4.77 (-19)	5.16 (-20)	163	5.88 (-18)	5.98 (-19)
200	6.82 (-19)	1.02 (-19)	159	5.15 (-18)	6.87 (-19)
197	9.77 (-19)	2.10 (-19)	155	3.89 (-18)	9.46 (-19)
194	1.35 (-18)	3.44 (-19)	151	4.76 (-18)	1.07 (-18)
191	1.78 (-18)	5.65 (-19)	148	7.74 (-18)	9.45 (-19)

[a]The number in parenthesis is the exponent of the power of ten by which the value of the cross section tabulated is to be multiplied.

We thank Dr. J. C. Person, D. Fowler, and P. P. Nicole (Argonne National Laboratory) for generously providing their photoabsorption cross sections for halocarbon 12 before publication, and Dr. P. Ausloos (National Bureau of Standards) for analyzing our gas samples.

References

1. Fluorocarbons — Impact on Health and Environment, Hearings before the Subcommittee on Public Health and Environment of the Committee on Interstate and Foreign Commerce, House of Representatives, Ninety-Third Congress, Second Session on H.R. 17577 and H.R. 17545, December 11 and 12, 1974, Ser. No. 93-110, U.S. Government Printing Office, Washington, D.C. (1975).
2. Doucet, J., P. Sauvageau, and C. Sandorfy, J. Chem. Phys. 58, 3708–3716 (1973).
3. Rowland, F. S. and M. J. Molina, Rev. Geophys. Space Phys. 13, 1–35 (1975).
4. Huebner, R. H., S. R. Mielczarek, and C. E. Kuyatt, Chem. Phys. Lett. 16, 464–469 (1972).
5. Huebner, R. H., R. J. Celotta, S. R. Mielczarek, and C. E. Kuyatt, J. Chem. Phys. 59, 5434–5443 (1973); J. Chem. Phys. 63, 241 (1975).
6. Gilbert, R., P. Sauvageau, and C. Sandorfy, J. Chem. Phys. 60, 4820–4824 (1974).
7. Bushnell, D. L., Jr., R. H. Huebner, R. J. Celotta, and S. R. Mielczarek, this report, paper 3.

A TROCHOIDAL ELECTRON ENERGY ANALYZER

David Spence and O. J. Steingraber

In this report we describe the use of a trochoidal electron energy analyzer, employing crossed electric and magnetic fields for the measurement of electron energy-loss spectra.

In the past, such measurements have usually been made using purely electrostatic instruments (for example, see Refs. 1 and 2). Though electrostatic instruments may be extremely versatile, providing high resolution often combined with angular capabilities, they tend to be rather complex and costly, demanding high mechanical tolerances. In addition, purely electrostatic instruments tend to suffer from poor electron transmission properties, which may vary as an unknown function of analysis energy because of electron-optical effects.

Electron-optical effects may often be effectively negated if the electron beam can be confined by an axial magnetic field. Such confinement precludes the ability to make angular measurements. However, this is not always a necessary feature.

We have developed an instrument to measure energy-loss spectra in forward scattering which employs magnetic confinement of the electron beam. For both monochromatization of the beam and for energy analysis, we use trochoidal dispersive elements first described by Stamatovic and Schulz.[3,4] In the past, such trochoidal devises have been used only as monochromators and not as scattered electron energy analyzers.[2] A schematic diagram of the apparatus we used for these studies is illustrated in Figure 1. Electrons are emitted from a thoria-coated iridium filament, and are confined by an axial magnetic field of a few hundred gauss. After initial acceleration by an anode, they enter an electric field perpendicular to their path provided by crossed plates TM in Figure 1. In this region the electrons experience the forces of crossed electric and magnetic fields and are dispersed along a plane perpendicular to their direction of motion according to their axial velocity on entering the crossed field region. A pseudomonochromatic beam is selected

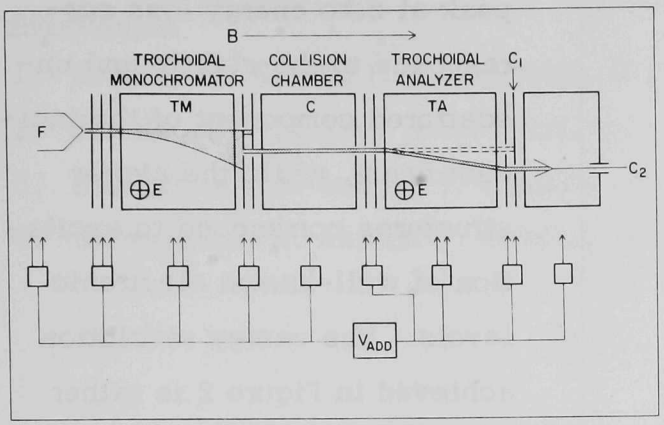

FIG. 1.--Schematic diagram of trochoidal monochromator-analyzer.

by placing the exit slit of the crossed field region off axis from the entrance slit. On leaving the crossed field region, the beam is accelerated to the desired energy and impinges on a gas target in the collision chamber, C. Electrons which lose energy in an inelastic collision with the target gas are magnetically confined by the magnetic field and their energy is analyzed by the trochoidal analyzer, TA, which is identical in construction to the monochromator TM. The operation of the trochoidal analyzer is as follows.

The analyzer is tuned to pass unscattered electrons of approximately the same energy as the monochromator (typically a few tenths of an eV), such that these unscattered electrons follow the curved path shown in Figure 1 and exit the analyzer through the off-axis aperture, where they are collected on a collector, C_2, and are detected. Under such conditions electrons which have lost energy in the collision chamber have insufficient energy to enter the analyzer and are thus not detected. By increasing the potential of all electrodes downstream of the collision chamber by an "add on" voltage, V_{add}, it is possible to give unscattered electrons sufficient energy in the analyzer to become essentially undeflected in the weak ExB field, and they pass straight through the analyzer (dashed line) and exit by the axial aperture, where they are collected by the collector, C_1. However, when eV_{add} is equal to a particular energy-loss process, these inelastically scattered electrons have the correct energy to follow the curved trajectory in TA and are detected. Thus, a voltage scan of V_{add} produces an energy-loss spectrum for the particular gas under study.

An example of such a spectrum obtained for 110-eV electrons incident on molecular nitrogen at a pressure of about 1×10^{-3} torr is shown in Figure 2. This spectrum compares to about 5 min data acquisition time. The

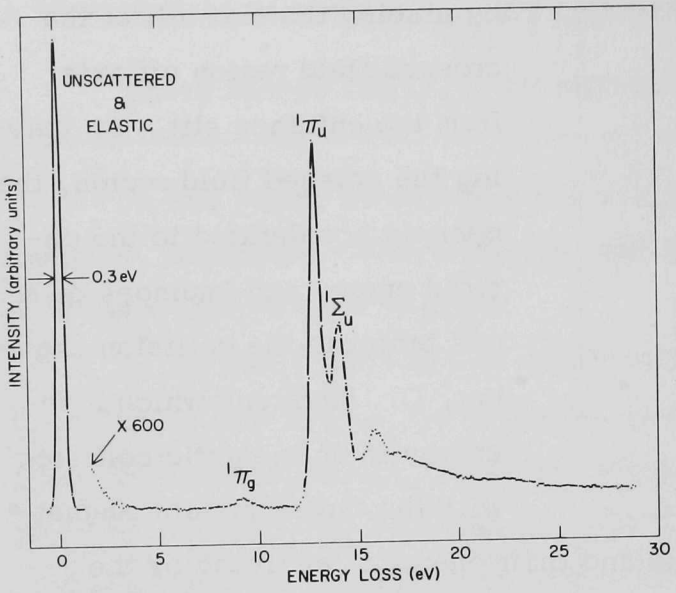

FIG. 2.--Electron energy-loss spectrum for 110-eV electron incident on molecular nitrogen.

peak at zero energy loss corresponds to the elastic and unscattered component of the incident beam, while the higher structures correspond to excitation of well-known electronic levels. The energy resolution achieved in Figure 2 is rather poor (about 0.3 eV), and so the structures correspond to excitation of bands rather than individual electronic vibrational levels. The poor resolution of this spectrum results from operation of the analyzer at rather high analysis energy, the width of the peaks being almost entirely due to the transverse electric field drop across the entrance slit of the analyzer. Later measurements have been made in which the combined monochromatic analyzer reaction is lowered to 0.08 eV. For incident currents of about 10^{-8} amp, we achieve a transmission through the analyzer of about 50%. This instrument has been operated at incident energies of 1.1 keV, and is presently being modified for 10-keV operation, and also for the ability to take spectra at very high energy loss in order to study inner-shell processes. Combined monochromator-analyzer resolution better than 0.1 eV is not required for these studies because of the intrinsic widths of the states involved.

The instrument described here is of much more simple construction and offers better energy resolution than the present generation of electrostatic instruments used for the study of K-shell spectra. The negation of electron optical effects in our instrument will potentially allow a much larger range of energy-loss measurements with respect to the incident electron energy, which is typically 10 to 20% in electrostatic instruments.

References

1. Kuyatt, C. E. and J. A. Simpson, Rev. Sci. Instrum. 38, 103 (1967).
2. Schulz, G. J., Rev. Mod. Phys. 45, 378 (1973).
3. Stamatovic, A. and G. J. Schulz, Rev. Sci. Instrum. 39, 1752 (1968).
4. Stamatovic, A. and G. J. Schulz, Rev. Sci. Instrum. 41, 423 (1970).

ABSORPTION CROSS SECTIONS FOR WATER, AMMONIA, METHANE, NEOPENTANE, THE CHLOROMETHANES, AND CF_2Cl_2

James C. Person, David E. Fowler,* and Paul P. Nicole

Experimental data on the absorption cross section (or differential oscillator strength) are presented for water, ammonia, methane, neopentane, CH_3Cl, CH_2Cl_2, $CHCl_3$, CCl_4, and CF_2Cl_2. In all cases the upper energy limit is 21.2 eV, and the lower energy limit is between 11 and 13 eV.

Introduction

The oscillator-strength distribution is a valuable input to theoretical radiation physics, as well as to fields such as photochemistry and upper-atmosphere chemistry. The differential oscillator strength, df/dE, is directly proportional to the absorption cross section, σ, and experimental results can be presented in either form. The double ion chamber[1] has proved to be a reliable apparatus for σ determinations, and we have improved conditions in order to obtain high precision. In this report we present σ (or df/dE) values for water, ammonia, methane, and a number of substituted methanes. The lower limit of the photon energy, E, is 11 to 13 eV, and the upper limit is 21.2 eV. Several of the molecules studied represent potential sources of chlorine atoms in the stratosphere[2] and are important when one estimates the impact of human activities on the ozone concentration.

Experimental

The apparatus, consisting of a light source, monochromator, and double ion chamber, has been described previously.[3-5] A hydrogen-discharge lamp was used for energies less than 13.3 eV, and a high-pressure helium lamp was used for $12.5 \leq E \leq 21.2$ eV. A new grating (1200 lines/mm, 80-nm blaze, gold coated, Bausch and Lomb No. 35-52-23-70) was installed, and data were

* Undergraduate Research Participant from Macalester College, St. Paul, Minnesota 55101.

taken using either 0.05-nm or 0.10-nm resolution (fwhm). Positive ions were collected in the double ion chamber using a voltage of 23 V.

The gas pressures were measured with an MKS Baratron Type 77H-1 capacitive manometer; this was calibrated by comparison with an oil manometer.[6,7] The oil was DC-704 vacuum-pump fluid; we measured the oil density as $1.0624/[1 + 0.00071\ (t - 23.7)]$, where t is the temperature in °C. Using this density, which is within 0.04% of Ruthberg's determination,[7] and taking the gravitational acceleration as 980.287 cm sec^{-2} gave a calibration that indicated the true pressure was 1.4% greater than the original (1966) factory calibration of the Baratron. Also, the nonlinearity corrections were some 2 to 3 mtorr larger than before. During the year the Baratron was returned to the factory for improvements of the head amplifier and for recalibration. The new factory calibration gave pressure readings that were 0.7% greater than our own calibration with the oil manometer; we have used our calibration and assumed that the error in calibration of the 1-torr head is around 1%.

The data were taken by stepping the monochromator wavelength-drive motor, unshorting the two vibrating-reed electrometers that measure the ion currents, and then determining the ion currents from the time derivatives of the voltage buildup on the integrating capacitors. The time derivatives are obtained by using voltage-to-frequency converters to send pulses to bidirectional counters that first count down and then, after a time delay, count up. The relative response for the two electrometers using the new system was determined to be 1.69:1. This value gave σ values that were within ± 0.3% for optical densities corresponding to values of $\exp(-\sigma N L_F)$ from 0.06 to 0.72 (where N is the gas density and L_F is the length of the front ion chamber). With a battery and a resistor (and correcting for contact-potential differences), we measured a relative response factor 1.4% smaller than the value that gave the minimum variation of σ when N was varied. Some of this difference may be accounted for by the $\approx$ 1% uncertainty in measuring the relative lengths of the two chambers. For typical optical densities, the error in σ is about one-half of the error in the response factor.

Thus, we can estimate limits for some of the systematic errors in σ as

$\approx$ 0.7% from the electrometer-response factor, $\approx$ 1% from L_F, and $\approx$ 1% from the pressure measurements; the random error is less than 1% for energies where the lamp has reasonable intensity. Another source of systematic error is scattered light present in the monochromator output, but all data in this report have scattered light intensities estimated to be less than 4% of the observed light intensities. Also, the σ values show good agreement in the energy region in which the data were taken with both lamps, even though different scattered-light corrections are used. Most of the data in this report were obtained for only one gas pressure, so that we did not demonstrate that the Beer-Lambert law was followed for the gas absorption. It is likely that the data for water for $E < 19$ eV are influenced by a failure of the Beer-Lambert law caused by the rapid variation of σ. For example, if 30% of the light had $\sigma' = 1.06\ \sigma$, the reported σ value would be in error by $\approx$ 2%.

An additional possible source of error is absorption by impurities, and the sample purities are uncertain, except for the methane and neopentane, which were Phillips Petroleum Company research grade with stated purities of 99.99% and 99.88%, respectively, and for NH_3, which was from the Matheson Company with a stated purity of 99.99%. All samples were degassed by freeze-pump cycles at liquid nitrogen temperature.

Results and Discussion

In this section we present the spectra with only a minimum of discussion. Except for the energy region between 20.8 and 21.2 eV, the noise level is low for the helium lamp data. The spectra presented were taken at a single gas pressure, although σ values that are within 1% have been observed at another pressure of methane.

The differential oscillator strength, df/dE, is directly porportional to the absorption cross section, with $df/dE = 0.0091116\ \sigma$ when df/dE is in units of $(eV)^{-1}$ and σ is in Mb (1 Mb = 10^{-18} cm^2). In Figure 1 we show the df/dE data for water vapor measured using the helium lamp. This spectrum is similar to that given by Katayama, Huffman, and O'Bryan,[8] but detailed comparisons will be made at a later time.

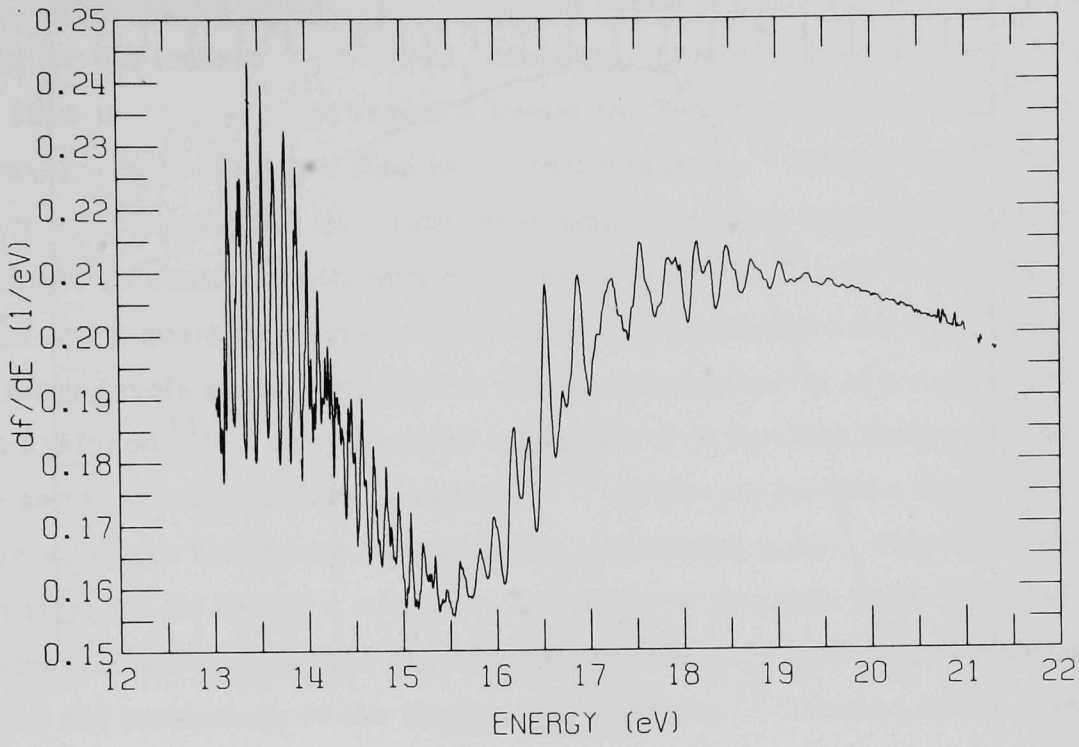

FIG. 1.--Differential oscillator-strength distribution for water vapor. The data for E < 15 to 19 eV may be influenced by a failure of the Beer-Lambert law.

Figure 2 shows the spectrum for ammonia obtained with the helium lamp. The low noise in this spectrum reveals a series of weak lines superimposed on the continuum in the 14- to 17-eV region, which was not reported by earlier workers, e.g., Watanabe and Snood.[9] As a further example, the spectrum of methane shown in Figure 3 shows a weak series of four or five lines, with spacings of ca. 0.27 eV, beginning at 19.84 eV. This feature is almost certainly the 3p Rydberg state of the series terminating at 22.4 eV.[10] This ionization potential corresponds to removal of an electron from the a_1 orbital, and the photoelectron spectrum[10] shows four or five lines spaced ca. 0.25 eV. The structure in the 13- to 15-eV region apparently corresponds to Rydberg levels converging on the upper vibronic levels (Jahn-Teller split) of the ionization of the t_2 electron (however, the small bump near 15.2 eV is not a reproducible feature).

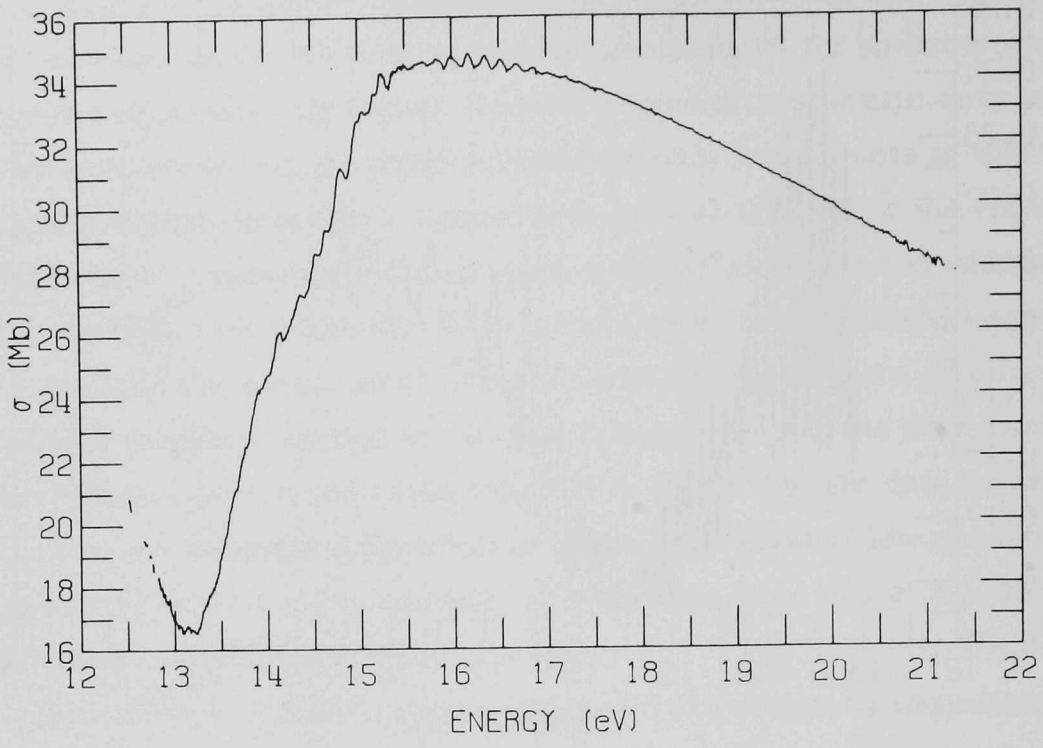

FIG. 2.--Absorption cross sections for ammonia (NH_3)

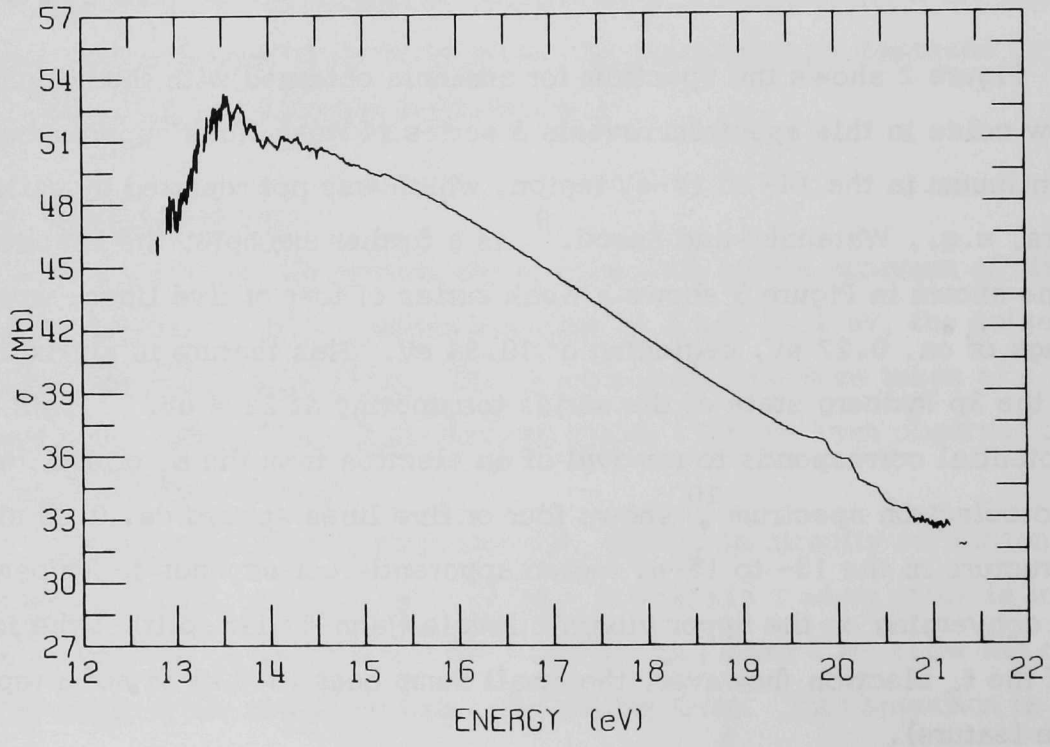

FIG. 3.--Absorption cross sections for methane (CH_4)

Neopentane (tetramethyl methane) shows a well-developed Rydberg series for the ionization of the $2a_1$ electron. Figure 4 shows the spectrum from 10.5 to 21.2 eV, and Figure 5 shows the Rydberg series in more detail. We resolve more structure than have other workers,[11] and we can observe the n = 3 to n = 9 levels that fit a Rydberg formula giving an ionization potential of 17.64 eV, in contrast with earlier values of 17.60 eV[12] and 17.68 eV.[11] This series has a quantum defect of 0.43, which is appropriate for a p series.[13] The lower levels show some five or six vibrational levels of a series that has been assigned[11,12] as the totally symmetric C-H bending mode ν_2, and we also see the weaker series assigned[11,12] as the combination band $\nu_2 + \nu_3$, where ν_3 is the totally symmetric C-CH_3 stretching mode. This combination band is sharp for the n = 4 members, but the n = 3 members show the band as shoulders. The line shapes are clearly asymmetric, but it will be difficult to extract the parameters of the Beutler-Fano profiles[14] because of the overlap of the various lines.

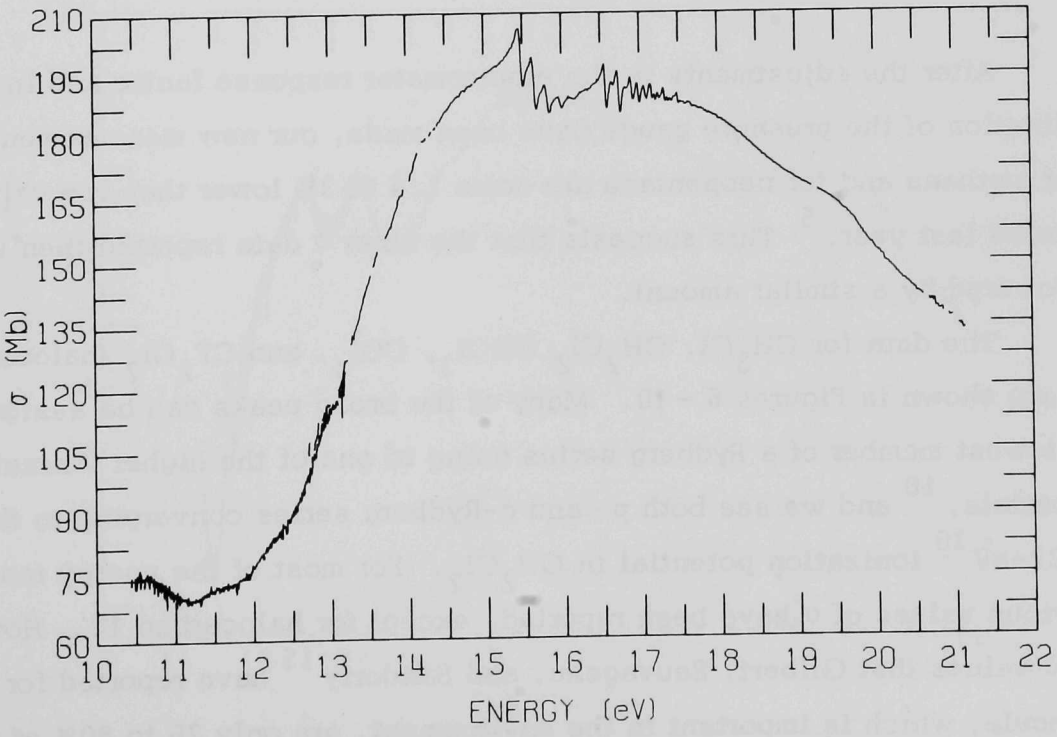

FIG. 4.--Absorption cross sections for neopentane [$C(CH_3)_4$]

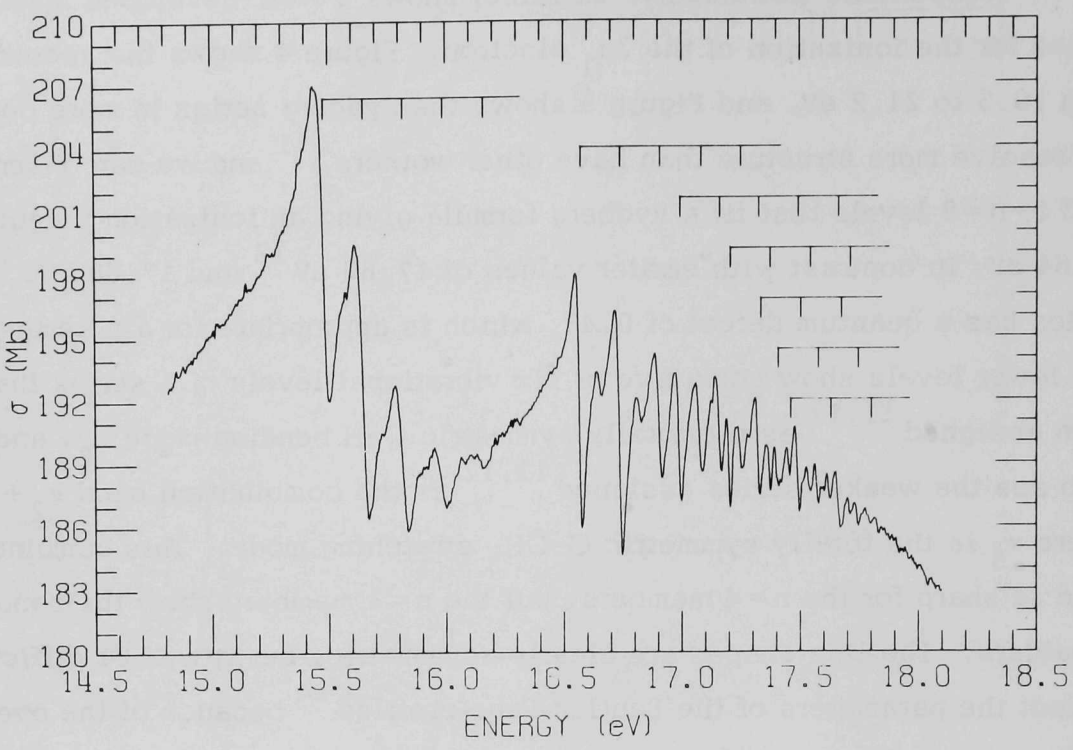

FIG. 5.--Rydberg series in neopentane. The vibrational levels of the ν_2 band of the n=3 (E=15.48 to 16.32 eV) to n=9 (E=17.46 to 17.97 eV) Rydberg states are indicated by the tick marks on the upper portion of the figure.

After the adjustments in the electrometer response factor and in the calibration of the pressure gauge have been made, our new measurements of σ for methane and for neopentane are some 1.4 to 3% lower than the values reported last year.[5] This suggests that the other σ data reported then should be lowered by a similar amount.

The data for CH_3Cl, CH_2Cl_2, $CHCl_3$, CCl_4, and CF_2Cl_2 (halocarbon 12) are shown in Figures 6 – 10. Many of the broad peaks can be assigned as the lowest member of a Rydberg series going to one of the higher ionization potentials,[10] and we see both p- and d-Rydberg series converging to the 12.22-eV[10] ionization potential in CH_2Cl_2. For most of the energy range, no previous values of σ have been reported, except for halocarbon 12. However, the σ values that Gilbert, Sauvageau, and Sandorfy[15] have reported for this molecule, which is important in the environment, are only 26 to 80% of the values we find.

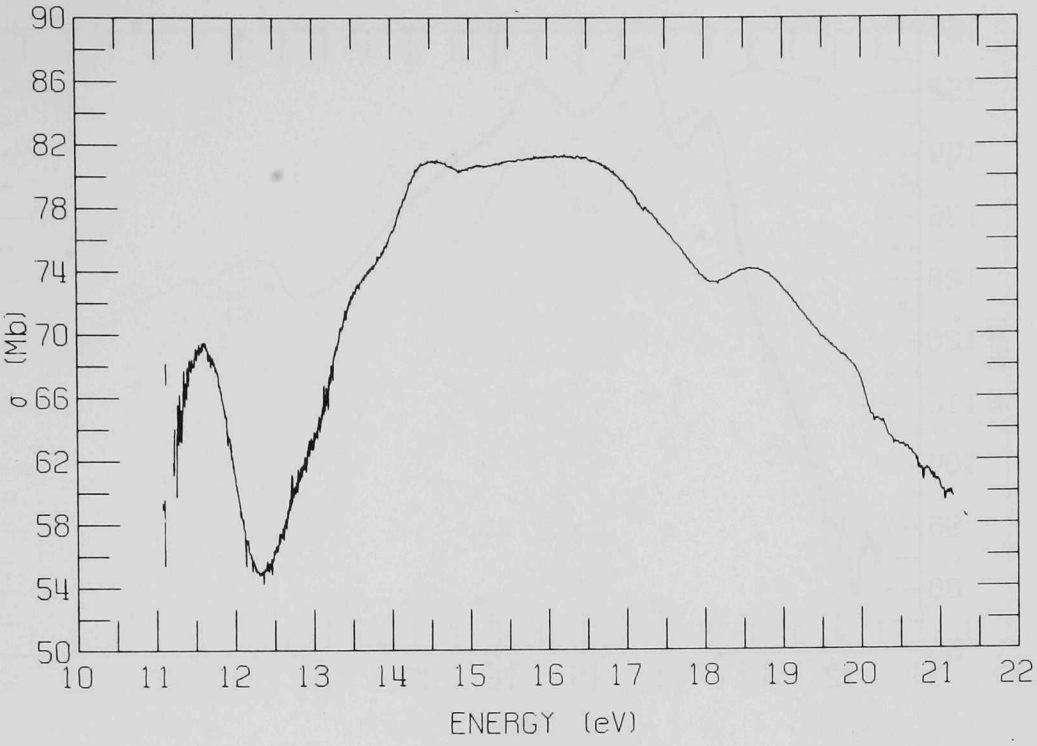

FIG. 6.--Absorption cross sections for methyl chloride (CH_3Cl)

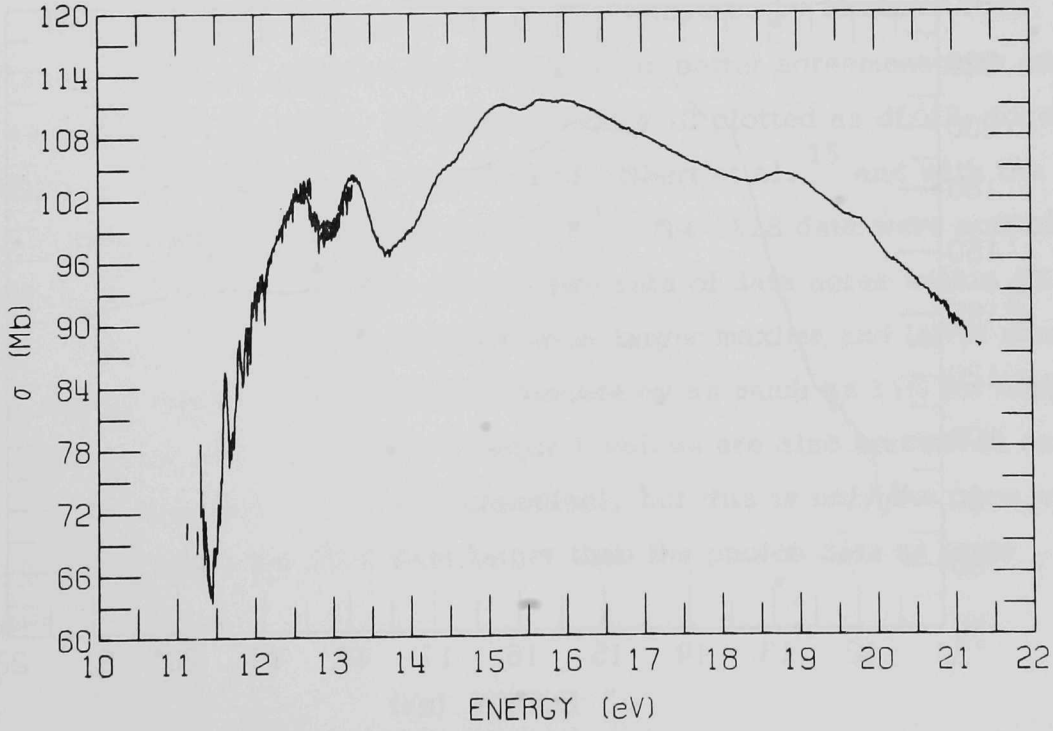

FIG. 7.--Absorption cross sections for dichloromethane (CH_2Cl_2)

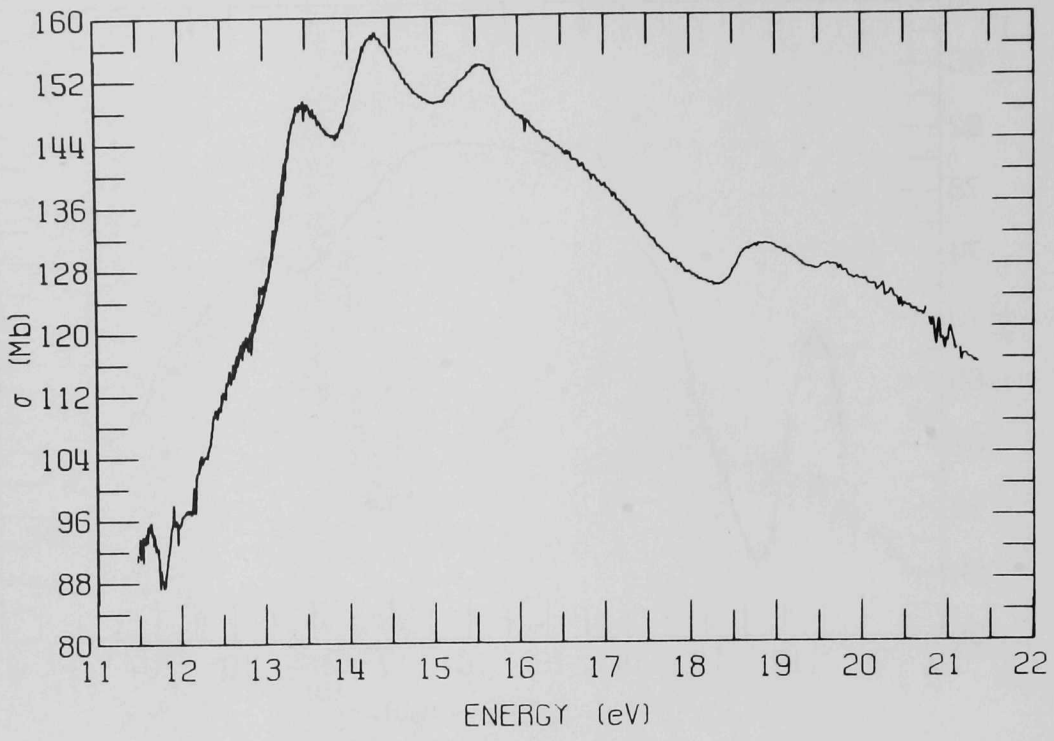

FIG. 8.--Absorption cross sections for chloroform ($CHCl_3$)

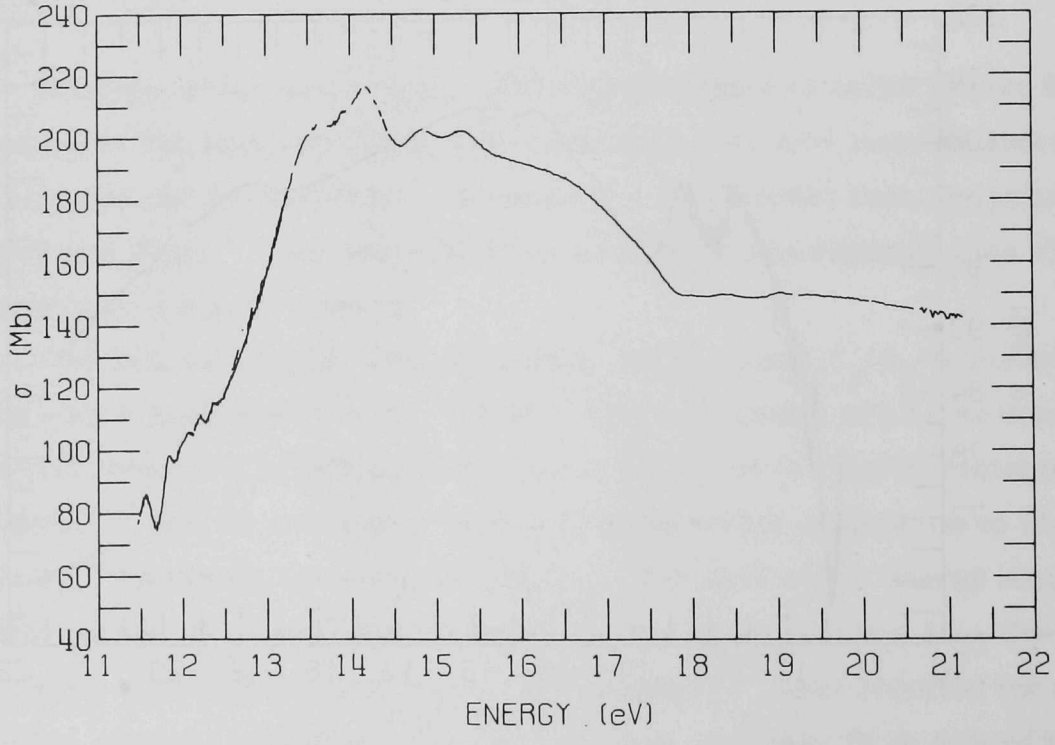

FIG. 9.--Absorption cross sections for carbon tetrachloride (CCl_4)

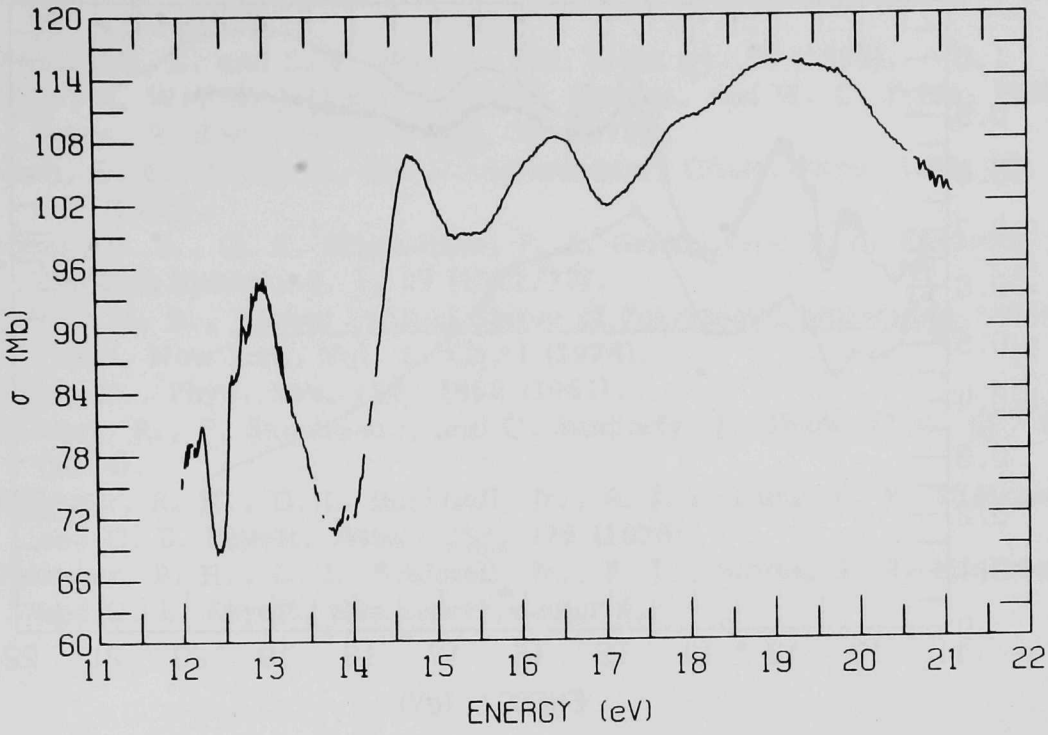

FIG. 10.--Absorption cross sections for halocarbon 12 (CF_2Cl_2)

The relative df/dE values for CF_2Cl_2 measured by Huebner et al.[16,17] using electron energy-loss spectroscopy (EELS) are in better agreement with our values, and Figure 11 shows the data of Figure 10 plotted as df/dE, together with representative points from the data of Gilbert et al.[15] and with the higher energy portion of the EELS data.[16,17] The EELS data were normalized to agree with ours at 12.22 eV, and the two sets of data agree within 4% for $12 < E < 14.4$ eV — although our data show larger maxima and lower minima in this energy region. The EELS data deviate by as much as 11% for higher energies ($E < 20$ eV). Deviation at large E values are also present in earlier comparisons (see Ref. 5 for some examples), but this is only the case where the deviations make the EELS data larger than the photon data at large energies.

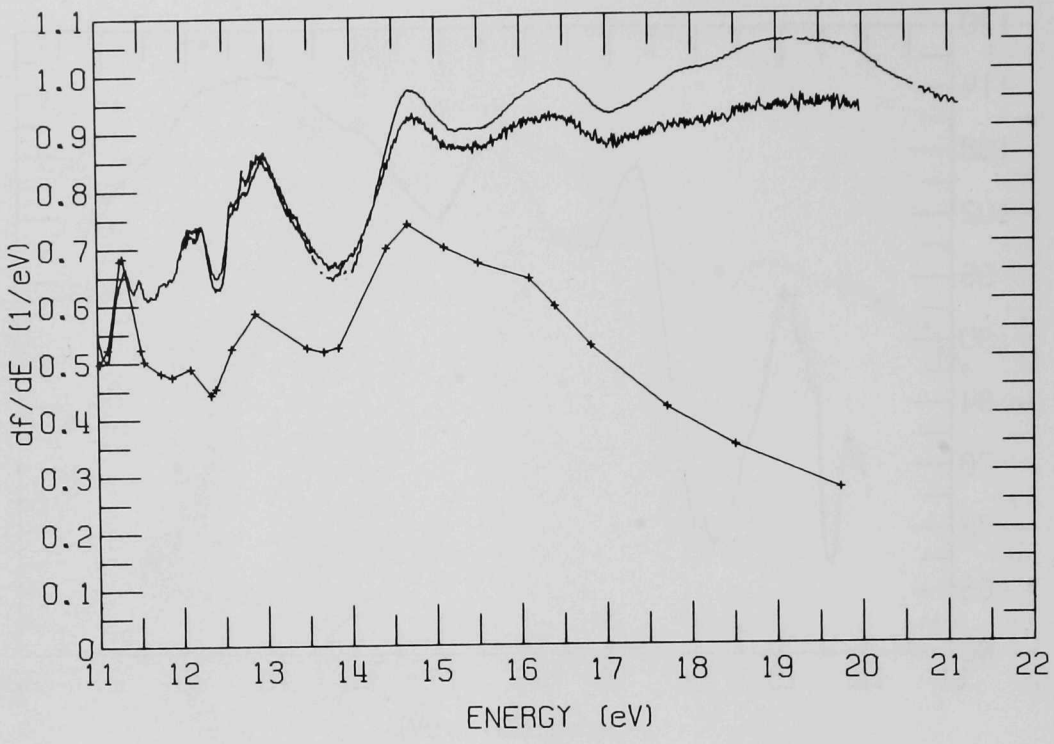

FIG. 11.--Differential oscillator-strength distribution for halocarbon 12 (CF_2Cl_2). The +'s connected by line segments are representative points from the photon data of Ref. 15. The EELS data of Refs. 16 and 17 go from 11 to 20 eV and our values go from 12 to 21.1 eV.

References

1. Samson, J. A. R., Techniques of Vacuum Ultraviolet Spectroscopy, John Wiley, New York, p. 267 (1967).
2. Fluorocarbons — Impact on Health and Environment, Hearings before the Sub-committee on Public Health and Environment of the Committee on Interstate and Foreign Commerce, House of Representatives, Ninety-Third Congress. Second Session on H.R. 17577 and H.R. 17545, Dec. 11 and 12, 1974, Ser. No. 93-110, U.S. Government Printing Office, Washington, D.C. (1975).
3. Person, J. C. and P. P. Nicole, Radiological and Environmental Research Division Annual Report, July 1971 —June 1972, ANL 7960, Part I, p. 76.
4. Person, J. C. and P. P. Nicole, Radiological and Environmental Research Division Annual Report, July 1972–June 1973, ANL-8060, Part I, p. 158.
5. Person, J. C. and P. P. Nicole, Radiological and Environmental Research Division Annual Report, July 1973–June 1974, ANL-75-3, Part I, pp. 53 and 63.
6. Thomas, A. M. and J. L. Cross, J. Vac. Sci. Technol. 4, 1 (1967).
7. Ruthberg, S., J. Vac. Sci. Technol. 6, 401 (1969).

8. Katayama, D. H., R. E. Huffman, and C. L. O'Bryan, J. Chem. Phys. 59, 4309 (1973).
9. Watanabe, K. and S. P. Snood. Sci. Light 14, 36 (1965).
10. Potts, A. W., H. J. Lempka, D. G. Streets, and W. C. Price, Philos. Trans. R. Soc. London A 268, 59 (1970).
11. Koch, E. E., V. Saile, and N. Schwentner, Chem. Phys. Lett. 33, 322 (1975).
12. Jonas, A. E., G. K. Schweitzer, F. A. Grimm, and T. A. Carlson, J. Electron Spectrosc. 1, 29 (1972/73).
13. Robin, M. B., Higher Excited States of Polyatomic Molecules, Academic Press, New York, Vol. 1, Ch. I (1974).
14. Fano, U., Phys. Rev. 124, 1866 (1961).
15. Gilbert, R., P. Sauvageau, and C. Sandorfy, J. Chem. Phys. 60, 4820 (1974).
16. Huebner, R. H., D. L. Bushnell, Jr., R. J. Celotta, S. R. Mielczarek, and C. E. Kuyatt, Nature 257, 376 (1975).
17. Huebner, R. H., D. L. Bushnell, Jr., R. J. Celotta, S. R. Mielczarek, and C. E. Kuyatt, this report, paper 4.

COLLISIONAL IONIZATION OF HIGHLY EXCITED POLYATOMIC MOLECULES*

James C. Person, R. L. Watkins,† and Dana Lee Howard‡

Most observations of collisional ionization of highly-excited Rydberg states have involved excited rare gas atoms,[1,2] and very large cross sections have been reported[1] for thermal collisions of the excited atoms with polyatomic molecules. When the molecule has a dipole moment, ionization via a rotational de-excitation of the molecule has been shown to be an important process.[3–5] Collisional ionization has also been observed for molecular Rydberg states (see Ref. 6 and the references therein), and we report further studies of the ionization of highly-excited polyatomic molecules by thermal collisions in pure gases or in mixtures with atomic gases.

The apparent ionization yield, $y(E,n)$, the probability that ionization is observed following absorption of a photon with energy, E, by a gas at a number density, n, is measured using monochromatic light (≈ 0.008 eV band width) in an apparatus previously described.[7]

Let y^* represent the quantum yield for producing the highly-excited states; these have a unimolecular decay (e.g., radiation or predissociation) rate constant of k_1, a bimolecular collisional ionization specific rate of k_2, and a bimolecular deactivation specific rate of k_3. Stated another way, we consider the overall collisional ionization rate constant to be the product of k_2 times the ionization yield for collisional ionization, $\eta_c \equiv k_2/(k_2+k_3)$.

In routine measurements[7,8] of the ionization yield, collisional ionization has been detected for eight different gases. For four of these gases, sufficient data were collected to determine the parameters listed in Table 1 to an

---

*Summary of a paper presented at the IXth Int. Conf. on Physics of Electronic and Atomic Collisions, Seattle, 24–30 July 1975. A full account of this work is being prepared for publication as a journal article.

†Undergraduate Research Participant from Fort Hays Kansas State College, Hays, Kansas 67602.

‡Undergraduate Research Participant from Wisconsin State University—Superior, Superior, Wisconsin 54881.

TABLE 1. Results for Collisional Ionization in Pure Gases

	I, eV	E, eV	$\eta_c y^*$	$k_2 y^*/k_1$ (10^{-18} cm^3)	$(k_2+k_3)/k_1$ (10^{-18} cm^3)
Acetone	9.705	9.69	0.066	2.5	38.
		9.68	0.09	1.3	14.
		9.66	0.07	0.2	3.
		9.65	0.03	0.15	5.
		9.64	0.01	0.07	7.
C_2H_4O	10.21	10.20	0.17	1.7	10.
		10.18	0.20	0.3	1.5
		10.15	0.02	0.04	2.
C_2D_4O	10.22	10.22	0.17	0.73	4.3
C_2D_4	10.53	10.56	0.019	0.13	7.
		10.54	0.014	0.24	17.
		10.52	0.024	0.14	6.
CH_3Br	10.53	10.52	0.26	8.1	31.
		10.50	0.39	0.74	1.9

accuracy of 10 to 30%. Gas mixtures of acetone with He, Ne, Ar, or N_2 and helium mixtures with CH_3Br and C_2H_4O indicates that the inert gases are less than 0.008 as efficient at producing ionization as are the polyatomics, and most ratios were measured in the range of 0.0006 to 0.003. Thus, the mixture results are consistent with the rotational de-excitation process being important, and the low value indicated for η_c for the case of C_2D_4, which has no dipole moment, also suggests the importance of this mechanism. Additional experiments are planned using SF_6 mixtures to study the energy dependence of collisional ionization for $E > I$, and to use the competition with collisional ionization by SF_6 to estimate the magnitude of k_2 for the organic molecules.[6]

References

1. Hotop, H. and A. Niehaus, J. Chem. Phys. 47, 2506 (1967).
2. Stockdale, J. A., F. J. Davis, R. N. Compton, and C. E. Klots, J. Chem. Phys. 60, 4279 (1974).
3. Matsuzawa, M., J. Electron Spectrosc. 4, 1 (1974).
4. Matsuzawa, M., Argonne National Laboratory Radiological and Environmental Research Division Annual Report, July 1973–June 1974, ANL-75-3, Part I, p. 105.
5. Chupka, W. A., Bull. Am. Phys. Soc. 19, 70 (1974).
6. Klots, C. E., J. Chem. Phys. 62, 741 (1975).
7. Person, J. C. and P. P. Nicole, J. Chem. Phys. 49, 5421 (1968).
8. Person, J. C. and P. P. Nicole, Argonne National Laboratory Radiological and Environmental Research Division Annual Report, July 1969–June 1970, ANL-7760, Part I, p. 97.

SHAPE RESONANCES IN K-SHELL PHOTOIONIZATION OF DIATOMIC MOLECULES*

J. L. Dehmer and Dan Dill†

Our recent calculations have shown that K-shell photoionization spectra of diatomic molecules can exhibit strong shape resonances near threshold. The molecular field is decisive in this phenomenon. It induces the resonant contraction of high-ℓ components of the ionization channels, and it couples these components with low-ℓ components produced in the atomic cores by K-shell photoionization. Clear evidence for this phenomenon exists for N_2, CO, and NO.

Figures 1–3 illustrate the essential features of this phenomenon for the case of N_2. Figure 1 shows the eigenphase sums for the allowed ionization channels for K-shell photoionization of N_2. The σ_u channel shows resonant behavior due to the contraction of the $\ell = 3$ component. Figure 2 shows the resulting shape resonance in the photoabsorption cross section. Figure 3 shows that this shape resonance causes the asymmetry parameter governing photoelectron angular distributions to oscillate.

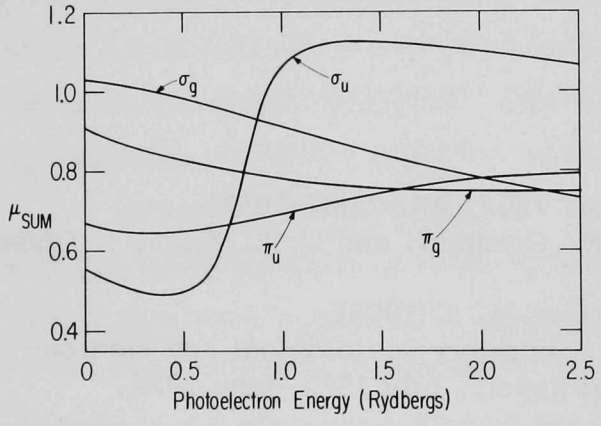

FIG. 1.--The eigenphase sum μ_{sum} for the even-ℓ and odd-ℓ components of the σ and π ionization channels of N_2.
(ANL Neg. 149-75-34)

*A report on this work has been published [Phys. Rev. Lett. 35, 213 (1975)].

†Alfred P. Sloan Foundation Fellow; also consultant, RER Division. Permanent address: Department of Chemistry, Boston University, Boston, Mass. 02215.

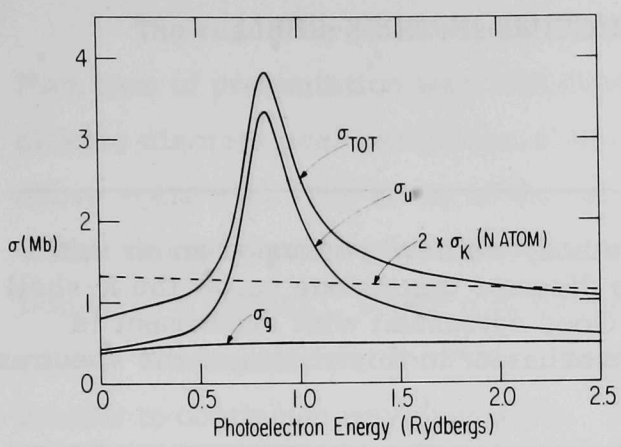

FIG. 2.--The K-shell photoionization cross section for N_2, showing breakdown into g and u components of the ionization channels. For comparison, the dashed line represents twice the K-shell photoionization cross section for atomic nitrogen.
(ANL Neg. 149-75-32)

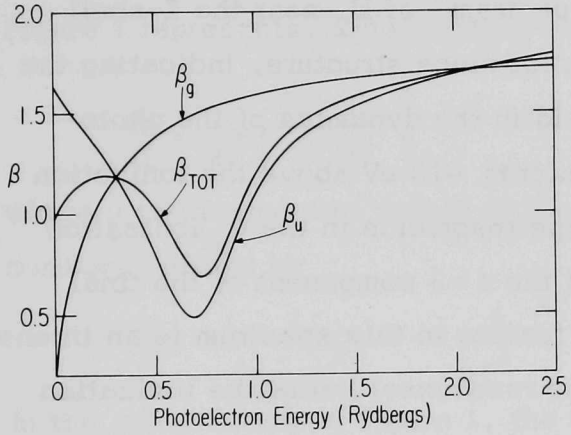

FIG. 3.--The asymmetry parameter, β_{tot}, for K-shell photoionization in N_2 and the asymmetry parameters for ionization into g and u components of the total ionization channels.
(ANL Neg. 149-75-33)

ANALYSIS OF THE AUTOIONIZATION STRUCTURE IN THE K-SHELL PHOTOIONIZATION SPECTRUM OF N_2

J. L. Dehmer and Dan Dill*

Using the multiple-scattering method, we have performed an ab initio calculation of the cross sections for the discrete transitions below the K-shell ionization threshold in N_2 (409.9 eV). Good agreement with experiment is achieved and the strongly nonhydrogenic behavior in this region of the spectrum is explained.

The "pseudo-photon" absorption spectrum[1] of N_2 near the K-shell threshold (409.9 eV) exhibits pronounced resonance structure, indicating the prominent role played by the molecular field in the dynamics of the photoionization process. The broad feature centered ~10 eV above the ionization limit has been shown[2] to arise from a shape resonance in the σ_u ionization channel due to the resonant contraction of the $\ell = 3$ component of the final state. However, by far the most striking feature in this spectrum is an intense peak ($\simeq$15 times stronger than the σ_u shape resonance) below the ionization threshold at ~401 eV.

In order to account for the extremely selective absorption in the discrete (autoionizing) part of this spectrum, we use the multiple-scattering method which was developed for discrete states by Johnson[3] and co-workers. Using this now standard technique, we calculated all dipole-allowed discrete σ_g, σ_u, π_g, and π_u states with binding energies greater than 0.02 Rydbergs. These states were all calculated in the field of the ground state charge distribution utilizing the Slater exchange approximation[4] with $\alpha = 1$ and the Latter cutoff[5] to achieve the proper asymptotic potential. Partial wave expansions on the atomic centers and the molecular centers were extended to $\ell = 5$ to achieve convergence to one part in a thousand in all quantities discussed.

*Consultant, RER Division, Argonne National Laboratory. Permanent address: Department of Chemistry, Boston University, Boston, Massachusetts 02215.

The resulting photoabsorption cross sections are shown in Figure 1. This type of presentation was introduced by Fano and Cooper[6] to permit displaying discrete peaks on an equal footing with the continuum (the solid lines above ~410 eV). The areas of the rectangles are proportional to the f-numbers of the discrete transition. The heights are proportional to the quantities $f(dn/dE)_n = (df/dE)_n$, where n is the principal quantum number of the excited state. This operation, in effect, renormalizes the final state per unit energy, similar to continuum wavefunctions. The differential oscillator strength is proportional to the photoabsorption cross section which the ordinate scale in Figure 1 represents. The quantity dn/dE is given by the expression

$$\frac{dn}{dE} = \frac{1}{2} n^{*3} + \frac{d\mu}{dE} ,$$

where μ is the quantum defect of the final state and n* is its effective quantum number, defined by

$$E_f = -\frac{1}{(n-\mu)^2} = -\frac{1}{n^{*2}} .$$

In the construction of Figure 1, the approximation

$$\frac{dn}{dE} \simeq \frac{1}{2} n^{*3}$$

was used with the restriction that dE/dn < 1 Ry. For all but the lowest one or two levels, this approximation is a good one; however, for the first one or two levels, the $d\mu/dE$ term is non-negligible. Unfortunately, in the absence of a continuous $\mu(E)$ function, $d\mu/dE$ is difficult to estimate in the lower part of the discrete spectrum where its effect is non-negligible. Therefore, since dE/dn represents the "width" of the rectangular peaks, the restriction dE/dn < 1 Ry imposes the observed width and gives a realistic representation of the experimental spectrum.

The experimental spectrum contains four main peaks between 400 eV and 410 eV. These lie at 401, 406, 407, and 408 eV with relative intensities 1:0.017:0.045:0.028. The theoretical spectrum contains three isolated peaks at 402.9, 406.6, and 407.5 eV, with final-state symmetries π_g, σ_g, and π_u (the photon energy has been derived from the computed binding energies of the

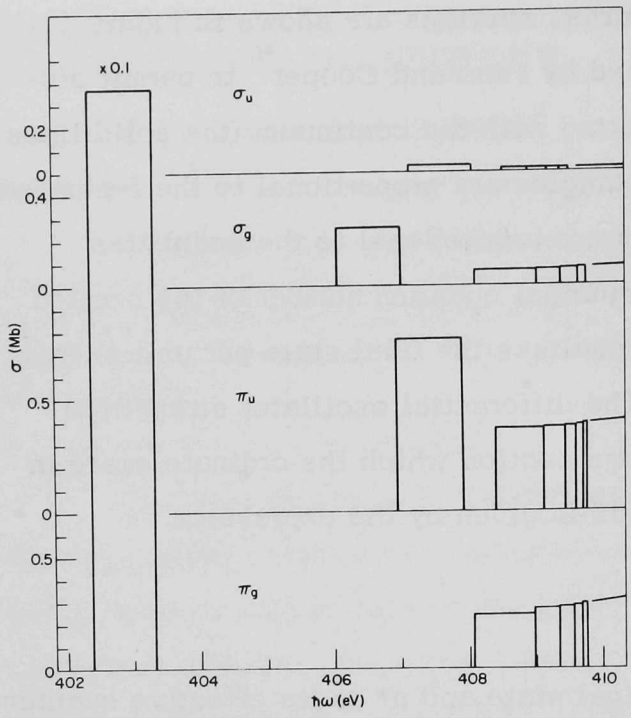

FIG. 1.--Histogram representation of the discrete part of the K-shell photoabsorption spectrum of N_2. (ANL Neg. 149-75-232)

states combined with the experimental ionization potential). The intensity ratios are 1:0.010:0.030, which is in qualitative agreement with experiment, and, of course, is subject to the somewhat arbitrary choice of dE/dn for the lowest level. The parameter dE/dn could be varied to produce agreement with experiment, but this would add nothing to the major observation, namely, that an extremely intense π_g peak dominates the discrete part of the spectrum. The feature at 408 eV derives from overlapping peaks in the two π channels. Note that in every channel the discrete and continuous part of the spectrum join at threshold, as required in an independent electron model.

The nature of the intense π_g peak is worthy of special comment since it relates to a well-known feature in $e-N_2$ scattering. At an incident electron kinetic energy of ~ 2.5 eV, the $e-N_2$ cross section in many observation channels[7] exhibits a strong shape resonance. The analysis[8,9] of this peak has shown it is produced when the incident electron enters a highly localized orbit of π_g symmetry. The localization of this orbit is attributed to the centrifugal barrier in the average potential of the $\ell = 2$ lead term of a spherical harmonic expansion of a π_g wavefunction. In photoionization of N_2, we deal with a closely related but more attractive $e-N_2^+$ potential. The net effect is that the π_g resonance moves to lower total energy and appears in the discrete part of the spectrum.

In summary, the K-shell photoabsorption spectrum of N_2 is dominated by two resonant features, one arising from the $\ell = 2$ component of the π_g channel

and one arising from the $\ell = 3$ component of the σ_u channel. By the time the total energy is high enough for the $\ell = 4$ component of the gerade channels to penetrate the molecular significantly, the circumstances necessary to produce resonant contraction no longer exist. The importance of resonant structure should be prominent in inner-shell spectra of most molecules, and can be successfully analyzed using the multiple-scattering method. At this time we do not have enough experience to predict precisely which high-ℓ components of which channels will be resonant, but hopefully some predictability will result from the study of several examples in the near future.

References

1. Wight, G. R., C. E. Brion, and M. H. van der Wiel, J. Electron Spectrosc. 1, 457 (1973).
2. Dehmer, J. L. and Dan Dill, Phys. Rev. Lett. 35, 213 (1975).
3. Johnson, K. H., Advances in Quantum Chemistry, P. O. Löwdin, Ed., Academic Press, New York, Vol. 7, p. 143 (1973).
4. Slater, J. C., Phys. Rev. 81, 385 (1951).
5. Latter, R., Phys. Rev. 99, 510 (1955).
6. Fano, U. and J. W. Cooper, Rev. Mod. Phys. 40, 441 (1968).
7. Schulz, G. J., Rev. Mod. Phys. 45, 378 (1973).
8. Krauss, M. and F. H. Mies, Phys. Rev. A 1, 1592 (1970).
9. Burke, P. G. and N. Chandra, J. Phys. B 5, 1696 (1972).

EXTENDED FINE STRUCTURE IN THE K-SHELL PHOTOIONIZATION SPECTRUM OF Br_2

Dan Dill* and J. L. Dehmer

The multiple-scattering approach to molecular wavefunctions in the electronic continuum[1] has been used recently to elucidate the structure of the shape resonance just above threshold in the K-shell photoionization spectrum of N_2.[2] A similar calculation for Br_2 has yielded significantly different results, i.e., there is no shape resonance; appearing instead is a single resonance in the discrete spectrum, and the photoionization spectrum is found to oscillate with appreciable amplitude throughout the spectral range investigated, from threshold to 60 Ry.

The calculation was carried out in the same manner as the N_2 calculation reported in Ref. 2. The multiple-scattering potential for the Br_2 ground state was obtained using Johnson's† bound-state multiple-scattering code modified to apply the Latter[4] cutoff condition to the large-r region of the potential. The statistical exchange parameter[5] was set at $\alpha = 1.0$. Convergence of the multiple-scattering expansion of the continuum wavefunction was determined by adjusting the maximum orbital angular momenta ℓ_I and ℓ_{III}, in region I and region III, respectively, until the eigenphase sum for each continuum channel converged to four significant figures. The values determined in this way for each energy range are given in Table 1.

In Figure 1 we plot the spectral variation of the eigenphase sums for the four continuum channels accessible from the K-shell, namely, σ_g, σ_u, π_g, and π_u. The overall rise of the π symmetry phaseshifts is to be contrasted with the overall flat but oscillatory structure of the σ symmetry phaseshifts. Each local enhancement of phase (in all four channels) is due to penetration

*Department of Chemistry, Boston University, Boston, Mass. 02215. Consultant, RER Division, ANL. Alfred P. Sloan Fellow.

†It is recommended that the reader consult Ref. 3 for a detailed account of the applications of the multiple-scattering method to the electronic structure of the molecules.

TABLE 1. Conditions Required for Numerical Convergence

Energy range, Ry	Maximum ℓ Region I	Region III
0 – 5	7	11
5 – 10	9	15
10 – 20	11	21
20 – 30	13	25
30 – 40	15	29
40 – 50	17	33
50 – 60	19	35

into the molecular core of a particular ℓ component of the continuum wavefunction. Even-ℓ components contribute to the g phaseshifts and odd-ℓ components contribute to the u phaseshifts. As a result, the oscillatory pattern alternates between the σ_g and π_g channels on the one hand and the σ_u and π_u channels on the other hand.

Each local enhancement in phaseshift results in a corresponding enhancement in the integrated cross section. This is seen most clearly in Figure 2 where the resultant cross sections due to even-ℓ and odd-ℓ are plotted separately. In Figure 3 the (observable) sum of these cross sections is plotted, together with twice the atomic K-shell photoionization cross section, computed in the Hartree-Slater model.[6] Near threshold the molecular cross

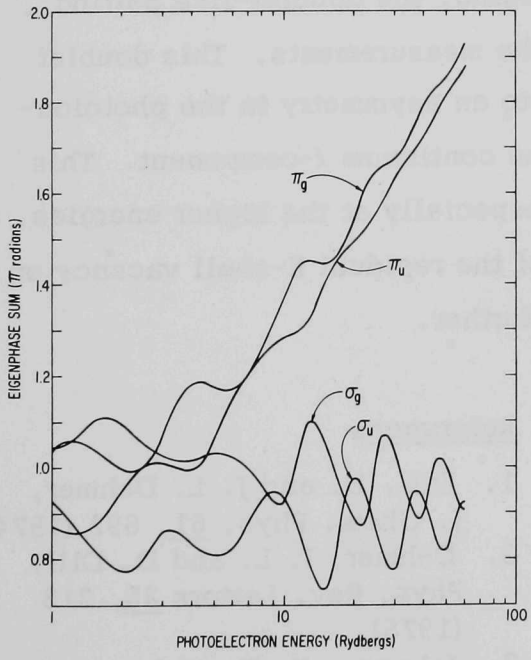

FIG. 1.--Eigenphase sums for the allowed ionization channels in K-shell photoionization of Br_2.

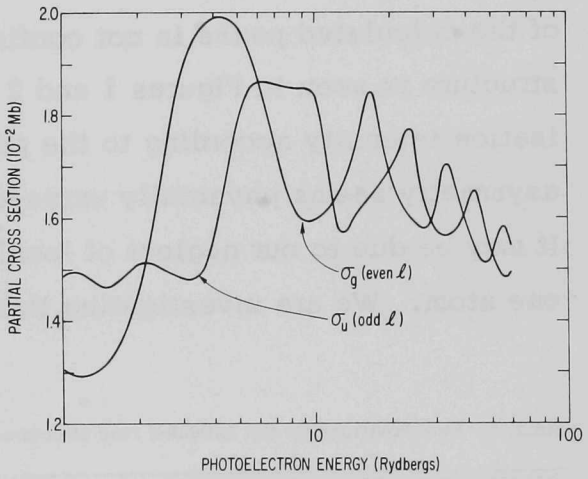

FIG. 2.--Decomposition of the theoretical K-shell photoabsorption cross section for Br_2 into partial cross sections corresponding to even-ℓ and odd-ℓ components of the final state wavefunction.

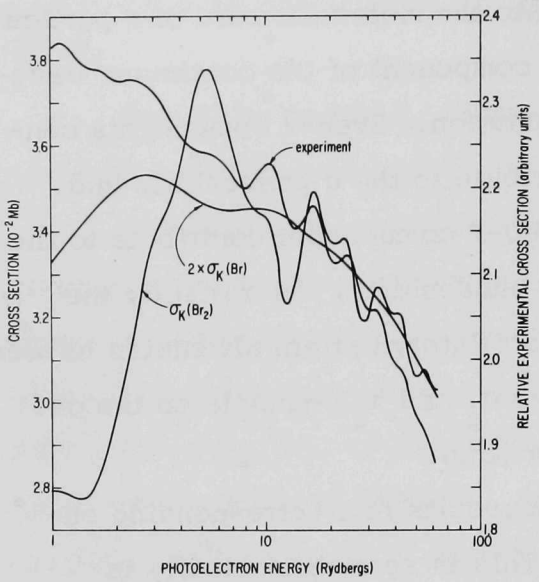

FIG. 3.--Comparison of theoretical K-shell photoabsorption cross sections of Br_2 and Br with experimental results for Br_2 (Ref. 7).

section is depressed relative to the reference atomic cross section. This reflects the concentration of oscillator strength below threshold brought on by the enhanced binding properties of the molecular field.[2] However, the molecular cross section rises rapidly to a broad maximum at 5 Ry, and thereafter it oscillates about the atomic cross section with an amplitude of 2 to 3%.

These oscillations are seen in the recent experimental work of Kincaid and Eisenberger.[7] Their relative cross section results are plotted in Figure 3. This permits a comparison of calculated and observed peak positions, given in Table 2 (the peak numbers are arbitrary). While agreement in peak positions is encouraging, the doublet-like pairing of the calculated peaks is not confirmed by the measurements. This doublet structure is seen in Figures 1 and 2 to trace to an asymmetry in the photoionization intensity according to the parity of the continuum ℓ-component. This asymmetry seems physically unreasonable, especially at the higher energies. It may be due to our neglect of localization of the residual K-shell vacancy on one atom. We are investigating this aspect further.

TABLE 2. Peak Positions for the Extended Fine Structure in Br_2

Peak number	Peak position, Ry Calculated	Observed	% difference
1	5.3	5.8	8.6
2	10.0	10.8	7.4
3	16.8	16.6	1.2
4	23.0	24.0	4.2
5	33.2	32.0	3.8
6	41.5	42.5	2.4
7	55.0	55.0	—

References

1. Dill, D. and J. L. Dehmer, J. Chem. Phys. 61, 692 (1974).
2. Dehmer, J. L. and D. Dill, Phys. Rev. Letters 35, 213 (1975).
3. Johnson, K. H., Advances in Quantum Chemistry, P.-O. Lowdin, Ed., Academic Press, New York, Vol. 7, p. 143 (1973).

4. Latter, R., Phys. Rev. 99, 510 (1955).
5. Slater, J. C., Phys. Rev. 81, 385 (1951).
6. Herman, F. and S. Skillman, Atomic Structure Calculations, Prentice-Hall, New Jersey (1963).
7. Kincaid, B. M. and P. Eisenberger, Phys. Rev. Letters 34, 1361 (1975).

CONTINUUM AND BOUND ELECTRONIC WAVEFUNCTIONS FOR ANISOTROPIC MULTIPLE-SCATTERING POTENTIALS

Jon Siegel,* Dan Dill,*† and J. L. Dehmer

Standard multiple-scattering treatments of bound and continuum one-electron states are restricted to a monopole potential in each of the various spherical regions. We have extended the treatment within these regions to a general potential. The corresponding multiple-scattering equations should facilitate accurate treatment of effects of the build-up of charge due to bonding, of the dipole character of polar molecules, and of external fields.

Introduction

Multiple-scattering treatments of bound [1] and continuum [2] wavefunctions have yielded results in good agreement with experiment.[1,3] However, a shortcoming of these treatments is their restriction of the potentials in the atomic spheres (region I) and asymptotic region (region III) to spherical symmetry. This restriction hampers accurate treatment of effects of the build-up of charge density due to bonding, of the dipole character of polar molecules, and of external fields. To study these effects we derive here the multiple-scattering equations for arbitrary (local) potentials in regions I and III.

Below we obtain the set of coupled Schroedinger equations for an electron in an arbitrary potential. Then, in the following section these equations are adapted to the specific spatial and spectral regions. In the next section solutions of these equations are matched at the region boundaries and appropriate multiple-scattering equations are derived. We conclude with a brief discussion of some applications in progress. Throughout we will use the notation and terminology of Ref. 2.

One-Electron Schreodinger Equations for a General Potential

The wavefunction $F(k,\vec{r})$ for an electron in an arbitrary potential $V(\vec{r})$ can be expressed as an expansion in spherical harmonics,

*Department of Chemistry, Boston University, Boston, Mass. 02215.

†Alfred P. Sloan Research Fellow; Consultant, RER Division

$$F(k,\vec{r}) = \sum_L f_L(kr)\, Y_L(\hat{r}) \ , \tag{1}$$

where we use the notation $\vec{r} = (r,\theta,\phi)$, $\hat{r} = (\theta,\phi)$, $L = (\ell,m)$. Energies k^2 are measured in rydbergs and lengths, r, are measured in bohrs. The radial functions, f(kr), are determined by solving the Schroedinger equation,

$$\sum_L \left[-\frac{1}{r}\frac{d^2}{dr^2} r + \frac{\ell(\ell+1)}{r^2} + V(\vec{r}) - k^2 \right] f_L(kr) Y_L(\hat{r}) = 0 \ . \tag{2}$$

Substituting the multipole expansion

$$V(\vec{r}) = \sum_{L''} V_{L''}(r)\, Y_{L''}(\hat{r}) \ , \tag{3}$$

left-multiplying by $Y_{L'}(\hat{r})^*$, and integrating over $\hat{r}$, we generate the set of coupled radial equations

$$\left\{ -\frac{1}{r}\frac{d^2}{dr^2} r + \frac{\ell(\ell+1)}{r^2} + \left[V_0(r) + V_{LL}(r) \right] - k^2 \right\} f_L(r)$$

$$= - \sum_{\substack{L(\neq L') \\ L'(>0)}} V_{LL'}(r)\, f_{L'}(r) \ . \tag{4}$$

The matrix elements $V_{LL'}(r)$ are[4]

$$V_{LL'}(r) = \sum_{L''=1}^{\infty} V_{L''}(r) \int_0^{\pi}\int_0^{2\pi} \sin\theta d\theta d\phi\, Y_L(\hat{r})^* Y_{L''}(\hat{r})\, Y_{L'}(\hat{r})$$

$$= \sum_{L''=1}^{\infty} V_{L''}(r)\, (-)^{-m} (4\pi)^{-1} \left[(2\ell+1)(2\ell''+1)(2\ell'+1) \right]^{\frac{1}{2}}$$

$$\times \begin{pmatrix} \ell & \ell'' & \ell' \\ -m & m'' & m' \end{pmatrix} \begin{pmatrix} \ell & \ell'' & \ell' \\ 0 & 0 & 0 \end{pmatrix} \ ; \tag{5}$$

note that $V_{LL}(r) = 0$ if $L = (0,0)$.

In practice one truncates the infinite set of Eqs. 4 and the infinite series in Eqs. 4 and 5 as dictated by a physical situation of interest. Designating as ℓ_{max} the highest value of ℓ kept in the expansions, one has

$(\ell_{max} + 1)^2$ coupled Eqs. 4, if ℓ ranges from 0 to ℓ_{max} and m ranges from $-\ell$ to $+\ell$.

Coupled Equations in the Spherical Regions

The coupled Schroedinger Eqs. 4 and their solutions, Eq. 1, are adapted to the particular regions of the multiple-scattering potential by insertion of the expansion of the potential and by imposition of the boundary conditions at the origin of the atomic spheres and at large distance in region III. The forms of the solutions (Eq. 1) are chosen to satisfy these boundary conditions as follows. Solutions in regions I are chosen to be regular at the center of the regions. Continuum solutions in region III are chosen to include components with both sine and cosine asymptotic forms, to allow imposition of K-matrix boundary conditions. Finally, discrete solutions in region III are chosen with decreasing exponentials, to ensure a bounded wavefunction.

Atomic Regions I

The wavefunction in the atomic region I_i is expanded as

$$\Psi_i = \sum_L A_L^{I_i} F_L^{I_i}(k, \vec{r}_i) \ . \tag{6}$$

The expansion coefficients $A_L^{I_i}$ are determined by imposing continuity of the wavefunction and its derivative across the region I_i–region II boundary. The basis functions are given by

$$F_L^{I_i}(k, \vec{r}_i) = \sum_{L'} f_{LL'}^{I_i}(kr_i) Y_{L'}(\hat{r}_i), \tag{7}$$

where the radial functions are the solutions to Eqs. 4 having first derivatives at the origin given by

$$d/dr_i \left[f_{LL'}^{I_i}(kr_i)\right]\Big|_{r_i \to 0} = \delta_{LL'} \ . \tag{8}$$

Combining Eqs. 6 and 7 we obtain

$$\Psi_i = \sum_{L'} \left[\sum_L A_L^{I_i} f_{LL'}^{I_i}(kr_i)\right] Y_{L'}(\hat{r}_i) \ . \tag{9}$$

Region III, Continuous Spectrum

The wavefunction in region III for positive energies is expanded as

$$\Psi_{III} = \sum_L \left[A_L^{III} F_L^{III}(k, \vec{r}_0) + B_L^{III} G_L^{III}(k, \vec{r}_0) \right] \quad . \tag{10}$$

The expansion coefficients A_L^{III} and B_L^{III} are determined by imposing continuity of the wavefunction and its derivative across the regionII-region III boundary and by imposition of K-matrix boundary conditions at large r_0. The basis functions are given by

$$F_L^{III}(k, \vec{r}_0) = \sum_{L'} f_{LL'}^{III}(kr_0) Y_{L'}(\hat{r}_0) \quad , \tag{11a}$$

$$G_L^{III}(k, \vec{r}_0) = \sum_{L'} g_{LL'}^{III}(kr_0) Y_{L'}(\hat{r}) \quad , \tag{11b}$$

where the radial functions are the solutions to Eqs. 4 having the asymptotic forms

$$\lim_{r_0 \to \infty} f_{LL'}^{III}(kr_0) = \delta_{LL'}(kr_0)^{-1} \sin(kr_0 - \tfrac{1}{2}\ell\pi + \omega) \quad , \tag{12a}$$

$$\lim_{r_0 \to \infty} g_{LL'}^{III}(kr_0) = -\delta_{LL'}(kr_0)^{-1} \cos(kr_0 - \tfrac{1}{2}\ell\pi + \omega) \; ; \tag{12b}$$

ω is the Coulomb phase

$$\omega = -(z/k)\ln(2kr) + \arg \Gamma[\ell + 1 - i(z/k)] \tag{13}$$

for interaction of an electron with an ion of charge z. Note that $\omega = 0$ for electron-neutral molecules ($z = 0$) interactions. Combining Eqs. 10 and 11, we obtain

$$\Psi_{III}(k, \vec{r}_0) = \sum_{L'} \left\{ \sum_L \left[A_L^{III} f_{LL'}^{III}(kr_0) + B_L^{III} g_{LL'}^{LLL}(kr_0) \right] \right\} Y_{L'}(\hat{r}_0) \quad . \tag{14}$$

Region III, Discrete Spectrum

The wavefunction in region III for negative energies is expanded as

$$\Psi_{III}(k, \vec{r}_0) = \sum_L C_L^{III} S_L^{III}(k, \vec{r}_0) \quad . \tag{15}$$

The expansion coefficients C_L^{III} are determined by imposing the continuity of

the wavefunction and of its derivative across the region II-region III boundary. The basis functions are given by

$$S_L^{III}(k, \vec{r}_0) = \sum_{L'} s_{LL'}^{III}(kr_0)\, Y_{L'}(\hat{r}_0) \ , \tag{16}$$

where the radial functions are the solutions to Eqs. 4 having the asymptotic form

$$\lim_{r_0 \to \infty} s_{LL'}^{III}(kr_0) = \delta_{LL'}\, y(kr) \ , \tag{17}$$

where y(kr) vanishes exponentially for large r. Combining Eqs. 15 and 16 we obtain

$$\Psi_{III}(k, \vec{r}_0) = \sum_{L'} \left[\sum_L C_L^{III}\, s_{LL'}^{III}(kr_0) \right] Y_{L'}(\hat{r}_0) \ . \tag{18}$$

Generating the Radial Functions

It is convenient to define the integer

$$N_j \equiv (\ell_{max,j} + 1)^2 \ , \tag{19}$$

where $\ell_{max,j}$ is the largest value of ℓ occurring in region I_j or (for $j = 0$) region III expansions. Assuming for purposes of discussion that m ranges from $-\ell$ to $+\ell$ the required number of solutions to Eqs. 4 is N_i in region I_j, $2N_0$ in region III for positive energies, and N_0 in region III for negative energies. Each member of these sets of solutions is generated by numerical integration of the corresponding N_j coupled equations, with starting conditions given by Eqs. 8, 12, or 17, respectively. The integration is outward for the atomic region I_j and inward for region III. A recent survey of integration methods is given by Allison.[5] Simplification can be achieved by factorization of the full system of equations into uncoupled subsets of equations characterized by the irreducible representations of the molecular point group.

Multiple-Scattering Equations

To match the wavefunction at the various spherical boundaries, we use the following expansions (Eqs. 13 and 15 of Ref. 2) for the wavefunction in region II, with respect to the center of region I_j and the center of the molecule, respectively:

$$\Psi_{II}(k,\vec{r}_j) = \sum_L \left\{ {}^{II_j}B_L \, n_\ell(\kappa r_j) + j_\ell \kappa r_j) \right.$$

$$\left. \times \sum_{L'} \left[{}^{II_0}A_{L'} \, J^{0j}_{L'L} + \sum_i (1-\delta_{ij}) \, {}^{II_i}B_{L'} \, N^{ij}_{L'L} \right] \right\} Y_L(\hat{r}_j) \, , \qquad (20)$$

$$\Psi_{II}(k,\vec{r}_0) = \sum_L \left[{}^{II_0}A_L \, j_\ell(\kappa r_0) \right.$$

$$\left. + \sum_i \sum_{L'} {}^{II_i}B_{L'} \, J^{i0}_{L'L} \, n_\ell(\kappa r_0) \right] Y_L(\hat{r}_0) \, . \qquad (21)$$

The constant potential V_{II} in region II determines κ through $\kappa = (k^2 - V_{II})^{\frac{1}{2}}$. The regular and irregular Bessel functions $j_\ell(\kappa r_0)$ and $n_\ell(\kappa r_0)$, and the structure factors $J^{ij}_{L'L}$ and $N^{ij}_{L'L}$ are defined in Ref. 2.

Region I_i – Region II Matching

Matching the region-I_i wavefunction (Eq. 9) with the region-II wavefunction (Eq. 20) at the surface of region I_i ($r_i = \rho_i$, the radius of the region), and a similar matching of the derivative of these functions gives

$$\sum_L \left\{ {}^{I_i}A_L \, {}^{I_i}f_{LL'}(k\rho_i) - j_{\ell'}(\kappa\rho_i) \left[{}^{II_0}A_L \, J^{0i}_{LL'} \right.\right.$$

$$\left.\left. + \sum_j (1-\delta_{ij}) \, {}^{II_j}B_L \, N^{ji}_{LL'} \right] \right\} = {}^{II_i}B_{L'} \, n_{\ell'}(\kappa\rho_i) \qquad (22)$$

and the equation obtained by the substitutions

$$\left[{}^{I_i}f_{LL'}(k\rho_i), \, n_{\ell'}(\kappa\rho_i), \, j_{\ell'}(\kappa\rho_i) \right]$$

$$\rightarrow \left[{}^{I_i}f'_{LL'}(k\rho_i), \, n'_{\ell'}(\kappa\rho_i), \, j'_{\ell'}(\kappa\rho_i) \right] \, , \qquad (23)$$

where we denote by primes derivatives taken with respect to r_i. The sum over L in Eq. 22 and its counterpart obtained by the substitution in Eq. 23 are in principle infinite. However, they are truncated in practice according to the physical situation being considered. In general, however, convergence in the

different regions I will require different numbers of terms. Thus, all $A_L^{I_i}$ and $B_L^{II_i}$ are set to zero for $L > (\ell_{i,max}, m_{i,max})$ and all $A_L^{II_0}$ are set to zero for $L > (\ell_{0,max}, m_{0,max})$ where the maximum values are chosen to ensure convergence in each region.

Region II-Region III Matching, Continuous Spectrum

In a similar way, the region-II wavefunction (Eq. 21) and the region-III continuum wavefunction (Eq. 14) are matched at $r_0 = \rho_0$, the region-III radius, to give

$$\sum_L \left[A_L^{III} f_{LL'}^{III}(k\rho_0) + B_L^{III} g_{LL'}^{III}(k\rho_0) - \sum_i B_L^{II_i} J_{LL'}^{i0} n_{\ell'}(\kappa\rho_0) \right] = A_{L'}^{II_0} j_{\ell'}(\kappa\rho_0) \tag{24}$$

and the equation obtained by the substitutions

$$\left[f_{LL'}^{III}(k\rho_0),\ g_{LL'}^{III}(\kappa\rho_0),\ n_{\ell'}(\kappa\rho_0),\ j_{\ell'}(\kappa\rho_0) \right] \rightarrow \left[f'^{III}_{LL'}(k\rho_0),\ g'^{III}_{LL'}(\kappa\rho_0),\ n'_{\ell'}(\kappa\rho_0),\ j'_{\ell'}(\kappa\rho_0) \right], \tag{25}$$

where here primes denote differentiation with respect to r_0. The coefficients A_L^{III} and B_L^{III} must be set to zero if $L > (\ell_{0,max}, m_{0,max})$.

The wavefunction $\Psi_{III}(\vec{r}_0)$ must satisfy K-matrix normalization at large r_0. Owing to Eqs. 12 the asymptotic form of the wavefunction (Eq. 10) in the coupled formulation is the same as for the uncoupled formulation of Ref. 2. Accordingly, K-matrix normalization is imposed by[2]

$$A_{L'}^{III} = \delta_{LL'} (k/\pi)^{\frac{1}{2}} , \tag{26}$$

$$B_{L'}^{III} = - (k/\pi)^{\frac{1}{2}} K_{LL'} . \tag{27}$$

With these two relations, Eqs. 22 and 24 and their counterparts obtained by the substitution (Eqs. 23 and 25) from a well-determined linear inhomogeneous system for the expansion coefficients of the wavefunction throughout the

multiple-scattering regions. Successive solutions of the linear system, with L varying from (0,0) to $(\ell_{0,max}, m_{0,max})$, yields, row by row, the entire K matrix.

Region II-Region III Matching, Discrete Spectrum

Matching of the region-II wavefunction (Eq. 21) and the region-III discrete wavefunctions (Eq. 18) at $r_0 = \rho_0$ gives

$$\sum_L \left[C_L^{III} s_{LL'}^{III}(k\rho_0) - \sum_i B_L^{II_i} J_{LL'}^{i0} n_{\ell'}(\kappa\rho_0) \right] = A_{L'}^{II_0} j_{\ell'}(\kappa\rho_0) \qquad (28)$$

and the equation obtained by the substitutions

$$\left[s_{LL'}^{III}(k\rho_0),\ n_{\ell'}(\kappa\rho_0),\ j_{\ell'}(\kappa\rho_0) \right] \rightarrow \left[s'^{III}_{LL'}(k\rho_0),\ n'_{\ell'}(\kappa\rho_0),\ j'_{\ell'}(\kappa\rho_0) \right] . \qquad (29)$$

The expansion in region III, Eq. 15, is truncated at $L = (\ell_{0,max}, m_{0,max})$.

Equations 22 and 28 and their counterparts obtained by the substitutions (Eqs. 23 and 29) form a well-determined linear homogeneous system for the wavefunction expansion coefficients. The discrete eigenvalues $|k_i|$ are determined as those values of $|k|$ for which the determinant of this linear system vanishes.

Limit of Isotropic Potentials

In the limit of isotropic potentials (Eq. 3 restricted to monopole terms), Eq. 4 reduces to the set of Schroedinger equations for the uncoupled formulation, Eq. 3 of Ref. 2. Accordingly, all of the radial functions are everywhere zero unless $L = L'$, and the multiple-sdattering equations reduce to those of Ref. 2.

Discussion

Anisotropy in the multiple-scattering potentials may be due to a number of factors. Besides intrinsic anisotropies of the molecular charge

density due to bonding and polar character, additional anisotropies can arise through exchange and polarization potentials, or through external fields, e.g., due to a surface on which the molecule is absorbed. The only restriction on these potentials is that they be expressed in terms of the multipole expansions (Eq. 3) about the center of each multiple-scattering region. Any re-expansions about different centers that may be required can be carried out using standard formulas.*

In conclusion, we have extended the multiple-scattering treatment of bound and continuum wavefunctions to include arbitrary potentials in the spherical regions, without unduly sacrificing the computational simplicity of the method. The resulting modifications in the multiple-scattering equations can be readily incorporated into existing computer codes and permit the direct investigation of potential anisotropies on electronic wavefunctions. Implementation of these equations is in progress.

References

1. Johnson, K. H., Scattered-Wave Theory of the Chemical Bond, Advances in Quantum Chemistry, P.-O. Löwdin, Ed., Academic Press, New York, Vol. 7, p. 143 (1973).
2. Dill, D. and J. L. Dehmer, J. Chem. Phys. 61, 692 (1974).
3. Dehmer, J. L. and D. Dill, Phys. Rev. Lett. 35, 213 (1975).
4. Rotenberg, M., R. Bivins, N. Metropolis, and J. K. Wooten, Jr., The 3-j and 6-j Symbols, Technology Press, MIT, Cambridge, Mass. (1959).
5. Allison, A. C., J. Comp. Phys. 6, 378 (1970).
6. Steinborn, E. O. and K. Ruedenberg, Rotation and Translation of Solid Spherical Harmonics, Advances in Quantum Chemistry, P.-O. Löwdin, Ed., Academic Press, New York, Vol. 7, p. 1 (1973).

*See, for example, Ref. 6.

WAVELENGTH DEPENDENCE OF THE PHOTOELECTRON ANGULAR DISTRIBUTIONS OF THE RARE GASES*

J. L. Dehmer, W. A. Chupka,†‡ J. Berkowitz,‡ and W. T. Jivery‡

Photoelectron angular distributions for the valence p shells of the rare gases have been measured up to a photon energy of 40.8 eV (48.4 eV for Ne) by use of resonance radiation from a hollow-cathode discharge lamp. The apparatus is shown in Figure 1. This work extends the range of existing absolute measurements on Ne, Kr, and Xe. Comparison with Hartree-Fock and RPAE (random-phase approximation with exchange) calculations indicates excellent agreement for Ne, as shown in Figure 2. However, the present results, particularly for Xe (Figure 3), add to earlier evidence that data for Ar, Kr, and Xe show systematic deviations from theory, especially in the higher photoelectron kinetic energies. For Kr and Xe, we have measured asymmetry parameters, β, separately for processes leading to the $^2P_{\frac{3}{2}}$ and $^2P_{\frac{1}{2}}$ spin-orbit states of the residual ion. The Xe results indicate that $\beta_{\frac{3}{2}} - \beta_{\frac{1}{2}}$ is positive for $\lambda \geq 461$ Å but changes sign in the range $\lambda \sim 350$ to 400 Å. At 304 Å, $\beta_{\frac{3}{2}} - \beta_{\frac{1}{2}} = -0.30$, which agrees with a recent calculation based on the Dirac-Slater model.

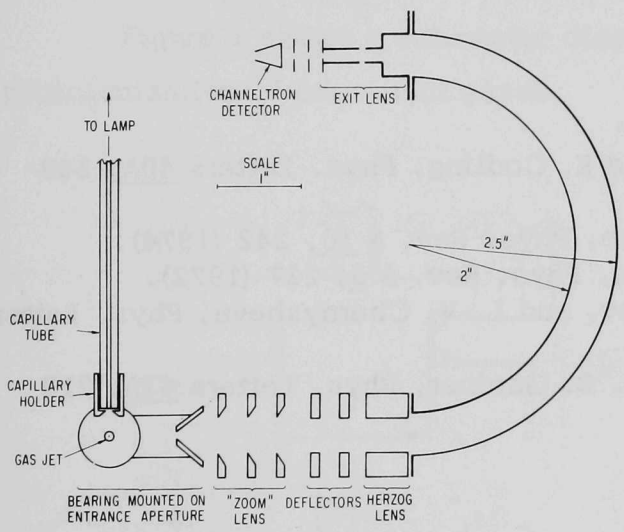

FIG. 1.--Schematic diagram of the experimental apparatus.

*A full report was published in Phys. Rev. A 12, 1966 (1975), and was also presented at the IXth International Conference on the Physics of Electronic and Atomic Collisions, Seattle, Washington, 24–30 July 1975.

†Present address: Dept. of Chemistry, Yale University, New Haven, Conn. 06520.

‡Physics Division, Argonne National Laboratory.

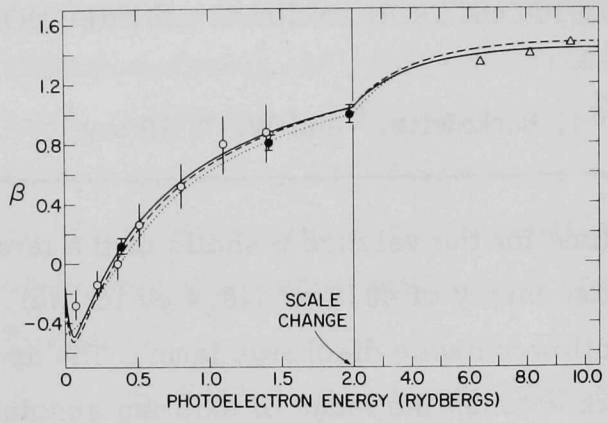

FIG. 2.--Energy dependence for β for the 2p subshell of Ne: ●, present work; O, Lynch et al., Ref. 1; △, Wuilleumier and Krause, Ref. 2; ——, HF-L, Ref. 3; ---, HF-V, Ref. 3; ..., RPAE, Ref. 4.

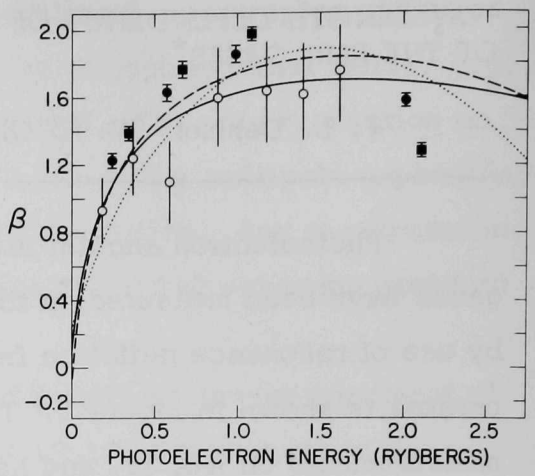

FIG. 3.--Energy dependence of β for the 5p subshell of Xe; ●, $^2P_{\frac{1}{2}}$, present work; ■, $^2P_{\frac{3}{2}}$, present work; O, Lynch et al., Ref. 5; —, HF-L, Ref. 3; ---, HF-V, Ref. 3; ..., RPAE, Ref. 4.

References

1. Lynch, M. J., A. B. Gardner, and K. Codling, Phys. Letters 40A, 349 (1972).
2. Wuilleumier, F. and M. O. Krause, Phys. Rev. A 10, 242 (1974).
3. Kennedy, D. J. and S. T. Manson, Phys. Rev. A 5, 227 (1972).
4. Amusia, M. Ya., N. A. Cherepkov, and L. V. Chernysheva, Phys. Letters 40A, 15 (1972).
5. Lynch, M. J., K. Codling, and A. B. Gardner, Phys. Letters 43A, 213 (1973).

AN ELECTRON SPECTROMETER FOR MEASUREMENT OF THE ENERGY DISTRIBUTIONS AND ANGULAR DISTRIBUTIONS OF ELECTRONS EJECTED BY IONIZING RADIATION

J. L. Dehmer

Ionizing collisions of all kinds result in ejected electrons which carry with them information about the energy and angular momentum of the other collision products, as well as information about the dynamics of the ionization process. Consequently, electron spectrometry is a very flexible tool which can be applied to many diverse problems, e.g., photoionization, electron scattering, heavy-ion-induced ionization, Penning ionization, chemi-ionization, and Auger effect. With a broad range of applications in mind, a new electron spectrometer has been constructed which is flange mountable, has an easily accessible source region, is rotatable over the range $25° \leq \theta \leq 335°$, and has a wide dynamical range and a wide range of resolving power.

Figure 1 shows a schematic diagram of the apparatus, set up to observe photoionization of permanent gases.

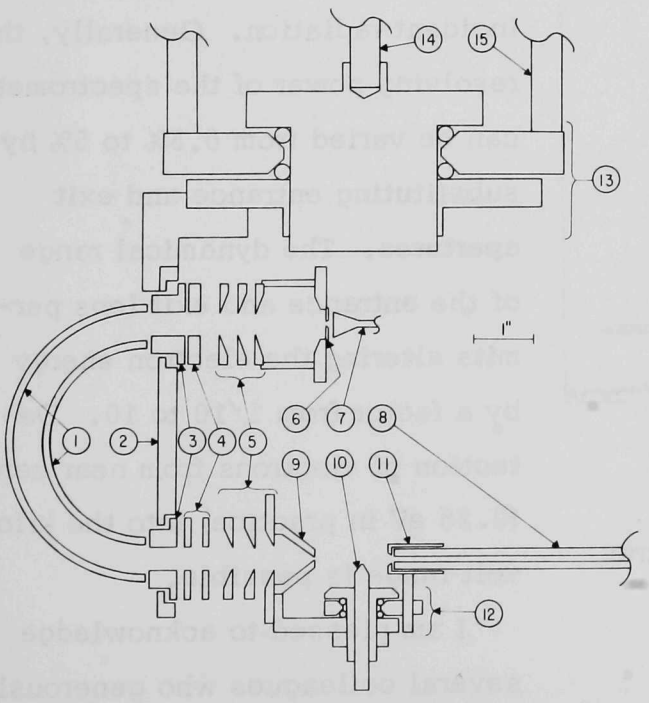

FIG. 1.--Schematic diagram of the rotatable hemispherical electron spectrometer. 1, inner and outer hemispheres; 2, main mounting plate; 3, Herzog lens; 4, deflector plates; 5, three-aperture lens operated as a "zoom lens;" 6, exit aperture; 7, channeltron multiplier; 8, capillary tubing used to channel the photons from the light source into the collision zone; 9, entrance aperture; 10, gas inlet; 11, capillary-tube holder; 12, sapphire-ball bearing to permit the analyzer to rotate around the collision zone while the capillary tube remains stationary; 13, main bearing upon which the analyzer rotates; 14, drive shaft coupled to drive train outside the vacuum chamber; 15, standoffs used to mount the entire assembly on a 10-in. O.D. conflat flange. (ANL Neg. 149-75-231)

The fabrication of the hemispheres calls for special mention. Normally, hemispheres are machined from solid blocks of metal. For this analyzer, hemispheres were hydroformed from 0.125-in copper plate. After minor touching up on a lathe, the finished product was lightweight and accurate to ± 0.001 in. This procedure is not only less expensive, but also permits making duplicate sets of hemispheres at negligible costs. The light weight makes precision alignment and movement of the resulting assembly easier.

The final assembly was aligned to ensure the top of the gas inlet tube was at the center of rotation to within 0.002 in. The analyzer was placed in a vacuum chamber lined with two layers of high permeability shielding, resulting in a residual magnetic field of < 0.001 G. The performance of the analyzer in its high resolution mode (0.020-in apertures and 0.75-eV analysis energy) is shown in Figure 2, where a portion of the Ar spectrum resulting from NeI excitation is shown. Under these conditions the theoretical resolution is ~0.004 eV. The observation of 0.006-eV resolution indicates a 0.0045-eV residual width due to doppler broadening and to the energy width of the incident radiation. Generally, the resolving power of the spectrometer can be varied from 0.5% to 5% by substituting entrance and exit apertures. The dynamical range of the entrance and exit lens permits altering the electron energy by a factor from 1/10 to 10. Detection of electrons from near zero (0.25 eV in practice) into the kilovolt range is possible.

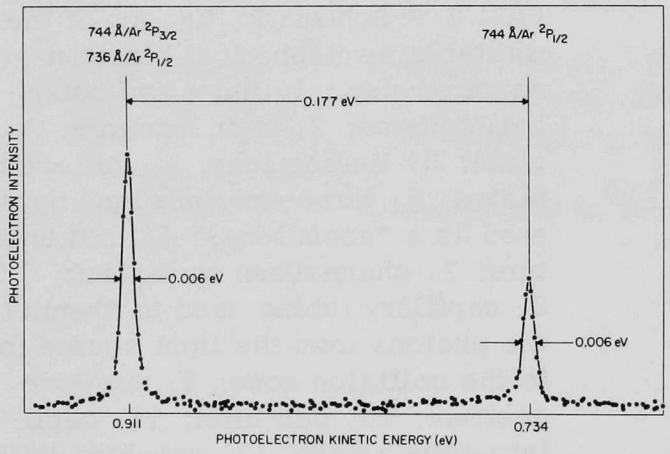

FIG. 2.--A portion of the photoelectron spectrum resulting from NeI (744 Å, 736 Å) photoionization of Ar. (ANL Neg. 149-75-230)

I am pleased to acknowledge several colleagues who generously contributed significant suggestions during the development of this device. They include B. Martinka and several machinists in the Building 203 section

of the ANL Central Shops, W. T. Jivery, W. A. Chupka, D. Spence, and P. M. Dehmer.

References

1. Herzog, R., Z. Phys. 97, 596 (1935).
2. Read, F. H., J. Sci. Instrum. 3, 127 (1970).

CROSS SECTIONS AND THRESHOLD EFFECTS FOR ELECTRON-IMPACT EXCITATION OF THE $(2s^2)^1S$ AND $(2s2p)^3P$ STATES OF HELIUM*

David Spence

The energy and intensity of scattered electrons resulting from excitation of the $(2s^2)^1S$ and $(2s2p)^3P$ autoionizing states of helium have been measured as a function of incident electron energy. For incident energies only slightly higher than the threshold for $(2s^2)^1S$ excitation, postcollision interactions between the scattered and ejected electrons cause the slowly moving scattered electron to lose an amount of energy proportional to $E_{ex}^{-1.25\pm0.05}$ (where E_{ex} is the energy the scattered electron would have had in the absence of a postcollision interaction). The energy dependence, shown in Figure 1, compares well with an energy gain of the ejected electron proportional to $E_{ex}^{-1,2}$, obtained by previous workers.[1] Measurements of the intensity of scattered electrons show that both ^1S and ^3P total cross sections peak at threshold, as shown in Figure 2, and have magnitudes about 2.0 and 4.0×10^{-20} cm^2, respectively, then rise to broad maxima of magnitudes about 2.5 and 5×10^{-20} cm^2 about 4.0 eV above their thresholds. A subsidiary peak at 59.0 eV in the ^3P cross section is attributed to decay of the previously unidentified $(2s2p^2)^2S$ He^- state[2] into the $^3P_3$ channel. The magnitude, energy, and width of this resonant structure in the ^3P channel agree with theoretical predictions.[3]

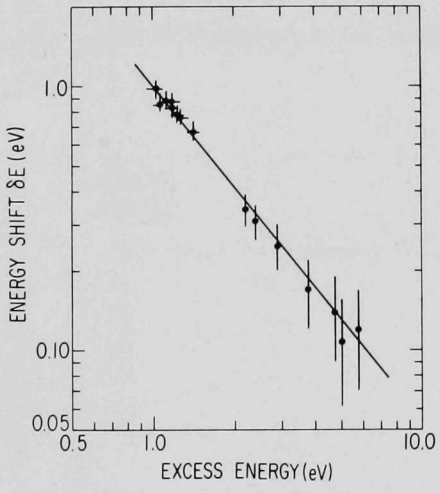

FIG. 1.--Log-log plot of the energy shift δE of the $(2s^2)^1S$ state of He as a function of excess energy E_{ex} obtained from measurements of the scattered electron energy. The slope, -1.25, compares with the value -1.2 obtained by Smith et al.[1] from ejected electron spectra.

*Summary of a paper published in Phys. Rev. A 12, 2353 (Dec 1975).

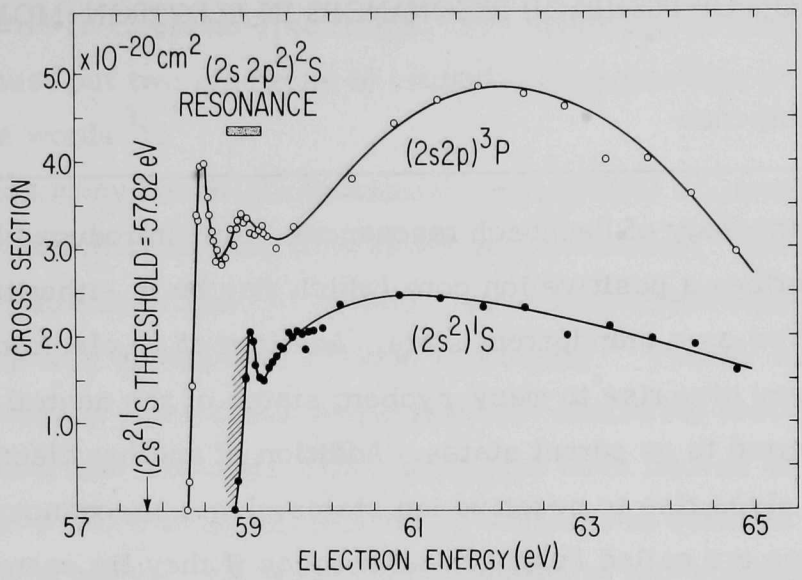

FIG. 2.--Total cross sections for electron impact excitation of the $(2s^2)^1S$ and $(2s2p)^3P$ states of He. The cross-hatch below the apparent $(2s^2)^1S$ threshold indicates that we cannot measure this cross section below 58.8 eV from measurements of the scattered electron (as the incident electron never emerges from the intermediate complex), and not that the $(2s^2)^1S$ excitation cross section is zero between 57.82 and 58.8 eV. The sharp rise at threshold of both cross sections is probably due to the $(2s^22p)^2P$ and $(2s2p^2)^2D$ He^- states which occur just below the inelastic thresholds. The "hump" at 59.0 eV in the $(2s2p)^3P$ state is interpreted as decay of the broad $(2s2p^2)^2S$ resonance into the ^3P channel.

References

1. Smith, A. J., P. J. Hicks, F. H. Read, S. Cvejanovic, G. C. M. King, J. Comer, and J. M. Sharp, J. Phys. B 7, L469 (1974).
2. Fano, U. and J. W. Cooper, Phys. Rev. 138, A400 (1965).
3. Ormande, S., F. Kets, and H. G. M. Heideman, Phys. Lett. 50a, 147 (1974).

CLASSIFICATION OF FESHBACH RESONANCES IN ELECTRON-MOLECULE SCATTERING

David Spence

The genealogy of Feshbach resonances, first introduced by Sanche and Schulz,[1] describes a positive ion core (which may be in either its ground or an excited state) as a grandparent state. Addition of an electron to the grandparent state may give rise to many rydberg states of the neutral molecule which are referred to as parent states. Addition of another electron to the parent states gives rise to negative ion states, i.e., resonances. Such negative ion states are called Feshbach resonances if they lie energetically below the parent excited states.

Feshbach resonances are a general phenomenon which, nevertheless, form a subclass of the broader problem of understanding the dynamics of two excited electrons moving in the field of a positive ion core, i.e., electron correlation effects in Coulomb-like fields. Related phenomena in this broader category in which electron correlation effects play a dominant role (and are thus difficult to handle theoretically) include threshold electron excitation and ionization,[2,3] and doubly-excited states.[4,5]

For Feshbach resonances in molecules, the problem is further complicated since the ion core is aspherical in shape and has internal structure (rotation, vibration, and perhaps electronic excitation).

Despite all these complications, however, spectra of Feshbach resonances are often strikingly simple, permitting straightforward analysis and configuration assignment. Further, despite the large number of all conceivable resonance configurations, the number of strong resonance features observed in electron-molecule scattering is fairly small, a situation which must imply stability rules (some of which are known) for pairs of electrons in

---

*Excerpt from a progress report presented at the Ninth Int. Conf. on the Physics of Electronic and Atomic Collisions, Seattle, July 1975. A full text will appear in Invited Papers and Progress Reports, Ed. J. S. Risley and R. Geballe (to be published by the University of Washington Press).

excited orbitals in Coulomb-like fields. For instance, to get a quasi-bound state, one must put two electrons in orbitals of similar size ("dynamic screening" in Rau's words [3]).

Though many bands of resonances and isolated resonances have been located by electron scattering from atoms and molecules,[6] the assignment of electron configurations has, in general, required detailed angular distribution measurements of resonant electron scattering.[6] Though such measurements will produce great detail of the resonant scattering processes, they are time-consuming and difficult. There have also been limited attempts to determine resonance electron configurations by comparison between resonance spectra and the spectra of neutral excited states in iso-electronic atoms and molecules.[7]

Studies of Feshbach resonances in electronically similar molecules and comparisons between recent experimental and theoretical results for resonant electron-atom scattering make it possible to derive certain systematics which often allow a simple determination of resonance configurations by a comparison between resonance spectra and known rydberg-state spectra. These systematics are important in the following respects.

(i) Determination of resonance grandparent states and the systematics of the binding energies of pairs of rydberg electrons in diatomic molecules;

(ii) The binding energies of electrons with various values of n and ℓ to parent rydberg states;

(iii) Application of guidelines provided by the above systematics to new systems.

References

1. Sanche, L. and G. J. Schulz, Phys. Rev. A 6, 69 (1972).
2. Wannier, G. H, Phys. Rev. 90, 817 (1953).
3. Rau, A. R. P., Phys. Rev. A 4, 207 (1971).
4. Madden, R. P. and K. Codling, Astrophys. J. 141, 364 (1965).
5. Fano, U., Atomic Physics, B. Bederson, V. W. Cohen, and F. M. J. Pichanek, Eds., Plenum Press, New York, p. 209 (1964).
6. Schulz, G. J., Rev. Mod. Phys. 45, 378 (1973).
7. Swanson, N., J. W. Cooper, and C. E. Kuyatt, Phys. Rev. A 8, 1825 (1973).

ADDITIONAL RESONANCES IN ELECTRON SCATTERING BY ATOMIC OXYGEN*

David Spence

Four new resonances, located at 10.73, 12.55, 14.40, and 15.65 eV are observed in electron scattering by atomic oxygen. Two of these resonances, located at 10.73 and 15.65 eV, have been predicted theoretically[1] to occur at 10.63 ($(^4S)3p^2\ ^6P$) and 15.75 eV ($(^2P)3p^2\ ^4D$), respectively. We attribute the two other resonances at 12.55 eV and 14.40 eV, to the configurations $(^2D)3s3p$ and $(^2P)3s3p$. With the addition of these new identifications, a total of ten resonances is now known to occur in atomic oxygen,[2,3] completing the triad of resonance configurations, $3s^2$, 3s3p, and $3p^2$, associated with each of the three lowest (^4S, ^2D, ^2P) positive ion states shown in Figure 1.

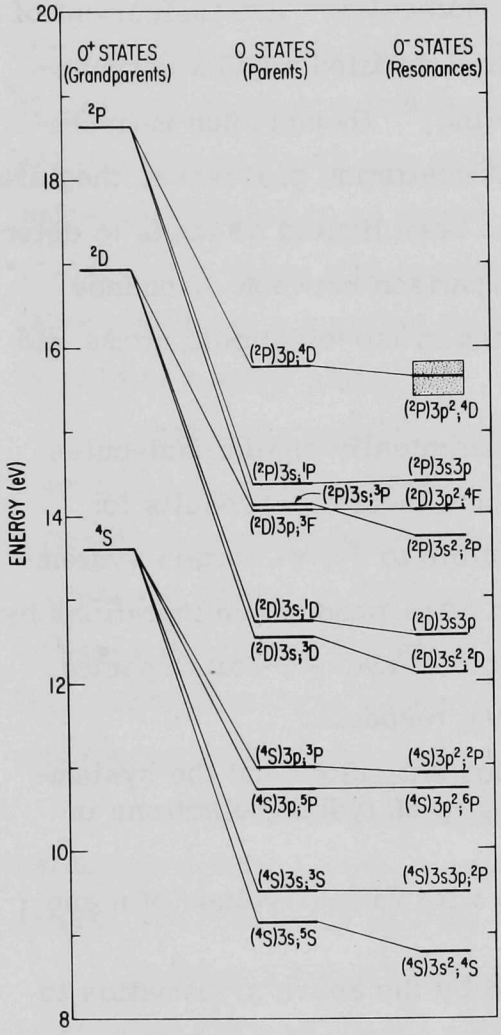

FIG. 1.--Energy level diagram of O^- states, together with their respective parent (O) states and grandparent (O^+) states. A triad of resonance configurations, $3s^2$, 3s3p, and $3p^2$, is associated with each of the ^4S, ^2D, and ^2P states. (ANL Neg. 149-6635

References

1. Matese, J. J., Phys. Rev. A 10, 1454 (1975).
2. Edwards, A. K. and D. C. Cunningham, Phys. Rev. A 8, 168 (1973).
3. Spence, D. and W. A. Chupka, Phys. Rev. A 10, 71 (1974).

*Summary of a paper published in Phys. Rev. A 12, 721 (1975).

FESHBACH RESONANCES ASSOCIATED WITH RYDBERG STATES OF THE HYDROGEN HALIDES*

David Spence and Tetsushi Noguchi †

Using an electron-transmission spectrometer, we locate Feshbach resonances, which consist of two rydberg electrons bound to a positive ion core, in the hydrogen halides HF, HCl, HBr, and HI. An example of these resonance spectra, that for HBr, is illustrated in Figure 1. Resonances in HCl, HBr, and HI are analogous to those previously observed in the isoelectronic rare gases Ar, Kr, and Xe, [1] an example of which (Kr) is shown in Figure 2. By dividing the resonances in Figure 2 into two series, each associated with a particular component of the ion core spin-orbit splitting, we plot the ladder of neutral and resonance states of Kr (Figure 3). The resonance electron configurations of Figure 3 are deduced from the requirements of minimized mutual screening of the ion core by the pair of rydberg electrons. Resonance configurations determined from rare-gas spectra are transferred to the analogous spectra for HCl, HBr, and HI, leading to resonance configurations of the type shown in Figure 4, which illustrates HBr as an example.

We find that most of the observed resonances whose grandparent positive-ion states have term value $X^2\Pi$, are associated with rydberg parent states of symmetry $(X^2\Pi)ns\sigma$, $(X^2\Pi)np\sigma$, and $(X^2\Pi)nd\lambda$. In HF, only one resonance series, associated with the $(X^2\Pi)3s\sigma\,^{1,3}\Pi$ rydberg state is observed.

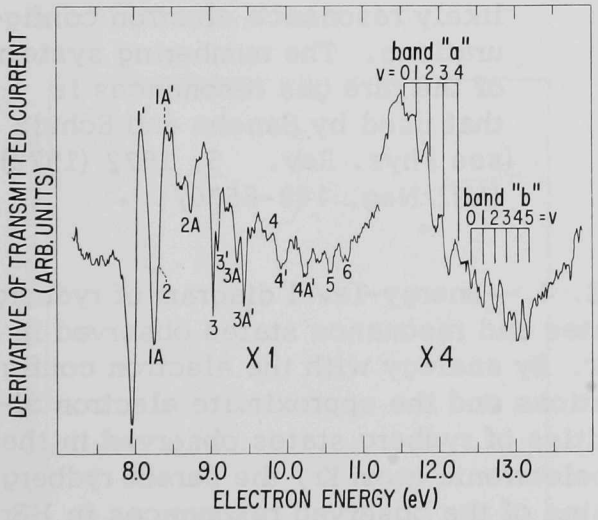

FIG. 1.--Derivative of the transmitted current vs. electron energy in HBr. Structures marked 1 to 6 derive from the addition of pairs of rydberg electrons to the $X^2\Pi_{\frac{3}{2}}$ and $^2\Pi_{\frac{1}{2}}$ positive ion cores. The separation of features marked n(1 to 4) - n(1 to 4)A is equal to the spin-orbit splitting of the ion core. Band "a" derives from the addition of a pair of $5s\sigma$ electrons to the $^2\Sigma^+$ positive ion core. (ANL Neg. 149-6541 R1).

*Summary of a paper published in J. Chem. Phys. 63, 505 (1975).

†Undergraduate Thesis student, Dept. of Physics, Kalamazoo College, Kalamazoo, Mich., 49001. Present address: Dept. of Physics, University of Chicago, Chicago, Ill., 60637.

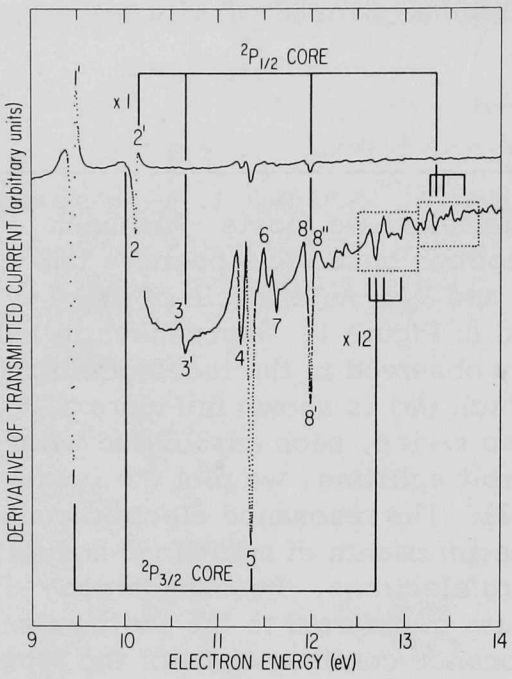

FIG. 2.--Krypton resonance spectrum of Sanche and Schulz [1] showing how we separate the resonance features into two sets, each associated with the appropriate $X^2P_{\frac{3}{2},\frac{1}{2}}$ ion core. For Kr there are four main sets of features, as in the spectra for HCl, HBr, and HI. The numbering system used in this spectrum is that used in Ref. 1. (ANL Neg. 149-6566).

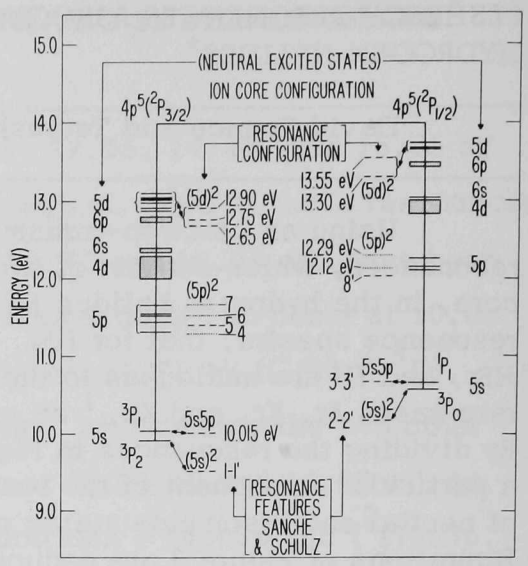

FIG. 3.--Energy-level diagram of excited states and resonance states in Kr. By separating the observed resonance into two sets, each associated with a particular component of the $X^2P_{\frac{3}{2},\frac{1}{2}}$ positive ion core, we identify the appropriate parent excited state of each observed resonance and deduce likely resonance electron configurations. The numbering system of the rare gas resonances is that used by Sanche and Schulz (see Phys. Rev. 5, 1672 (1972). (ANL Neg. 149-6570)

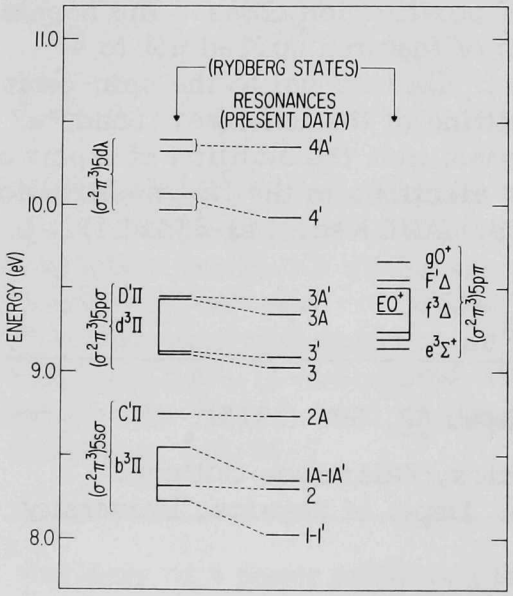

FIG. 4.--Energy-level diagram of rydberg states and resonance states observed in HBr. By analogy with the electron configurations and the approximate electron affinities of rydberg states observed in the isoelectronic atom Kr, the parent rydberg states of the observed resonances in HBr are determined. Also by analogy with krypton, we see that indeed we do expect to observe a resonance (associated with the $^3\Pi_1$ parent state) at the small feature marked 2 in Figure 3. Most resonances are observed to be associated with states whose rydberg electron has σ symmetry. (ANL Neg. 149-6567).

FESHBACH RESONANCES IN THE METHYL HALIDES

David Spence

We have previously reported measurements of Feshbach resonances in the molecular halogens [1] and in the hydrogen halides. [2] Both of these previous studies have enhanced our understanding of resonances from observation of systematic changes in resonance energies as a function of molecular size. We complete this study of resonance systematics by reporting here measurements we have made in CH_3Cl, CH_3Br, and CH_3I. The apparatus we use for these studies is a standard electron-transmission spectrometer of the type previously described by Sanche and Schulz. [3]

Results

Spectra of resonances we observe in CH_3I, CH_3Br, and CH_3Cl are shown in Figures 1–3. These resonances consist of pairs of rydberg electrons bound to a positive ion core (which may be in the ground state or in some excited state). [3] Such resonances may be visualized as an electron binding to

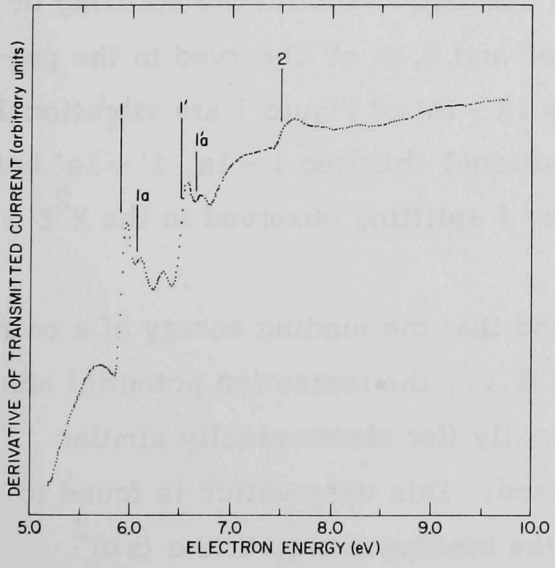

FIG. 1.--Derivative of the transmitted electron current vs. electron energy in methyl iodide (ANL Neg. 149-75-243)

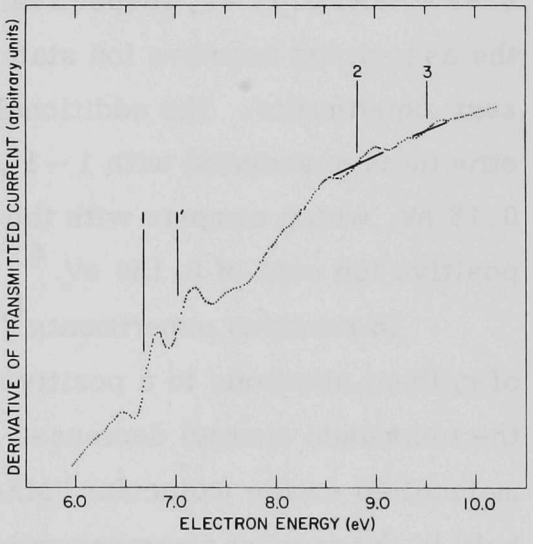

FIG. 2.--Derivative of transmitted electron current vs. electron energy in methyl bromide (ANL Neg. 149-75-241)

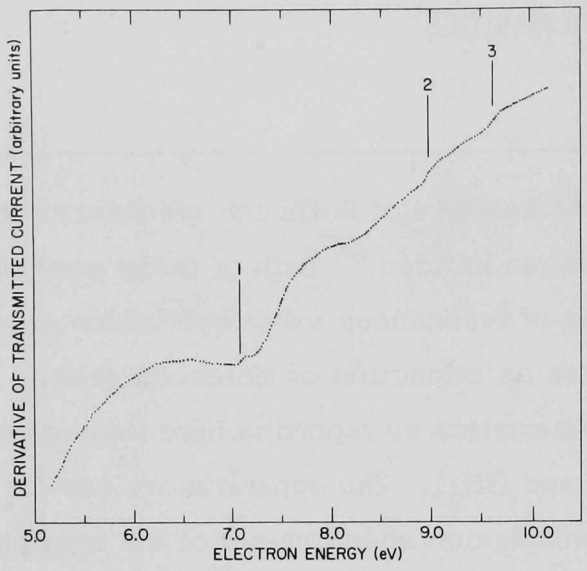

FIG. 3.--Derivative of the transmitted electron current vs. electron energy in methyl chloride
(ANL Neg. 149-75-238)

an already existing rydberg state of the molecule, with the resultant resonance (negative ion state) lying energetically below this neutral rydberg state.

The energetically lowest lying resonance in Figures 1–3 are clearly associated with rydberg states formed by the promotion of an $np\pi$ halogen lone-pair electron into an $(n+1)s\sigma$ orbital, where $n=5$ for I, 4 for Br, and 3 for Cl. Addition of another electron leads to resonance configuration $\{(n+1)s\sigma\}^2$. In Figures 1 and 2, the doubling of the resonance features $1-1'$ is clearly associated with the $^2E_{\frac{3}{2},\frac{1}{2}}$ spin-orbit splitting of the positive ion core. The positive ion core splittings for CH_3I and CH_3Br were measured by Potts et al.,[4] using photoelectron spectroscopy, and found to be 0.62 eV and 0.33 eV, respectively, which compare well with the splitting of the associated negative ion states 0.625 eV and 0.35 eV observed in the present experiments. The additional features $1a-1a'$ of Figure 1 are vibrational structures associated with $1-1'$, the vibrational splitting $1-1a$, $1'-1a'$ being 0.15 eV, which compare with the $v=0 \rightarrow v=1$ splitting observed in the X^2E positive ion core of 0.156 eV.[4]

In previous experiments[1,2] we found that the binding energy of a pair of rydberg electrons to a positive ion core (i.e., the ionization potential minus the resonance energy) decreased monotonically (for electronically similar molecules) as the molecular "size" increased. This observation is found to hold in the present measurements, where the binding energy of the $(s\sigma)^2$ resonance pair to the X^2E positive ion core is determined to be 4.22 eV, 3.86 eV, and 3.64 eV for CH_3Cl, CH_3Br, and CH_3I.

At present we are not able to assign unambiguous resonance configurations to the structures marked 2 and 3 in Figures 1, 2, and 3. Although these structures are very broad and "weak" compared to structures 1, they are nevertheless very reproducible. These additional structures may be associated with excited states of the positive ion core, or alternatively, consist of pairs of rydberg electrons with $\ell > 0$ associated with the ground state of the positive ion core. Although in the past we have been able to attribute high-lying resonances in the hydrogen halides to both these configurations,[2] such simple classifications as we achieved previously do not appear applicable to the higher resonances of the methyl halides. In this respect, further analysis of the present data is necessary.

References

1. Spence, David, Radiological & Environmental Research Division Annual Report, July 1973–June 1974, ANL-75-3, Part I, pp. 91–93.
2. Spence, D. and T. Noguchi, this report, paper 17.
3. Sanche, L. and G. J. Schulz, Phys. Rev. A 6, 69–86 (1972).
4. Potts, A. W., H. J. Lempka, D. G. Streets, and W. C. Price, Phil. Trans. R. Soc. London A 268, 59–76 (1970).

PRELIMINARY TOTAL CROSS SECTION MEASUREMENTS USING A HIGH TEMPERATURE RAMSAUER APPARATUS

D. Spence, T. Noguchi,* and O. J. Steingraber

In this report we describe construction and testing of an apparatus to measure total cross sections for electron scattering from substances which are gaseous only at high temperatures.

Our motivation for measuring the total cross sections for scattering of electrons by high temperature vapors is their relevance to the MHD (magneto-hydrodynamic) power-generation program.

In MHD power generation a conducting fluid (usually an ionized gas) is passed through a supersonic duct, with a magnetic field perpendicular to the direction of motion. The interaction of the moving charges with the magnetic field causes a current of electrons to flow in a direction perpendicular to both the magnetic field and the direction of bulk gas flow. With suitably placed electrodes, this current can be picked up and passed through an external circuit. In the open-cycle MHD generator, electrons are usually produced by thermal ionization of K atoms (i.e., seed atoms). The high temperatures needed for this are provided by burning a suitable fuel in the presence of air or oxygen. Typical fuels are methane, kerosene, fuel oil, and coal; potassium is introduced in the form of potassium sulphate. At the temperatures necessary to produce reasonable ionization of the potassium ($\approx$ 3000 C), a partial list of molecular species present in the MHD duct includes H_2O, CO_2, CO, O_2, O, H_2, N_2, OH, K, and KOH.[1] The main reaction for electron production is $K \rightleftarrows K^+ + e$, and that for electron removal is $OH + e \rightleftarrows OH^-$. In the MHD duct the electrons perform trochoidal or epicychoidal motions in the E $\times$ B field, and make many collisions with neutral molecules before being collected. As the electron energy in a thermal duct is low (at most a few eV), the most important cross sections necessary for an analysis of the system are elastic

*Summer student 1975. Present address: Department of Physics, The University of Chicago, Chicago, Illinois 60637.

cross sections and vibrational excitation cross sections of all the constituent molecules. One of the principal constituents in the open-cycle MHD generator, for which electron collision cross sections are urgently needed, is KOH;[1] because of its large dipole moment, total electron-scattering cross sections are expected to be large at low electron energies. At present no measurements are available for MHD duct constituents such as KOH.

The Apparatus

The oldest, and probably still the most reliable, method for measuring total electron-scattering cross sections is that developed in the 1920's and 1930's by Ramsauer and Kollath.[2] The basis of the technique of Ramsauer and Kollath is best described with reference to Figure 1.

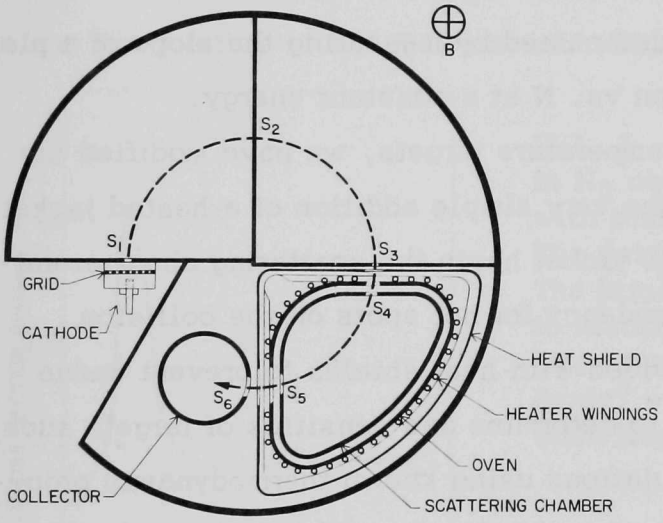

FIG. 1.--Schematic diagram of the apparatus (ANL Neg 149-75-240)

Electrons are emitted from a heated filament or cathode, and are selected for momentum by the combination of 3 slits, S_1, S_2, and S_3, and a uniform magnetic field applied perpendicular to the plane of the drawing. The selected beam of electrons collides with a target gas in the scattering chamber, and the transmitted electron signal at the collector is studied as a function of gas density in the scattering region at a particular value of electron energy.

Assume that a current of electrons, $I_{c0} + I_{s0} = I_0$, enters the scattering chamber, where I_{c0} is that part of the current entering the scattering region that would reach the collector in the absence of scattering and I_{s0} is

that part of the current entering the scattering chamber which would reach the scattering chamber walls owing to mechanical imperfection in the absence of scattering. Then, in the presence of scattering, the current reaching the collector is given by

$$I_c(E) = I_{c0}(E) \exp [-\sigma_t(E) N x] , \quad (1)$$

where $\sigma_t(E)$ is the total cross section, N is the gas density, and x is the path length of the electron beam through the scattering region, and E is the electron energy.

The current reaching the scattering chamber is given by

$$I_s = I_{s0} + I_{c0} [1 - \exp (-\sigma_t N x] . \quad (2)$$

Then, combination of Eqs. 1 and 2 gives

$$\ln [(I_c + I_s)/I_c] = \ln [(I_{c0} + I_{s0})/I_{c0}] + \sigma_t N x . \quad (3)$$

The total cross section is directly determined by measuring the slope of a plot of the left-hand side of this equation vs. N at a constant energy.

For measurements on high-temperature targets, we have modified the design of Ramsauer and Kollath by the very simple addition of a heated jacket around the scattering chamber. This jacket heats the scattering chamber uniformly by radiation, removing the tendency for hot spots on the collision chamber. The heated jacket is provided with heat shields to prevent undue heat loss. As it will be necessary to determine gas densities of targets such as KOH and NaOH solely from calculations using known thermodynamic properties, it is essential that the scattering chamber be uniformly heated. Measurements made by platinum-platinum-iridium thermocouples attached to the sides, bottom, and top of the scattering chamber indicate that the temperature variation over the scattering chamber surface is < 2 K at a temperature of 1000 K, much higher than necessary to provide sufficient target gas densities. All current-collecting electrodes have been provided with guards to minimize electrical leakage at high temperatures, and all insulators are optically shielded to prevent deposition of condensate. The entire apparatus is constructed from 304 stainless steel because of this material's great resistance to corrosion from molten KOH and NaOH.

There is a tendency of 304 stainless steel to become magnetic at high temperatures. However, this condition is readily noticeable, and residual magnetization is removed by application of a large degaussing field generated by a solenoid surrounding the apparatus.

Results

In order to check the general performance of our apparatus we have measured relative total scattering cross sections in molecular nitrogen — a system which has received previous detailed study. We measured the relative rather than the absolute cross section in this case as our apparatus has no facility for absolute pressure measurement, a facility not required for high-temperature vapor measurements. We have measured the $e - N_2$ cross section at both room and elevated temperatures. A representative set of data taken at a gas temperature of 731 K is shown in Figure 2, together with a comparison of

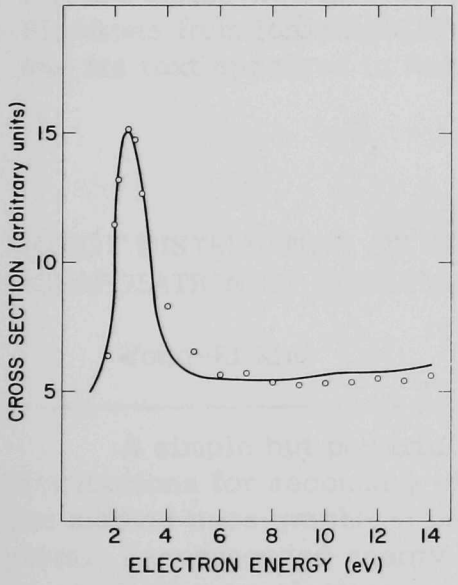

FIG. 2.--Comparison of total cross sections in N_2 obtained in the present experiment with that obtained by Ramsauer and Kollath. The data have been normalized at 2.5 eV. The large peak in the data at 2.3 eV is due to resonant scattering by the $N_2^- X\,\Pi_g$ state. Open circles, present data — 731 K; line, Brode[3] — room temperature. (ANL Neg. 149-75-244)

earlier measurements compiled by Brode.[3] Our data are normalized to the earlier measurements at 2.5 eV, and the functional agreement between the two curves is excellent. No noticeable difference in data is observed between room and elevated temperatures, indicating no dimensional distortion of the apparatus due to thermal stress.

The system has been operated at high temperatures while containing a charge of KOH, and long-term stability over many hours is achieved. For now, however, no complete set of data has been taken for KOH.

References

1. Zeilinski, A., Electricity from MHD, Proc. I.A.E.A. Symp. on MHD Power Generation, Warsaw, 24–30 July 1968, Int. Atomic Energy Agency, Vienna, Vol. IV, p. 2211 (1968).
2. Massey, H. S. W. and E. H. S. Burhop, Electronic and Ionic Impact Phenomena, Oxford University Press, Oxford, Ch. I–IV (1952).
3. Brode, R. B., Rev. Mod. Phys. 5, 257 (1933).

BASIC ASPECTS OF SECONDARY-ELECTRON DISTRIBUTIONS*

Yong-Ki Kim

Graphical methods proposed by Platzman and by Fano are applied to the analysis of the basic features observed in secondary electron spectra. These methods are useful not only in checking the consistency of experimental data, but also in extrapolating the spectra to the range of primary- and secondary-electron energies not covered by experiments. Illustrative examples include He, Ne, and NO. For incident protons of moderate energy (< 300 keV) charge transfer to the hydrogen continuum accounts for a substantial fraction (< 25%) of the total ionization cross section. Suggestions are given for desirable experiments that would be useful in determining reliable secondary-electron spectra.

*Summary of a progress report presented at the IXth Int. Conf. on the Physics of Electronic and Atomic Collisions, Seattle, July 1975. A full text will be included in Invited Papers and Progress Reports, edited by J. S. Risley and R. Geballe (University of Washington Press). Also, a lecture on closely related topics was delivered at the Symposium on Distributions of Secondary Electrons from Ionizing Collisions, London, Ontario, Canada, December 1974, and its text appeared in Radiat. Res. 64, 96 (1975).

ENERGY DISTRIBUTION OF SECONDARY ELECTRONS. II. NORMALIZATION AND EXTRAPOLATION OF EXPERIMENTAL DATA*

Yong-Ki Kim

A simple but powerful method of constructing a consistent set of energy distributions for secondary electrons produced by electron impact is presented. The method uses graphical presentations known as the Platzman and the Fano plots. Recommended energy distributions for He and N_2 are given for a wide range of primary-electron energies (50 eV to 100 keV). Data necessary for extrapolating the distribution to higher incident energy are also included.

*Abstract of a paper published in Radiat. Res. 64, 205 (1975).

EFFECTS OF PARTIAL CROSS SECTIONS ON THE ENERGY DISTRIBUTION OF SLOW SECONDARY ELECTRONS*

Henry C. Tuckwell† and Yong-Ki Kim

The shapes of the energy distribution of secondary electrons can be predicted for fast incident charged particles by using dipole oscillator strengths in conjunction with the Born formula. Target atoms or molecules may have one or more ionization potentials close to the first one, and the corresponding partial photoionization cross sections are sometimes large. Allowance must then be made for the differences in kinetic energies of photoelectrons that leave alternative ionic states. This produces a significant change in the expected secondary electron spectrum at low energies. The photoionization data for NO are analyzed, and the predicted shape of the secondary electron energy distribution agrees well with that of the experimental distribution at those secondary electron energies where a comparison is possible. Predicted low energy results from a preliminary analysis for N_2 are also reported.

---

*Abstract of a paper published in J. Chem. Phys. 64, 333 (1976).

†Present address: Department of Mathematics, University of British Columbia, Vancouver, B.C., Canada.

ELECTRON-COLLISION CROSS SECTIONS FOR ENERGY-DELIVERY ANALYSIS*

Mitio Inokuti

Although the study of individual collisions of electrons with molecules has been a major enterprise of atomic physics for over half a century, our knowledge remains fragmentary for any given molecule. For this reason, Platzman and co-workers devised a series of methods, such as use of suitable plots, for testing the consistency of cross-section data with independent information. The quantities treated include the spectral distribution of the oscillator strength, the total inelastic-collision cross section, the discrete-excitation cross section, the ionization cross section, and especially important, the secondary-electron energy distribution. On the basis of cross sections thus constructed for several basic gases, we can describe the earliest phase of the energy deposition in much greater detail and with much greater certainty than ever before. The analysis also lends itself to systematic extensions to many gases.

In amplification of Fano's plenary lecture[1] entitled "Platzman's Analysis of the Delivery of Radiation Energy to Molecules," it is appropriate to make several remarks, including an indication of areas that call for future study.

One general point of emphasis is that we need a comprehensive determination of electron-collision cross sections for a given molecule. The word "comprehensive" here implies cross sections in absolute units for all major processes (which account for say 99% of the stopping power) at all incident energies. This emphasis distinguishes our interest from the interest of a pure physicist who looks for novel phenomena, which are often specific to a particular process, a particular energy, or a particular molecule. Indeed, the need for the comprehensive determination of cross sections is not at all limited to radiation research, but is common to modeling studies of macroscopic phenomena, e.g., plasma simulations, chemical aeronomy, dynamics

---

*Excerpt of an invited paper presented at the XXIII Annual Meeting of the Radiation Research Society, May 1975, Miami Beach, Florida.

of gas lasers. An obvious corollary of this emphasis is a persistent inquiry as to the possibility of kinetic competition among different processes. Every time someone brought up a new process for consideration, Platzman used to ask, "Does that process effectively compete with all other known processes?" This attitude is crucial to successful execution of the energy-delivery analysis.

Some of the present outstanding problems are as follows.

1. Secondary-electron spectra. Experimental data on very slow secondary electrons (with energies below several eV) are scanty in general, and appear inconclusive or imcomplete for a few examples so far reported on. Although a semi-empirical analysis [2] provides reasonable estimates, their verification by direct measurements is highly desirable.

2. Electronic excitation by slow electrons. Despite its long history and its obvious importance to many applications, the absolute measurement of discrete-excitation cross sections for near-threshold electrons remains a difficult task. Also, current theories bearing on the subject matter are rudimentary.

3. Inner-shell excitations. Much of the energy-delivery analysis has so far dealt with aspects chiefly related to excitation and ionization of the valence shell. Although inner-shell excitations are rare, they involve large energy transfer per event; indeed, they account for nearly 20% of the stopping power for atoms in the first row of the periodic table, and a greater fraction for heavier atoms. A vacancy in an inner shell of a light atom leads through a succession of Auger effects to a highly charged ion, and therefore possibly to many chemical and biological consequences. [3] The role of inner-shell excitation in the radiation-energy delivery awaits further scrutiny, especially in the light of contemporary cross-section data. The recognition [4] of notable molecular effects on the K-shell ionization exemplifies new elements to be considered in this respect.

4. Systematics of cross sections and related properties for many atoms. A full analysis of cross sections for any single atom or molecule is a major task demanding over a man-year effort. In order to clarify general implications of such an analysis, we need to understand variations of cross sections from one atom to another. Our effort toward this end [5,6] has led to certain

important systematics for atoms up to krypton. A comparable study on molecules is desirable.

5. Subexcitation electrons. Once an electron becomes too slow to excite electronic levels of molecules, its energy loss is much less efficient. The major energy-loss processes of subexcitation electrons [7] are vibrational excitation, rotational excitation, and elastic scattering. The current knowledge of cross sections for these processes is certainly incomplete, but appears substantial enough to justify some application to electron moderation calculations.

6. Later stages of radiation action. By use of a set of comprehensive cross-section data, one evaluates cumulative consequences of many electron collisions and obtains yields of initial species, e.g., ions and excited states. It is important to appreciate that these yields pertain to the earliest stage in the radiation action. Thermal collisions of the initial species with other molecules (mostly in the ground state) may cause inter-conversion. Indeed, most observations in radiation chemistry (even in the fastest of pulse-radiolysis measurements) concern species that have experienced thermal collisions. This is certainly true in condensed phases and probably so in gas phases unless the gas pressure is very low. Evidence of thermal-collision effects has been established in ionization yields of some gases; an appreciable fraction of excited states convert into ions by chemi-ionization processes. This observation points to the importance of studying the interactions of excited species with other molecules, as a link of the energy-delivery analysis to radiation chemistry. Also, these interactions are important to some other applications such as chemical aeronomy, gaseous magnetohydrodynamic power-generation processes, and gas-dynamic laser developments.

References

1. Fano, U., Radiat. Res. 64, 96 (1975).
2. Kim, Y.-K., Radiat. Res. 61, 21 (1975); 64, 96 (1975); 64, 205 (1975).
3. Durup, J. and R. L. Platzman, Disc. Faraday Soc. 31, 156 (1961); Int. J. Radiat. Phys. Chem. 7, 121 (1975).

4. Dehmer, J. L. and D. Dill, Phys. Rev. Lett. 35, 213 (1975).
5. Inokuti, M., J. L. Dehmer, and J. D. Hanson, this report, paper 24.
6. Dehmer, J. L., J. D. Hanson, and M. Inokuti, this report, paper 25.
7. Platzman, R. L., Radiat. Res. 2, 1 (1955).

TOTAL CROSS SECTIONS FOR INELASTIC SCATTERING OF CHARGED PARTICLES BY ATOMS THROUGH THE THIRD ROW OF THE PERIODIC TABLE

Mitio Inokuti, J. L. Dehmer, and J. D. Hanson*

The systematic study of the Bethe cross sections has now been extended to include all neutral atoms through the third row, i.e., $Z \leq 36$.

For a structureless particle of charge ze and velocity $v = \beta c$, the total inelastic-scattering cross section, σ_{tot}, is given as[1]

$$\sigma_{tot} = \frac{8\pi a_0^2 z^2}{mv^2/R} \left\{ M_{tot}^2 \left[\ln\left(\frac{\beta^2}{1-\beta^2} \right) - \beta^2 \right] + C_{tot} \right\} , \quad (1)$$

where a_0 is the Bohr radius, R is the Rydberg energy, m is the electron rest mass. Two nontrivial parameters, M_{tot}^2 and C_{tot}, embody the atomic dynamics pertinent to total inelastic scattering at sufficiently great v. In the nonrelativistic domain, Eq. 1 may be put in the form

$$\sigma_{tot} = 4\pi a_0^2 z^2 (R/T) M_{tot}^2 \ln(4c_{tot} T/R) , \quad (2)$$

where $T = \frac{1}{2}mv^2$, and c_{tot} is related to C_{tot} through[1]

$$C_{tot} = M_{tot}^2 [\ln c_{tot} + \ln(2mc^2/R)]$$

$$= M_{tot}^2 [\ln c_{tot} + 11.2268] . \quad (3)$$

Extending an earlier study[2] on atoms with atomic number $Z \leq 18$, we evaluated M_{tot}^2 and $\ln c_{tot}$ for all neutral atoms with $19 \leq Z \leq 36$ by the use of Hartree-Fock and Hartree-Slater models.[3]

Figures 1 and 2 summarize our results. The dependence of σ_{tot} on Z is primarily governed by M_{tot}^2, which may be regarded as representing the

---

*Appointee, Undergraduate Research Participation Program, Fall 1974, from Kalamazoo College, Kalamazoo, Mich., 49001. Present address: Lawrence Livermore Laboratory, Livermore, California 94550.

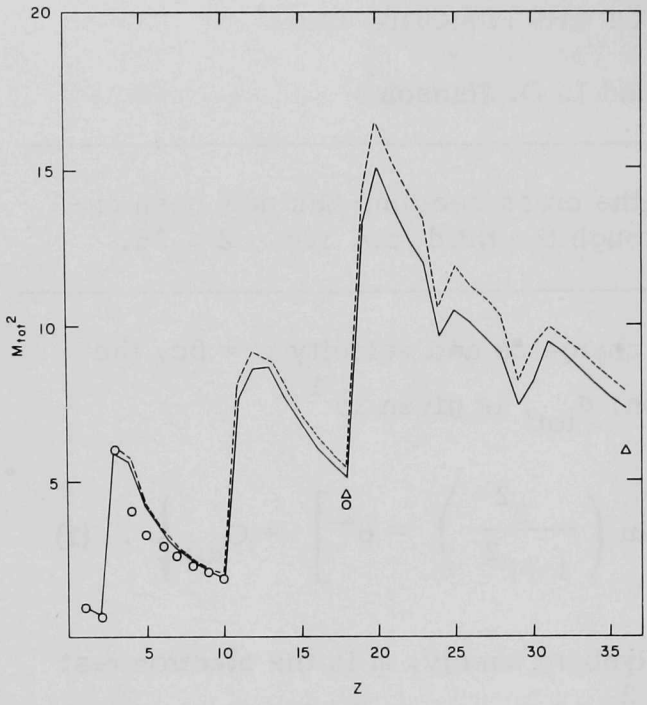

FIG. 1.--The total dipole matrix element M_{tot}^2 as a function of atomic number Z. The points connected with heavy lines show the Hartree-Slater values obtained in the present work; those connected by broken lines show the Hartree-Fock values taken from the literature; and the circles show accurate theoretical values also taken from the literature. The triangles represent values computed from experimental oscillator-strength distributions.

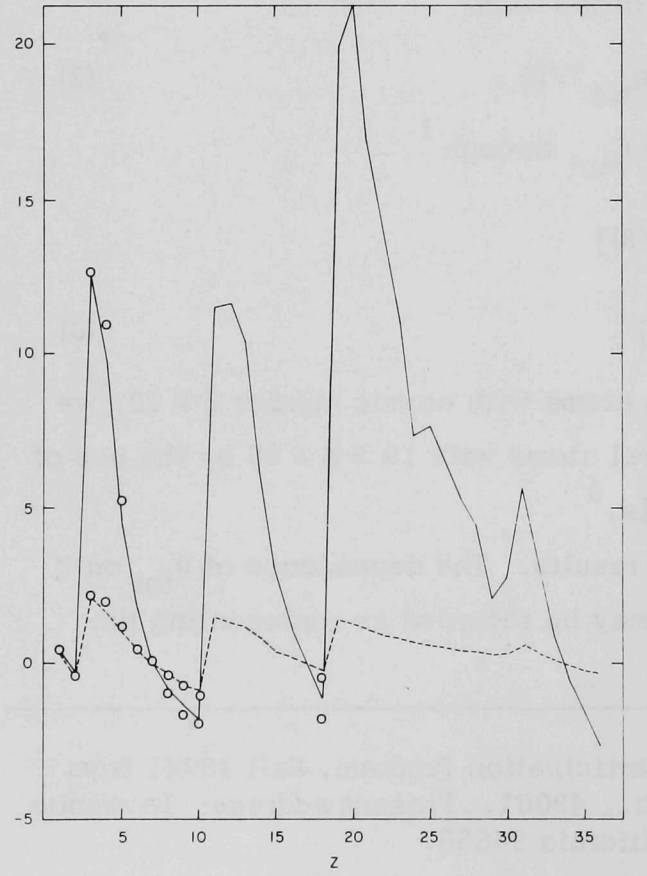

FIG. 2.--The quantities M_{tot}^2 ln c_{tot} (solid line) and ln c_{tot} (broken line) as functions of atomic number Z. The points connected with heavy lines represent results from a combined use of Hartree-Fock and Hartree-Slater data, and the open circles represent results including more accurate theoretical data.

squared atomic size because of the relation

$$M_{tot}^2 = \langle (\sum_j x_j)^2 \rangle \ , \qquad (4)$$

where x_j is a Cartesian component of jth electron coordinate and $\langle \ldots \rangle$ denotes the ground-state expectation value. The strong variation of M_{tot}^2 with Z, shown in Figure 1, clearly arises from the periodic shell structure. In contrast, the variation of $\ln c_{tot}$ is only moderate, and becomes especially weak for $19 \leq Z \leq 36$ (see Figure 2). Considering the weak variation and the modest size of $\ln c_{tot}$ compared to the constant 11.2268 in Eq. 3, we can readily see that the parameter C_{tot} is nearly proportional to M_{tot}^2. Therefore, σ_{tot} in the relativistic domain is proportional to M_{tot}^2 to a good approximation, especially for $19 \leq Z \leq 36$.

A comprehensive account of the present series of work will be soon prepared for publication as a journal article.

References

1. Inokuti, M., Y.-K. Kim, and R. L. Platzman, Phys. Rev. 164, 55 (1967).
2. Inokuti, M., R. P. Saxon, and J. L. Dehmer, Int. J. Radiat. Phys. Chem. 7, 109 (1975).
3. Dehmer, J. L., J. D. Hanson, and M. Inokuti, this report, paper 25.

MOMENTS OF THE DIPOLE OSCILLATOR-STRENGTH DISTRIBUTIONS FOR ATOMS IN THE THIRD ROW OF THE PERIODIC TABLE

J. L. Dehmer, J. D. Hanson,* and Mitio Inokuti

Our ongoing study of the systematics of the Z dependence of moments of the dipole oscillator-strength distributions has now been extended to include the atoms of the third row of the periodic table, K through Kr.

As in the earlier phases of this study[1,2] we employ the realistic atomic potentials tabulated by Herman and Skillman.[3]

The quantities of primary interest are the moments $S(\mu)$ and $L(\mu)$ defined as

$$S(\mu) = \int (E/R)^{\mu} (df/dE)\, dE \,, \tag{1}$$

and

$$L(\mu) = \int (E/R)^{\mu} \ln(E/R)\, (df/dE)\, dE \,, \tag{2}$$

where the integration over energy includes a summation over the discrete transition energies. The moments defined in Eqs. 1 and 2 for $19 \leq Z \leq 36$ and $-6 \leq \mu \leq 2$ are listed in Tables 1 and 2. For $\mu \leq 0$ the accuracy is $< 0.1\%$. The accuracy declines for $\mu = 1$ ($\sim 1\%$) and $\mu = 2$ (5 to 10%) because of truncation at the high energy limit of the integrals in Eqs. 1 and 2, which is usually ~ 500 Ry.

The earlier study on the first two rows of the periodic table exhibited pronounced periodic behavior in the moments and in the physical quantities which depend upon them. In most cases, the period structure could not be discerned from the sparse experimental data which are typically limited to the rare gases. This attaches great significance to realistic theoretical estimates of these quantities. The purpose of extending the study to the third row was to elucidate the effect of the filling of the 3d subshell on these systematics.

---

* Participant in the Fall 1974 Undergraduate Research Participation Program from Kalamazoo College, Kalamazoo, Mich. 49001. Present address: Lawrence Livermore Laboratory, Livermore, California 94550.

TABLE 1. The Moments $S(\mu)$ $-6 \leq \mu \leq 1$

Z	S(-6)	S(-5)	S(-4)	S(-3)	S(-2)	S(-1)	S(0)	S(1)
19	5.538 + 5	6.154 + 4	6.842 + 3	7.618 + 2	8.648 + 2	1.302 + 1	1.900 + 1	1.350 + 3
20	8.572 + 4	1.455 + 4	2.471 + 3	4.204 + 2	7.260 + 1	1.500 + 1	2.000 + 1	1.520 + 3
21	4.119 + 4	7.895 + 3	1.515 + 3	2.919 + 2	5.742 + 1	1.380 + 1	2.101 + 1	1.699 + 3
22	2.295 + 4	4.840 + 3	1.023 + 3	2.171 + 2	4.726 + 1	1.280 + 1	2.201 + 1	1.890 + 3
23	1.394 + 4	3.189 + 3	7.309 + 2	1.685 + 2	3.994 + 1	1.197 + 1	2.301 + 1	2.092 + 3
24	1.763 + 4	3.518 + 3	7.057 + 2	1.435 + 2	3.082 + 1	9.664 + 0	2.401 + 1	2.304 + 3
25	5.792 + 3	1.529 + 3	4.044 + 2	1.077 + 2	2.959 + 1	1.056 + 1	2.501 + 1	2.534 + 3
26	4.197 + 3	1.167 + 3	3.254 + 2	9.138 + 1	2.652 + 1	1.010 + 1	2.601 + 1	2.774 + 3
27	2.904 + 3	8.576 + 2	2.539 + 2	7.572 + 1	2.336 + 1	9.556 + 0	2.701 + 1	3.028 + 3
28	2.122 + 3	6.594 + 2	2.055 + 2	6.452 + 1	2.098 + 1	9.130 + 0	2.802 + 1	3.295 + 3
29	3.078 + 3	8.051 + 2	2.122 + 2	5.703 + 1	1.645 + 1	7.497 + 0	2.903 + 1	3.570 + 3
30	1.164 + 3	3.989 + 2	1.371 + 2	4.751 + 1	1.708 + 1	8.362 + 0	3.003 + 1	3.871 + 3
31	8.979 + 3	1.670 + 3	3.400 + 2	7.941 + 1	2.247 + 1	9.522 + 0	3.103 + 1	4.186 + 3
32	1.087 + 3	3.312 + 2	1.089 + 2	3.957 + 1	1.632 + 1	9.146 + 0	3.203 + 1	4.517 + 3
33	2.091 + 2	9.164 + 1	4.282 + 1	2.159 + 1	1.200 + 1	8.618 + 0	3.304 + 1	4.865 + 3
34	5.643 + 1	3.267 + 1	1.996 + 1	1.299 + 1	9.168 + 0	8.132 + 0	3.404 + 1	5.230 + 3
35	1.896 + 1	1.374 + 1	1.045 + 1	8.391 + 0	7.245 + 0	7.709 + 0	3.504 + 1	5.613 + 3
36	7.381 + 0	6.466 + 0	5.918 + 0	5.700 + 0	5.869 + 0	7.337 + 0	3.604 + 1	6.015 + 3

TABLE 2. The Moments $L(\mu)$ $-6 \leq \mu \leq 1$

Z	L(-6)	L(-5)	L(-4)	L(-3)	L(-2)	L(-1)	L(0)	L(1)
19	-1.217 + 6	-1.352 + 5	-1.503 + 4	-1.670 + 3	-1.848 + 2	-1.759 + 1	4.783 + 1	7.787 + 3
20	-1.520 + 5	-2.580 + 4	-4.380 + 3	-7.436 + 2	-1.256 + 2	-1.843 + 1	4.979 + 1	8.916 + 3
21	-6.806 + 4	-1.304 + 4	-2.499 + 3	-4.795 + 2	-9.148 + 1	-1.459 + 1	5.336 + 1	1.013 + 4
22	-3.574 + 4	-7.530 + 3	-1.588 + 3	-3.352 + 2	-7.029 + 1	-1.174 + 1	5.711 + 1	1.144 + 4
23	-2.058 + 4	-4.702 + 3	-1.075 + 3	-2.462 + 2	-5.585 + 1	-9.518 + 0	6.100 + 1	1.285 + 4
24	-2.846 + 4	-5.663 + 3	-1.130 + 3	-2.266 + 2	-4.510 + 1	-5.574 + 0	6.596 + 1	1.435 + 4
25	-7.720 + 3	-2.035 + 3	-5.369 + 2	-1.417 + 2	-3.685 + 1	-6.139 + 0	6.917 + 1	1.599 + 4
26	-5.374 + 3	-1.493 + 3	-4.149 + 2	-1.154 + 2	-3.153 + 1	-5.049 + 0	7.328 + 1	1.773 + 4
27	-3.544 + 3	-1.045 + 3	-3.085 + 2	-9.101 + 1	-2.631 + 1	-3.924 + 0	7.762 + 1	1.959 + 4
28	-2.481 + 3	-7.699 + 2	-2.391 + 2	-7.420 + 1	-2.249 + 1	-3.038 + 0	8.197 + 1	2.157 + 4
29	-4.135 + 3	-1.077 + 3	-2.816 + 2	-7.387 + 1	-1.891 + 1	-7.993 - 1	8.730 + 1	2.363 + 4
30	-1.248 + 3	-4.267 + 2	-1.461 + 2	-4.993 + 1	-1.655 + 1	-1.545 + 0	9.094 + 1	2.592 + 4
31	-1.540 + 4	-2.945 + 3	-5.208 + 2	-1.087 + 2	-2.556 + 1	-3.230 + 0	9.449 + 1	2.833 + 4
32	-1.326 + 3	-3.821 + 2	-1.162 + 2	-3.782 + 1	-1.305 + 1	-1.358 + 0	9.839 + 1	3.089 + 4
33	-1.784 + 2	-7.286 + 1	-3.109 + 1	-1.386 + 1	-6.234 + 0	3.969 - 1	1.024 + 2	3.363 + 4
34	-3.222 + 1	-1.702 + 1	-9.236 + 0	-5.122 + 0	-2.654 + 0	1.785 + 0	1.066 + 2	3.652 + 4
35	-6.509 + 0	-4.109 + 0	-2.592 + 0	-1.577 + 0	-6.759 - 1	2.876 + 0	1.108 + 2	3.959 + 4
36	-1.126 + 0	-7.205 - 1	-3.811 - 1	-5.004 - 2	4.635 - 1	3.750 + 0	1.150 + 2	4.280 + 4

The first results of this analysis concern total inelastic cross sections and are discussed elsewhere.[4] These analyses are being extended to other physical quantities.

One example of these quantities is the mean excitation energy I_0 that appears in the Bethe stopping-power formula and is defined by

$$\ln (I_0/R) = L(0)/S(0) = L(0)/Z \ . \qquad (3)$$

Because I_0 is roughly proportional to Z, it is customary[1] to consider the ratio I_0/Z and its Z dependence. Figure 1 shows our results: the ratio I_0/Z varies with Z periodically with maxima at rare gases and at Cr (Z = 24) and Cu (Z = 29), and with shallow minima in between. The periodic behavior chiefly arises from valence-shell structure. Indeed, the variation of I_0/Z becomes damped for atoms with higher and higher Z, because a greater and greater fraction of electrons belongs to inner shells. Our results also agree with the general experimental conclusion that $I_0/Z \approx 10$ eV for large Z.

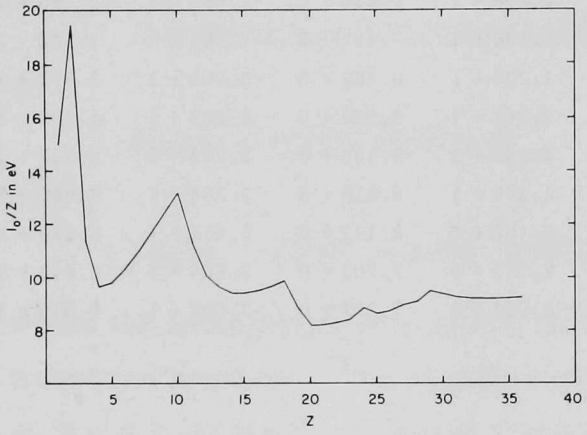

FIG. 1.--The ratio of the mean excitation energy I_0 for stopping power to atomic number Z, plotted as a function Z.

References

1. Dehmer, J. L., Mitio Inokuti, and R. P. Saxon, Phys. Rev. A 12, 102 (1975).
2. Inokuti, Mitio, R. P. Saxon, and J. L. Dehmer, Int. J. Radiat. Phys. Chem. 7, 109 (1975).
3. Herman, F. and S. Skillman, Atomic Structure Calculations, Prentice Hall, Inc., Englewood Cliffs (1963).
4. Inokuti, Mitio, J. L. Dehmer, and J. D. Hanson, this report, paper 24.

DEGRADATION SPECTRA AND IONIZATION YIELDS OF ELECTRONS IN GASES*

Mitio Inokuti, D. A. Douthat,† and A. R. P. Rau‡

Notable progress in the microscopic theory of electron degradation in gases recently made by Platzman, Fano, and co-workers is outlined. The theory consists of two principal components: first, the comprehensive cataloging of all major inelastic-collision cross sections for electrons (including secondary-electron energy distribution in a single ionizing collision), and second, the evaluation of cumulative consequences of individual electron collisions for the electrons themselves, as well as for target molecules (the so-called bookkeeping problem). Although current atomic physics offers a considerable volume of pertinent cross-section data, one must assess the data consistency and reliability through every possible means of critical analysis, and then extrapolate the data to the ranges of variables (such as electron energy) left unexplored by individual measurements. It is precisely for this reason that a series of plots devised by Platzman turns out to be especially powerful. By the use of realistic cross-section data thus established, the electron degradation spectra have been obtained through numerical solution of the Spencer-Fano equation for all electron energies down to the first ionization thresholds for a few concrete examples such as He and Ne. Remarkable systematics of the solutions thus obtained not only have led to the recognition of approximate scaling properties of the degradation spectra for different initial electron energies, but also point to new methods of more efficient treatment. At the same time, certain systematics of the ionization yields and their energy dependence on the initial electron energy have been recognized. Finally, we point out a close relation between the Spencer-Fano equation for the degradation spectra and the Fowler equation for the ionization and other yields; the two equations are tightly linked with each other by a set of variational principles.

---

*Abstract of an invited paper presented at the Fifth Symp. on Microdosimetry, Verbania-Pallanza, Italy, 22–26 September 1975. A full text will be included in the Proceedings to be published by the Commission of European Communities, Directorate General for Dissemination of Information, Luxembourg.

†Kennedy-King College, Chicago, Illinois 60621. Consultant, RER Division, Argonne National Laboratory.

‡Department of Physics and Astronomy, Louisiana State University, Baton Rouge, Louisiana 70803.

ENERGY DEPOSITION BY ELECTRONS AND DEGRADATION SPECTRA*

D. A. Douthat†

The energy distribution of particles in an irradiated system — the degradation spectrum — is perhaps the most fundamental piece of information in a description of the radiation field acting on the system. We discuss recent progress in the calculation of electron degradation spectra as well as some systematics of electron degradation spectra and compare this method with other viewpoints, e.g., CSDA, Monte Carlo, and Fowler-equation calculations. Deficiencies in the available data, as well as prospects for further calculations, are pointed out.

*Summary of a paper presented at the Symp. on Distributions of Secondary Electrons from Ionizing Collisions, Centre for Interdisciplinary Studies in Chemical Physics, The University of Western Ontario, London, Ontario, Canada, December 5–7, 1974. A full text appears in Radiat. Res. 64, 141 (1975).

†Kennedy-King College, Chicago, Illinois 60621. Consultant, RER Division, Argonne National Laboratory, Argonne, Illinois 60439.

CALCULATIONS OF ELECTRON DEGRADATION SPECTRA. II.

D. A. Douthat†

The sensitivity of computed electron degradation spectra with respect to the choice of cross-section data is under investigation. Fano's criterion for the validity of the continuous-slowing-down approximation was tested for the degradation of electrons and emerges as perhaps the most important factor affecting this sensitivity.

We have previously discussed the spectrum of electrons in an irradiated medium.[1] This spectrum is called the degradation spectrum and is represented by the function $y(T_0, T)$, where T_0 is the energy of the (monoenergetic) source electrons, and T is the spectral energy. A more detailed definition was given

†Kennedy-King College, Chicago, Illinois 60621. Consultant, RER Division, Argonne National Laboratory, Argonne, Illinois 60439.

by its inventors, Spencer and Fano.[2] Our initial calculations[3,4] dealt with gaseous helium and employed as input a self-consistent set of cross-section data assembled by W. F. Miller.[5] Although these data are still reliable in their major aspects, the difficulty of acquiring and analyzing data for other species[6,7] point to the following question: How sensitively do the computed spectra depend on the input data? This question has become especially important in view of the fact that other investigators have performed extensive calculations[8,9] for electron degradation in more complex gases than helium. The data for these media are less complete than those for helium. Furthermore, few investigators have employed consistency checks as extensively as Miller.

The last certain part of the input data is the low-incident energy portion of the secondary electron distribution. There has been substantial progress recently in both the experimental accumulation of such data[10,11] and in the analysis and extrapolation of the data by Kim and co-workers.[12–15] Miller's use of the form $q(T,E) = C(T)E^{-n}$ for the low-incident energy ($T \lesssim 400$ eV) differential ionization cross section is still reasonable. Here E is the energy loss. The total ionization cross section dictates the choice of the function C(T). Other workers also use similar analytic forms for q(T,E).

We find that changing n from 2 to 3 produces a decrease in the helium spectrum by about 10% at the ionization threshold. This result was obtained for $T_0 = 2$ keV, but the scaling properties[3] of the function $y(T_0,T)/T_0$ permit a simple extension to other source energies.

Our most important numerical result is the following: For factorizable q(T,E), i.e., those of the form f(T) g(E), degradation of the primary electron follows the continuous-slowing-down approximation (CSDA) to surprisingly low spectral energies. More specifically, the primary electron spectrum $y(T_0,T)$ calculated from the Spencer-Fano equations remains only a few percent lower than the reciprocal stopping power, $s^{-1}(T)$, over virtually the entire spectral range. The only regions where the difference is substantial are a) near the source energy where the transient effect raises $y_p(T_0,T)$ well above $s^{-1}(T)$, and b) for T within a few eV of the ionization threshold. Thus, the usual criterion for the validity of the CSDA — that the energy losses be only

a small fraction of the incident energy — is too restrictive. Fano[16] pointed this out in 1953, but his analytic result does not seem to be widely appreciated.

Our result explains in part why other investigators[17,18] found little difference between the CSDA result and more accurate results. The non-factorizing terms of the cross sections were of small magnitude.

We have not yet tested this result for the full degradation spectrum, i.e., the primary electron and all consequent secondary electrons. We expect that the transient[16] associated with the generation of each secondary electron will raise the full spectrum relative to the CSDA result. We plan to perform a calculation to test this expectation.

Acknowledgements

I wish to thank Dr. M. Inokuti and Dr. Y.-K. Kim for helpful discussions of this problem.

References

1. Douthat, D. A., Radiological and Environmental Research Division Annual Report, July 1973–June 1974, ANL-75-3, Part I, p. 25.
2. Spencer, L. V. and U. Fano, Phys. Rev. 93, 1172 (1954).
3. Douthat, D. A., Radiat. Res. 61, 1–20 (1975).
4. Douthat, D. A., Radiat. Res. 64, 141 (1975).
5. Miller, W. F., Ph.D. Thesis, Purdue University (1956) unpublished.
6. Gerhart, D. E., J. Chem. Phys. 62, 821 (1975).
7. Eggarter, E. J., Chem. Phys. 62, 833 (1975).
8. Green, A. E. S. and J. H. Miller, Physical Mechanisms in Radiation Biology, Proc. Conf. Airlie, Virginia, 11–14 October 1972, R. D. Cooper and R. W. Wood, Eds., U.S. Atomic Energy Commission Report, CONF-721001, p. 68 (1974).
9. Emerson, L. C., R. D. Bikrhoff, V. E. Anderson, and R. H. Ritchie, Phys. Rev. B 7, 1798 (1973).
10. Oda, N., F. Nishimura, and S. Tahira, J. Phys. Soc. Japan 33, 462 (1972).
11. Opal, C. B., E. C. Beaty, and W. K. Peterson, At. Data 4, 209 (1972).
12. Kim, Y.-K., Radiat. Res. 61, 21 (1975).
13. Kim, Y.-K., Radiat. Res. 64, 205 (1975).
14. Kim, Y.-K., Radiat. Res. 64, 96 (1975).
15. Tuckwell, H. C. and Y.-K. Kim, J. Chem. Phys. 64, 333 (1976); see also paper 22, this report.
16. Fano, U., Phys. Rev. 92, 328 (1953).
17. Peterson, L. R., Phys. Rev. 187, 105 (1969).
18. Klots, C. E. and H. Wright, Int. J. Radiat. Phys. Chem. 2, 191 (1970).

VARIATIONAL METHODS FOR IONIZATION YIELDS: A NUMERICAL APPLICATION

D. A. Douthat*

Our first numerical application of a recently devised variational method for the calculation of ionization yields gives a mean energy per ion pair of 43.5 eV for 1000 eV electrons in gaseous helium.

Variational principles were recently employed[1] in the elucidation of several features of the theory of electron energy degradation in gases. One result of this work is a unification of the two major bookkeeping methods: the Fowler equation and the Spencer-Fano theory. By the term "bookkeeping" we mean, following Platzman, the enumeration of the initial events in a medium as a consequence of the slowing down of an electron within the medium.

More specifically, if the incident electron of energy T is stopped completely within a volume of dilute gas, a number, $N_i(T)$, of ion pairs are produced. The mean energy per ion pair is $W(T) = T/N_1(T)$. The Spencer-Fano approach[2] for the computation of $N_i(T)$ (or any other primary product) consists of calculating first the degradation spectrum and then use of this reduced distribution function to compute the yield of ion pairs. Solution of the Fowler equation gives the number $N_i(T)$ directly. The merits of the various theoretical methods have been discussed elsewhere.[3,4]

The results for $N_i(T)$ obtained by numerical solution of the Fowler equation suggests a simple analytic solution. Inokuti[2] proposed that $N_i(T) \cong (T-U)/W_a$ for high T and verified the validity of this solution for He, H_2, and Ar. Furthermore, he deduced expressions for U and W_a in terms of the cross sections for electron impact. While his results for W(T) are substantially better than Fano's earlier result,[5] the values for W(T) are still several percent lower than the accurate results of full numerical solution of the Fowler equation.

*Kennedy -King College, Chicago, Illinois; consultant, RER Division, Argonne National Laboratory.

The variational expression (Eq. 28 of Ref. 1) permits an improvement on Inokuti's result. In this expression,

$$V(T_0) = N_{it}(T_0) - \int_I^\infty dT\, L_t(T_0, T)\,[\Omega_T N_{it}(T) - \sigma_i(T)] \ , \tag{1}$$

$N_{it}(T_0)$ is a trial approximate solution of the Fowler equation for $N_i(T_0)$, $L_t(T_0, T)$ is an approximate degradation spectrum, i.e., solution of the Spencer-Fano equation for an electron of initial energy T_0, $\sigma_i(T)$ is the total ionization cross section, and Ω_T is the operator that generates the Fowler equation. The factor in brackets vanishes if $N_{it}(T)$ is exactly $N_i(T)$. Hence, $V(T_0)$ given by this equation is a variational estimate of $N_i(T_0)$. The statements of this paragraph are amplified in Ref. 1.

As a test for the method, we computed $V(T_0)$ for helium for several values of T_0. The input for the calculation consisted of a) Inokuti's form for the trial $N_{it}(T)$, b) Smith's data[6] for $\sigma_i(T)$, and c) a polynomial fit to a function closely related to the degradation spectrum $y(T_0, T)$. The function chosen for (c) is

$$z^{tot}(\xi) \equiv \frac{T}{T_0}\ y(T_0, T)\, N\, \sigma^{tot}_{inelastic}\ (T) \ln (T_0/I) \ , \tag{2}$$

from which the values of $L_t(T_0, T) = N\, y(T_0, T)$ are computed. The number density of atoms is N, I is the ionization energy, and $\xi \equiv \ln (T/I)/\ln (T_0/I)$. Quasi-invariance of this type of function[7,8] permits extension to values of T_0 other than the initial choice (T_0 = 2 keV) for the third-order polynomial fit. Data for $y(T_0, T)$ were taken from Ref. 7 and data for the total inelastic cross section from Miller's thesis.[9]

Results

The results of the calculation are satisfactory, and, in view of the relative simplicity of the calculation, suggest that variational methods for degradation problems will be very useful. With an accurate fit to the functions $\sigma_i(T)$ and $\sigma^{tot}_{inelastic}(T)$ and our third-order polynomial fit to $z^{tot}(\xi)$, we found W = 43.5 eV for T_0 = 1000 eV. The more accurate Fowler-equation result is 46.3 eV, Fano's formulation[5] gives 40 eV using Miller's data, and Inokuti's

expression gives 42.9 eV. The variational results of several values of T_0 are given in Table 1, together with values computed from Inokuti's expression.

TABLE 1. Mean Energy in eV per Ion Pair for Helium

T_0, eV	$W(T) = W_a(T/(T-U))^a$	$W_{variational}$	% difference
500	43.52	44.13	1.40
1,000	42.90	43.51	1.40
4,000	42.45	43.03	1.35
16,000	42.34	42.91	1.35
32,000	42.32	42.90	1.36

[a] $W_a = 42.3$, $U = 14.0$.

Remaining problems include 1) full use of the expression for $V(T_0)$ as a variational principle, i.e., the stationary nature of the results, and 2) extension of the calculation to improve approximate values of other quantities including the function $y(T_0, T)$, and 3) tests of the sensitivity of $V(T_0)$ to the choice of input data.

Acknowledgements

I wish to thank Dr. M. Inokuti and Dr. A. R. P. Rau for useful suggestions and discussions concerning this work.

References

1. Inokuti, M., D. A. Douthat, and A. R. P. Rau, Proc. Fifth Symp. on Microdosimetry, Verbania-Pallanza, Italy, 22–26 September 1975 (to be published). See paper 26 of this report.
2. Spencer, L. V. and U. Fano, Phys. Rev. 93, 1172 (1954).
3. Inokuti, M., Radiat. Res. 64, 6 (1975).
4. Douthat, D. A., Radiat. Res. 64, 147 (1975).
5. Fano, U., Phys. Rev. 70, 44 (1946).
6. Smith, P. T., Phys. Rev. 36, 1293 (1930).
7. Douthat, D. A., Radiat. Res. 61, 1 (1975).
8. Fano, U. and L. V. Spencer, Int. J. Radiat. Phys. Chem. 7, 63 (1975).
9. Miller, W. F., Ph.D. Thesis, Purdue University, 1956 (unpublished).

MODELING OF THE ELECTRONIC ENERGY LOSS PROCESSES RELEVANT TO THE YIELDS AND DISTRIBUTIONS OF PRIMARY SPECIES PRODUCED BY THE PULSE RADIOLYSIS OF AQUEOUS SYSTEMS*

C. A. Naleway,† Yong-Ki Kim, M. C. Sauer, Jr.,† and A. C. Wahl†

A refined understanding of the physical stages of energy transfer associated with energy deposition by high energy electron or heavy ion beams is necessary in obtaining initial radical and electron distributions to be used as input into a classical diffusion kinetics model. A program has thus been initiated to investigate both the radical distribution functions and total yields of presolvated electrons and radicals. A parameterized form of the first order Born approximation properly correlated to parallel experimental scattering data has been implemented to obtain the required cross sections for energy loss. The cascading processes of energy loss have been simulated by use of a multi-leveled Monte Carlo procedure.

This program has been implemented in the investigation of both electron and heavy ion incident beams. Discussion focuses on various levels of sophistication (parameterization) used throughout these studies. Comparison between the obtained initial yields and experimental gas phase yield has been found to be encouraging. Readjustment and further refinement pertinent to the losses within a condensed phase are outlined, and preliminary results are presented.

*Abstract of a paper presented at the E. J. Hart Int. Conf. on Radiation Chemistry, Argonne National Laboratory, July 1975.

†Chemistry Division, Argonne National Laboratory.

SPECTRAL AND ELECTRON COLLISION PROPERTIES OF ATOMIC IONS*

K. D. Chao,† J. L. Dehmer, U. Fano,‡ M. Inokuti, S. T. Manson,† A. Msezane,† R. F. Reilman,† and C. E. Theodosiou‡

The aim of this study is to delineate the systematics of various properties of positive atomic ions over a wide range of nuclear charge, Z, and electron number, N. These properties include energy levels, transition rates, electron collision cross sections, and other directly observable quantities. From a theoretical point of view, many of these properties are derived from a few basic quantities: phase shifts of partial waves, $\delta_\ell(\epsilon)$, (including both $\epsilon > 0$ and $\epsilon < 0$) and their derivatives, enhancement factors,[1] $\alpha_\ell(\epsilon)$, and oscillator strength distributions, $df/d\epsilon$. It is these quantities that we calculate and map extensively over Z and N. The point of view taken here has been presented in a study[1] (hereafter called FTD) of these same basic quantities for neutral atoms.

Since any property of the ions can be considered as a function of two variables, Z and N, our data can be analyzed in terms of at least three alternative pictures: isoelectronic (N kept constant), isonuclear (Z kept constant), and isionic ($z = Z - N$ kept constant). Each of these pictures brings out different aspects of the variation of a given quantity over Z and N.

The isoelectronic picture is the most straightforward from a computational viewpoint and is widely used. In addition, it is directly applicable to 1/Z expansions.[2] Each of the properties approaches the known hydrogen values asymptotically[3] when plotted vs. 1/Z ($1/Z \to 0$). The isonuclear picture simplifies the variation of ionic properties from one order of the spectrum to

---

*Summary of a paper presented at the IVth Int. Conf. on Beam-Foil Spectroscopy and Heavy-Ion Atomic Physics Symposium, Gatlinburg, Tennessee, September 1975. A preliminary report of the work has also appeared in Abstracts of Papers, IXth Int. Conf. on the Physics of Electronic and Atomic Collisions, Seattle, July 1975, J. S. Risley and R. Geballe, Eds., University of Washington Press, Seattle, p. 693 (1975).

†Department of Physics, Georgia State University, Atlanta, Georgia 30303.

‡Department of Physics, The University of Chicago, Chicago, Illinois 60637.

the next. In particular, we shall see that inner-shell properties are virtually unaffected by stripping outer shell electrons. Further, the isonuclear picture is most suitable for certain applications. For example, if we consider a given impurity contamination in a CTR plasma, the many ions of that impurity which are relevant constitute an isonuclear sequence. This is also true for astrophysical applications.[4] The isoionic picture maintains a constant asymptotic potential, $(z + 1)/r$, in the ion, and focuses on the interplay between increasing Z and increasing N. This provides a framework for the transfer of the extensive experience with neutral atoms, $z = 0$, gained by traditional spectroscopy and collision physics.

The calculations presented in this paper are based on single-electron Hartree-Slater (HS) wavefunctions.[5] The HS model is used since it is quite amenable to large-scale calculations. In addition, HS functions have been shown to be reasonably realistic for neutral atoms by FTD[1] and can be expected to be better for ions. We view this study as the beginning of a first approximation to the (Z,N) mapping of ionic properties. This initial survey attempts to elucidate gross systematics and to identify areas for deeper examination, incorporating, e.g., correlation and relativistic effects.[6,7] In this paper we present several results exemplifying the usefulness of the different pictures.

As an example of the isoionic picture, Figure 1 shows the phase shift, $\delta_\ell(0) = \pi\mu_\ell$, which characterizes the scattering of zero-energy electrons in the field of ions at various stages of ionization. Two striking features are observed. First, the behavior of $\delta_\ell(0)$ shows the known[1] rich structure (associated with chemical properties) for the first spectrum (neutrals). This structure still persists to a lesser extent for the second spectrum (singly ionized species), but disappears completely for all higher-order spectra. Second, in the generally smooth behavior of $\delta_\ell(0)$ for each higher-order spectrum, prominent changes of the slope appear at the same Z for all partial waves. These slope discontinuities occur whenever the total number of electrons equals 28, 10, and 2. These values correspond to the complete filling through the $n = 3$, 2, and 1 shells, respectively, of a hydrogenic atom. Accordingly, we expect to observe a similar behavior of $\delta_\ell(0)$ for ions with 60 electrons which will correspond to

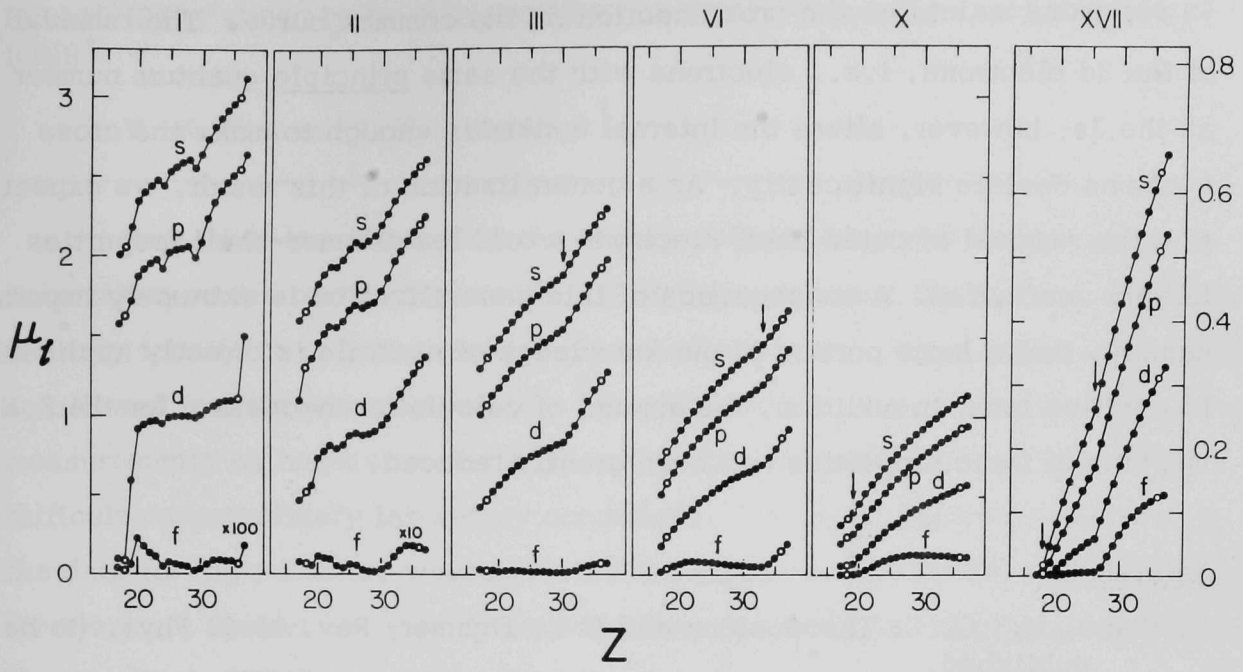

FIG. 1.--Quantum defects, μ_ℓ, as a function of atomic number, Z, and spectral order (denoted by the roman numerals above each set of data).

the n = 4 shell. This is in contrast to the neutral stom case where "closed-shell" systems occur when the electron number is 86, 54, 36, 18, 10, and 2, i.e., the noble gases.

As a second example, Figure 2 shows photoionization cross sections (or rather, oscillator-strength distributions) for the 3s subshell along the Z = 26 (Fe) isonuclear sequence. Note that the cross sections are plotted against photon energy, rather than photoelectron energy. Displaying the data in this fashion reveals an important simplification: the cross sections for the neutral, singly ionized, and doubly ionized species lie on a common curve, apart from the obvious shift of the threshold. This is in sharp contrast to the members of the sequence of higher ionicity, which follow independent curves. In other words, successive removal of outer

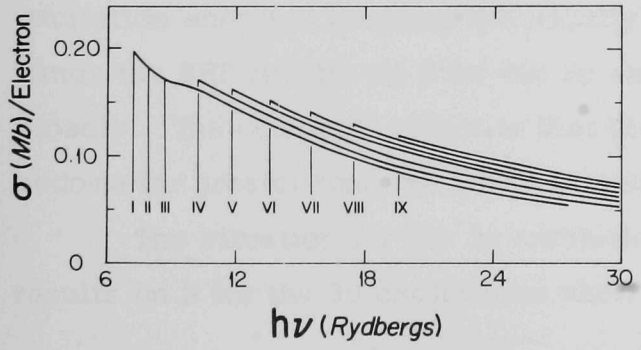

FIG. 2.--The 3s subshell photoionization cross sections for the Z=26 (Fe) isonuclear sequence. The roman numerals indicate the order of the spectrum (i.e., Z-N+1).

4s electrons maintains the cross section on the common curve. The removal of the 3d electrons, i.e., electrons with the same principle quantum number as the 3s, however, alters the internal dynamics enough to make the cross sections deviate significantly. As a generalization of this result, we expect that the removal of outer-shell electrons would leave inner-shell properties largely unaffected. A consequence of this generalization is extremely important, namely, that a large portion of our knowledge of neutrals is directly applicable to positive ions; in addition, the amount of calculation necessary for the Z,N mapping of ionic properties has been greatly reduced.

References

1. Fano, U., C. E. Theodosiou, and J. L. Dehmer, Rev. Mod. Phys. (to be published.
2. Layzer, D., Ann. Phys. 8, 271 (1959).
3. Smith, M. W. and W. L. Wiese, Ap. J. Supp. 23, 103 (1973).
4. Fawcett, B. C., Adv. At. Mol. Phys. 10, 223 (1974).
5. Herman, F. and S. Skillman, Atomic Structure Calculations, Prentice-Hall, Englewood Cliffs, N.J. (1963).
6. Doyle, H. T., Adv. At. Mol. Phys. 5, 337 (1969).
7. Armstrong, L. and S. Feneville, Adv. At. Mol. Phys. 10, 1 (1974).

RELATIVISTIC EFFECTS IN THE RESONANCE TRANSITIONS OF LITHIUM-LIKE IONS*

Y.-K. Kim and J. P. Desclaux†

Radiative-transition data for highly stripped ions are needed in the Tokamak-type fusion reactor studies, both for estimating the energy loss through impurity ions in the plasma and for plasma diagnosis.[1] Some experimental data on allowed transitions are available[2] for lithium-like ions of $Z < 30$. However, measurements on heavier atoms such as Mo ($Z=42$) and W ($Z=74$) would be difficult under ordinary laboratory conditions. To study relativistic effects in the data for high-Z ions, we calculated the dipole oscillator strengths (f values) for the $2s \rightarrow 2p$ and $2s \rightarrow 3p$ transitions from the nonrelativistic and relativistic Hartree-Fock (NRHF and RHF) wavefunctions.[3]

The f value is defined as the product of the excitation energy E and the line strength S (see Ref. 4, Eq. 10), i.e., $f=ES/3gR$, where $R=13.6$ eV and g is the degeneracy of the initial state. The relativistic effect in f could come from either E or S, or from both.

For the $2s \rightarrow 2p$ transition, the excitation energy vanishes in the nonrelativistic hydrogenic limit, and hence the nonrelativistic f values diminish as Z increases. In reality, however, the spin-orbit interaction splits $2p_{\frac{1}{2}}$ and $2p_{\frac{3}{2}}$, and our RHF results show that only $2p_{\frac{1}{2}}$ excitation energies diminish as the state is degenerate with $2s_{\frac{1}{2}}$ in the relativistic hydrogenic limit. The $2p_{\frac{3}{2}}$ excitation energies increase drastically for high Z (Table 1). On the other hand, the RHF results on S for the 2p excitation resemble the NRHF results closely. The combined effect is that the RHF f values for the $2p_{\frac{3}{2}}$ excitations become far greater than the NRHF results for higher Z (Table 1).

The situation for the 3p excitations is just the opposite. The RHF results on S for the 3p excitations show a significant reduction from the NRHF

---

*Summary of a paper presented at the IXth International Conference on the Physics of Electronic and Atomic Collisions, Seattle, July 1975.

†Institut Laue-Langevin, 38042 Grenoble, France.

TABLE 1. Dipole Oscillator Strengths f and Excitation Energies of Lithium-Like Ions

	N (Z=7)		Mo (Z=42)		W (Z=74)	
	f	E, Ry	f	E, Ry	f	E, Ry
$2s \rightarrow 2p$						
Adopted[a]	0.235	0.7348	—	—	—	—
NRHF	0.239	0.7381	0.0316	5.704	0.0175	10.19
RHF,[b] $2p_{\frac{1}{2}}$	0.0796	0.7402	0.0112	6.558	0.0069	15.80
$2p_{\frac{3}{2}}$	0.160	0.7424	0.0565	15.77	0.129	126.1
Z expansion[c]						
$2p_{\frac{3}{2}}$	—	0.9941	—	15.43	—	105.5
$2s \rightarrow 3p$						
Adopted[a]	0.233	4.354	—	—	—	—
NRHF	0.235	4.345	0.405	229.6	0.418	733.3
RHF,[b] $3p_{\frac{1}{2}}$	0.0784	4.349	0.134	237.7	0.136	824.7
$3p_{\frac{3}{2}}$	0.156	4.349	0.240	240.0	0.183	857.6

[a] Ref. 2.

[b] Nonrelativistic f values should be compared with the sum of the $p_{\frac{1}{2}}$ and $p_{\frac{3}{2}}$ relativistic f values.

[c] Ref. 5.

results. The RHF 3p excitation energies, on the other hand, show close agreement with the NRHF results. Thus, the RHF f values become smaller than the NRHF values as Z increases (Table 1).

The sum of the f values for the 2p and 3s transitions, however, is nearly the same for the NRHF and RHF results. In other words, the f value for the $2p_{\frac{3}{2}}$ excitation builds up at the expense of the 3p excitations. The excitation energies obtained from the relativistic Z-expansion method by Doyle[5] agree with our results only for intermediate Z (Table 1).

Similar calculations[6] on the Be sequence show that the f values for $2s^2\,{}^1S \rightarrow 2s2p_{\frac{3}{2}}\,{}^1P_1$ transitions deviate appreciably for $Z > 40$ from values extrapolated from low-Z ions.

References

1. Hinov, E., Princeton University Plasma Physics Laboratory Report MATT-1022 (1974).
2. Smith, M. W. and W. L. Wiese, Astrophys. J. Suppl., Ser. 23, No. 196, 103 (1971); also W. L. Wiese, M. W. Smith, and B. M. Glennon,

Atomic Transition Probabilities, Vol. I. Hydrogen Through Neon, NSRDS-NBS 4 (1966).
3. Desclaux, J. P., Comp. Phys. Comm. 9, 31 (1975).
4. Nichols, R. W. and A. L. Stewart, Atomic and Molecular Processes, D. R. Bates, Ed., Academic Press, New York, p. 47 (1962).
5. Doyle, H. T., Adv. Atom. Mol. Phys. 5, 337 (1969).
6. Kim, Y.-K. and J. P. Desclaux, Phys. Rev. Lett. 36, 139 (1976).

RELATIVISTIC EFFECTS IN OUTER SHELLS OF HEAVY ATOMS*

J. P. Desclaux† and Yong-Ki Kim

The relativistic contraction of inner-shell orbitals affects outer shells through the self-consistency requirements of the atomic field. The self-consistent field relativistic effects increase the binding energies of the 6s electrons of Au and Hg by about 30%, whereas those for the 4f and 5d electrons are decreased by about 15% compared to the nonrelativistic results. Also, the oscillator strengths for the resonance transitions (6S → 6P) of Au and Hg are reduced by about 30% as a consequence of the self-consistent field relativistic effects.

---

*Abstract of a paper published in J. Phys. B: Atom. Molec. Phys. 8, 1177 (1975).

†Institut Laue-Langevin, 38042 Grenoble, France.

REMARKS ON THE SIGNIFICANCE OF ELECTRON CORRELATIONS IN TWO OSCILLATOR-STRENGTH SUM RULES*

Mitio Inokuti

Sum rules for the dipole oscillator strength are powerful as a check on cross sections for photoabsorption[1] and for inelastic collisions of fast charged particles.[2] Let df/dE be the density of the dipole oscillator strength per unit interval of excitation energy, E, measured from the ground state of an atom, and consider the moment $S(\mu) = \int (E/R)^{\mu} (df/dE)\, dE$, where R is the Rydberg energy and the integral includes summation over discrete excitations. In particular, S(-1) and S(1) are expressed[1,2] in terms of ground-state expectation values (denoted by $\langle\ \rangle$) as

$$S(-1) = (3a_0^2)^{-1} \left[\sum_j \langle \vec{r}_j^{\,2} \rangle + \sum_j \sum_{k\neq k} \langle \vec{r}_j \cdot \vec{r}_k \rangle\right] , \tag{1}$$

a_0 being the Bohr radius, and as

$$S(1) = (4/3R) \left[\sum_j \langle \vec{p}_j^{\,2}/2m \rangle + \sum_j \sum_{k\neq j} \langle \vec{p}_j \cdot \vec{p}_k/2m \rangle\right] , \tag{2}$$

where $\vec{r}_j$ and $\vec{p}_j$ are the position and the momentum of the jth electron. The proof of Eq. 2 rests upon the relation

$$-(i\hbar/m) \langle E | \vec{p}_j | 0 \rangle = \langle E | [H, \vec{r}_j] | 0 \rangle = E \langle E | \vec{r}_j | 0 \rangle , \tag{3}$$

where H may be the standard nonrelativistic Hamiltonian including solely Coulomb interactions between a fixed nucleus and electrons, as well as among the electrons.

In contrast to the first terms of Eqs. 1 and 2, which are single-electron expectation values, the second terms

$$\Omega_r = \sum_j \sum_{k\neq j} \langle \vec{r}_j \cdot \vec{r}_k \rangle \quad \text{and} \quad \Omega_p = \sum_j \sum_{k\neq j} \langle \vec{p}_j \cdot \vec{p}_k \rangle ,$$

manifestly depend upon angular correlations of electrons, and, therefore, deserve special attention in the following respects.

---

*Summary of a paper presented at the IXth Int. Conf. on the Physics of Electronic and Atomic Collisions, Seattle, July 1975.

1. Within the Hartree-Fock approximation, $\Omega_r \leqq 0$ and $\Omega_p \leqq 0$ in general. Moreover, these two quantities receive contributions only from pairs of electrons that have the same spin but have orbital angular momenta differing unity.

2. The above statement also holds for central-field approximations in which all atomic electrons are subject to a single local potential. Further, in these approximations, Ω_r and Ω_p are numerically connected to each other because of Eq. 3. (Note that Eq. 3 holds for central-field approximations as well as for rigorous many-electron theories, but not for the Hartree-Fock approximation.) More interestingly, Ω_r and Ω_p are expressed in terms of probabilities of radiative transitions between hole states, i.e., inner-shell fluoresence rates tabulated by Manson and Kennedy.[3]

3. When one goes behond the HF (or other independent-electron) approximations and fully incorporates angular correlations, then Ω_r and Ω_p can be modified considerably. For the ground state[4,5] of He, as an example, $\Omega_r < 0$ but $\Omega_p > 0$; the signs of these quantities can be easily understood from elementary analysis of either Hylleraas or configuration-interaction wavefunctions. Surprisingly many authors (see, for example, Table 10, Ref. 6 and Refs. 7 and 8) incorrectly state the sign of Ω_p, which also gives rise to the specific nuclear-mass effect on atomic spectra.[9] Also, for the Li ground state,[5] $\Omega_p > 0$.

4. For atoms other than He, Li, and possibly Be, the modification due to electron correlations is usually too small to offset the negative sign of the HF Ω_p value. For example, data[10] based on configuration-interaction wavefunctions for Ne show $\Omega_p < 0$. The quantity Ω_r is invariably negative in all existing data.

5. Recent data[1,12] show other systematics of Ω_r and Ω_p concerning their magnitudes relative to the first terms in Eqs. 1 and 2.

References

1. Fano, U. and J. W. Cooper, Rev. Mod. Phys. 40, 441 (1968).
2. Inokuti, M., Rev. Mod. Phys. 43, 297 (1971).

3. Manson, S. T. and D. J. Kennedy, Atomic Data and Nucl. Data Tables 14, 111 (1974).
4. Pekeris, C. L., Phys. Rev. 115, 1216 (1959).
5. Cooper, J. W. and J. B. Martin, Phys. Rev. 131,1183 (1963).
6. Bethe, H. A. and E. E. Salpeter, Quantum Mechanics of One- and Two-Electron Atoms, Springer-Verlag, Berlin, p. 164 (1957).
7. Dalgarno, A. and N. Lynn, Proc. Phys. Soc. (London) A70, 802 (1957).
8. Massey, H. S. W., E. H. S. Burhop, and H. B. Gilbody, Electronic and Ionic Impact Phenomena, Oxford University Press, Cambridge, Vol. II, p. 1112 (1969).
9. Bethe H. and E. E. Salpeter, Quantum Mechanics of One- and Two-Electron Atoms, Springer-Verlag, Berlin, p. 166 (1957).
10. Saxon, R. P., Phys. Rev. A 8, 839 (1973).
11. Dehmer, J. L., M. Inokuti, and R. P. Saxon, Phys. Rev. A 12, 102 (1975).
12. Cummings, F. E., J. Chem. Phys. 63, 4960 (1975).

THEORETICAL ASPECTS OF ELECTRON CORRELATIONS IN ELECTRON COLLISIONS*

Mitio Inokuti

Electron-correlation effects manifest themselves in diverse facets of electron collisions with an atom or molecule. A fast incident electron acts largely as an external agent, and its inelastic collisions probe the structure, including correlations within the target (in both the initial state and the final state), nearly in the same way as photoionization processes do. In inelastic collisions of a slow electron, the central object of study is the correlated motion of the incident electron and an electron excited out of the target core. This elementary observation is illustrated by many examples and is elaborated by remarks on some current theoretical methods.

*Brief summary of lectures delivered at the NATO Advanced Study Institute on Photoionization and Other Probes of Many-Electron Interactions, Carry-le-Rouet, France, 31 August — 13 September 1975 (to be published by Plenum Press, New York).

MINIMA IN GENERALIZED OSCILLATOR STRENGTHS FOR INITIALLY EXCITED HYDROGEN-LIKE ATOMS

Michio Matsuzawa,† Kazem Omidvar,‡ and Mitio Inokuti

Generalized oscillator strengths for transitions from an initially excited state of a hydrogenic atom to final states (either discrete or continuum) have complicated structures, including minima and shoulders, as functions of the momentum transfer. Extensive calculations carried out in the present work have revealed certain systematics of these structures. Some implications of the minima for the energy dependence of the inner-shell ionization cross section of heavy atoms by proton impact are discussed.

*Abstract of a paper submitted for publication.

†Visiting Scientist, October 1972—March 1974. Permament address: Dept. of Engineering Physics, The University of Electron-Communications, Chofu-shi, Tokyo, Japan.

‡NASA Goddard Space Flight Center, Greenbelt, Maryland 20771.

NUMERICAL TESTS OF THE WEINBERG SEPARATE-POTENTIAL METHOD, THE ORTHOGONALITY-CONSTRAINT METHOD, AND OTHER RELATED METHODS*

Smio Tani,† Augustine C. Chen,‡ and Mitio Inokuti

We tested the three methods in the title with regard to the numerical efficienty of their respective modified Born series. Our example concerns model potentials that are pertinent to the low-energy electron-hydrogen single-S scattering. The Weinberg method gives an excellent result.

If a bound state can be formed by reducing the energy of the system below zero, the Born series for scattering in the same channel does not converge at low energies. The force (a certain potential in the Hamiltonian) that causes the bound state is treated by a nonperturbative method, and other forces in the system will be treated by means of a modified Born series that retains convergence. If the wavefunction of the bound state is known, we may utilize it in a specific way to formulate the modified Born series. Our purpose is to test the numerical aspects of two such methods, Weinberg's spearable-potential and the orthogonality-constraint methods.

Weinberg[1] developed a method of using a separable potential

$$V_W = |V\phi\rangle \langle \phi V| \langle \phi V\phi\rangle^{-1} , \tag{1}$$

where $|\phi\rangle$ is the bound-state wavefunction. This potential reproduces the bound state exactly and provides a set of distorted waves which becomes the basis of a convergent modified Born series. The original potential, V, is rearranged as

$$V = V_W + \hat{V} = V_W + [V - V_W] . \tag{2}$$

The modified Born series in $\hat{V}$ converges, while the simple perturbation series

*Summary of a paper presented at the IXth Int. Conf. on the Physics of Electronic and Atomis Collisions, Seattle, July 1975.

†Physics Department, Marquette University, Milwaukee, Wisconsin 53233.

‡Physics Department, St. John's University, Jamaica, New York 11432.

in V fails to do so. The numerical aspects of this method have been tested for the Yukawa and exponential potentials,[2] but have never been tested for a realistic potential pertinent to atomic physics.

In the method of orthogonality constraint,[3] one tackles the scattering problem after the bound state is worked out. The subspace orthogonal to the bound state will turn out to be sufficient for the scattering calculation. When the kinetic-energy operator is projected to that subspace, an eigenfunction satisfies

$$d^2|\psi\rangle/dr^2 + |\phi\rangle\langle\phi V\psi\rangle\langle\phi\phi\rangle^{-1} = E|\psi\rangle \ . \qquad (3)$$

According to Levinson's theorem, the phase shift becomes equal to π in the zero energy limit when there is one bound state. This will never follow from the simple perturbation calculation, because any individual term of the simple Born series for phase shift vanishes at zero energy, and hence the sum must vanish if the series converges. The eigenfunction that satisfies Eq. 3 produces a phase shift that becomes equal to π at zero energy. Hence, we may use such an eigenfunction as a basis of convergent modified-Born series. Theoretical advantages of using the orthogonalized subspace have been discussed earlier,[4] but the rapidity of the convergence has not been examined for any realistic potential.

As far as the analytic property as a function of potential strength is concerned, the Padé approximant is on a firm basis. Let the potential strength be λ and the Hamiltonian for a variable λ be written as

$$H(\lambda) = T + \lambda V \ , \qquad (4)$$

where T is the operator of kinetic energy. For the physical problem $\lambda = 1$. One can show (see Ref. 5 and references therein) that the scattering length, a, is a meromorphic function of λ, i.e.,

$$a = -\lambda \sum_n s_n/(1 - \lambda\lambda_n^{-1}) \ , \qquad (5)$$

where the λ_n is a pole and the s_n determines a residue. The Padé approximant is a continued fraction in λ, and it may closely represent a truncated form of the right-hand side of Eq. 5. The Padé approximant of a sufficiently high order

actually becomes a close approximation to the exact result. The exact result follows by an analytical continuation from the original Born series outside its radius of convergence. The Padé approximant may closely represent the analytically continued form of the series, if its order is sufficiently high. We shall examine how high the order should be to obtain a sufficient accuracy in the present problem.[6]

We examined several potentials that support a bound state with binding energy 0.0555 Ry and have an asymptotic form at a large distance

$$V(r) \sim -(9/2)\, r^{-4} \quad , \tag{6}$$

where 9/2 is the electric dipole polarizability (in atomic units) of atomic hydrogen. These potentials are pertinent to the e-H scattering in the ^1S state. Specifically, they include:

A. Biermann potential[7] (exponential approach to the asymptotic form)

$$V_a = -(9/2)\, r^{-4} \left[1 - \exp\left(-(r/r_0)^6\right)\right] ,$$

$$r_0 = 1.2355 \; ; \tag{7}$$

B. Buckingham-Bates potential[8,9] (inverse power approach to the asymptotic form)

$$V_b = -(9/2)\left(r^2 + r_0{}^2\right)^{-2} \quad ,$$

$$r_0{}^2 = 1.0688 \; . \tag{8}$$

The numerical results obtained by the Padé-approximant method are listed in Table 1. The computation was carried out using 16-digit double-precision arithmetic, and the results were truncated in Table 1. The exact result can be obtained analytically for the V_b; for the convenience of comparison with the exact result, an extra digit has been added inside the parentheses for that potential. Besides the discussion of the modified-Born series, some review of the properties of the simple Born series may be in order. For this purpose, the first six terms of the Born series are listed in the lower portion of Table 1.

As can be seen from Eq. 5, the nth order Born approximation to the

scattering length takes the form

$$a^{(n)} = -\lambda^n \sum_m s_m \lambda_m^{-(n-1)} \quad . \tag{9}$$

The poles are arranged according to their magnitude

$$\lambda_1 < \lambda_2 < \lambda_3 < \ldots \quad . \tag{10}$$

One may rewrite Eq. 9 as

$$a^{(n)} = -(\lambda^n/\lambda_1^{n-1})\,[s_1 + (\lambda_1/\lambda_2)^{n-1} s_2 + \ldots] \quad . \tag{11}$$

TABLE 1. Scattering Length Obtained by the Pade Approximation Method for Potentials V_a and V_b

Order	Potential V_a	Potential V_b
(1,1)	15.719	64.974 (3)
(2,2)	5.264	5.159 (1)
(3,3)	5.216	4.962 (3)
(4,4)	5.216	4.962 (0)
Exact		4.96128459
Born approximation[a]		
$a^{(1)}$	- 4.111	- 3.419
$a^{(2)}$	- 5.187 (1.262)	- 3.599 (1.053)
$a^{(3)}$	- 7.882 (1.520)	- 4.886 (1.358)
$a^{(4)}$	-12.131 (1.539)	- 6.819 (1.396)
$a^{(5)}$	-18.697 (1.541)	- 9.560 (1.402)
$a^{(6)}$	-28.821 (1.542)	-13.414 (1.403)

[a] The ratio of successive terms $a^{(n-1)}/a^{(n)}$ is given inside the parentheses.

The first few terms in the series dominate as the order n grows because the ratios λ_1/λ_m $(m = 2,3,\ldots)$ are less than one. A ratio of two successive Born approximations tends toward the constant (λ/λ_1) as n grows. Such a trend can be read off clearly around n = 6.

In determining the coefficient of the continued fraction, a ratio of two determinants made of $a^{(k)}$ $(k = 1,2,\ldots)$ must be determined accurately. For example, to determine the (N,N) approximant we need a reliable estimate of

$$\begin{vmatrix} a & \cdots & a^{(N+1)} \\ \vdots & & \vdots \\ a^{(N+1)} & \cdots & a^{(2N)} \end{vmatrix} \Bigg/ \begin{vmatrix} a^{(1)} & \cdots & a^{(N)} \\ \vdots & & \vdots \\ a^{(N)} & \cdots & a^{(2N-1)} \end{vmatrix}^{-1} \tag{12}$$

The general trend of $a^{(n)}$ for large n discussed after Eq. 11 causes each determinant to become small when N is large. To determine each determinant and hence the ratio accurately, higher-order Born approximations must be obtained to an extremely high precision. Thence, despite the firm theoretical basis for its convergence, numerical applications of the Padé approximant are impractical beyond a certain order. Table 1 demonstrates that the (1,1) approximant,

$$\alpha^{(1,1)} = a^{(1)} \left[1 - (a^{(2)}/a^{(1)}\right]^{-1} , \tag{13}$$

is very poor. An accuracy of 0.02% error may be achieved by using the (3,3) approximant. Our computation beyond the (3,3) approximant may be somewhat uncertain because of the difficulty discussed below Eq. 12. These results agree with observations made by Moiseiwitsch[10] regarding the applicability of the Padé approximant. The entries in parentheses in the lower portion of Table 1 show that the ratio $a^{(2)}/a^{(1)}$ used in the (1,1) approximant is not a good approximation to λ/λ_1 (roughly 30% in error), whereas the value of

$$1 - (\lambda/\lambda_1)$$

is crucially important in determining the first term in the series of Eq. 5, which dominates near a zero-energy resonance. This is one reason why the (1,1) approximant is poor.

The results obtained by Weinberg's separable potential are shown in Table 2. Before corrected by the higher-order terms of the modified Born series (regarding $\hat{V}$ of Eq. 2), the result is already within 6.13 and 7.23%, respectively for V_a and V_b, of the (3,3)-Padé approximant. When the modified Born series is summed up to the second order, the result agrees with the (3,3)-Padé approximant within 0.02%. Since the latter is in error up to 0.02 to 0.03%, the modified Born series summed up to the second order is in error perhaps by 0.5%. Thus, yielding both an excellent uncorrected value, as well as a rapidly converging modified Born series, Weinberg's method is superior in dealing with the scattering length in electron-hydrogen scattering. It can be shown that this is generally true when the system has one loosely bound state.

TABLE 2. Scattering Length Obtained by the Weinberg-Separable-Potential Method for Potentials V_a and V_b

Order	Potential V_a	Potential V_b
$\hat{a}_W^{(0)}$	5.558	5.322
$\hat{a}_W^{(1)}$	-0.348	-0.332
$\hat{a}_W^{(2)}$	-0.009	-0.011
Sum	5.217	4.963

TABLE 3. Scattering Length Obtained by the Orthogonality-Constraint Method for Potentials V_a and V_b

Order	Potential V_a	Potential V_b
$\hat{a}_{orth}^{(0)}$	8.926	8.828
$\hat{a}_{orth}^{(1)}$	-1.257	-1.115
$\hat{a}_{orth}^{(2)}$	-0.706	-0.615
$\hat{a}_{orth}^{(3)}$	-0.497	-0.464
$\hat{a}_{orth}^{(4)}$	-0.355	-0.361
Sum	6.111	6.274
(1,1)-Pade	6.058	6.343
(2,)-Pade	5.220	4.990

The results obtained by the orthogonality-constraint method are listed in Table 3 for the potentials. The modified Born series converges slowly. The slow rate of convergence can be enhanced by deriving the Padé approximants, which are shown in the lower portion of Table 3. Let the binding energy be $-\kappa^2$ Ry in the Schroedinger equation; the parameter κ in our problem is 0.2356. According to the effective-range theory, the scattering length is close to $\kappa^{-1} = 4.235$. In all examples to which we applied the orthogonality-constraint method, the scattering length uncorrected by the modified Born series is of the order of $2\kappa^{-1} = 8.470$. This discrepancy is likely to be inherent in the current method. Therefore, although the uncorrected value is much better than the (1,1)-Padé approximant, an improvement demands future study. It should be emphasized, nonetheless, that a converging modified Born series for scattering becomes available by simply limiting the subspace orthogonal to the bound state.

References

1. Weinberg, S., Phys. Rev. 130, 776 (1963); Phys. Rev. 131, 440 (1963).
2. Scadron, M. and S. Weinberg, Phys. Rev. 133, B1589 (1964); M. Scadron, S. Weinberg, and J. Wright, Phys. Rev. 135, B202 (1964).
3. Tani, S., Phys. Rev. 117, 252 (1960).
4. Chen, A., S. Tani, and S. Borowitz, Phys. Rev. 137, B236 (1965).
5. Tani, S. and M. Inokuti, J. Chem. Phys. 61, 4422 (1974).
6. Chen, A., Nuovo Cimento 52A, 474 (1967).
7. Bierman, L., Z. Astrophysik 22, 157 (1943).
8. Buckingham, R. A., Proc. R. Soc. A160, 94 (1937).
9. Bates, D. R. and H. S. W. Massey, Phil. Trans. R. Soc. A239, 33 (1943).
10. Moiseiwitsch, B. L., J. Phys. B: Atom. Mol. Phys. 3, 1417 (1970).

A PROGRAM TO TRANSLATE PUNCHED PAPER TAPES

Paul P. Nicole

A computer program is described that enables a user of the ANL IBM-370/195 computer system to process data punched in standard ASCII code on a paper tape as though they were punched on standard IBM cards.

Introduction

Paper tape is usually read into the ANL computer system through a remote access data station (RADS station). The RADS station reads the hole pattern in the tape and produces a corresponding bit pattern in storage. This is done one character (row of holes on tape) at a time until 79 characters have been read. An 80-character card image made up of hexidecimal (hex) 00 followed by the 79 characters is then assembled. These card images are sent to the computer to be processed.[1]

A translation is necessary before the data read by the tape reader can be processed in a normal way. Even after translation the way in which the characters are arranged on the card images may make them hard to read. Multi-digit numbers, for example, may be split between two card images. There may also be characters that must be removed or handled in a special way, such as carriage returns, line feeds, and other control characters.

A new program translates ASCII (American Standard Code for Information Interchange) coded tape, does some minor editing, reformats the resulting data, and then writes a card image dataset, which may be punched as a deck of cards, read directly by another program, or listed on the printer. The method used here could be easily adapted to translate codes other than ASCII as long as there is a one-to-one correspondence between input characters on the tape and output characters. Also, the output records could easily be changed from 80 characters (card images) to either longer or shorter records by making some minor changes in the program.

Theory

In this discussion, paper tape patterns will be represented by combinations of X's, O's and periods. An X represents an unpunched hole, an O represents a punched hole, and a period represents a sprocket hole. We will deal only with 8-level paper tape, which has room for 8 X's or O's, and 1 period per line (character). In this scheme, XXXXX.XXX would represent a line with no holes punched (blank tape with only a sprocket hole), and OOOOO.OOO would represent a line with all holes punched. Columns will be numbered from right to left. So, XOXOX.XXO has punches in columns 1, 5, and 7. Also, all numbers preceded by a Z will be hex (base 16) numbers.

When the computer reads the tape, it produces a binary bit pattern that is the same as the pattern punched in the tape with all punches (O's) becoming 1's and all unpunched positions (X's) becoming 0's. The result is a binary number in storage with a value equal to the value of the punches on the tape if we count column 1 as 1 ($=2^0$), column 2 as 2 ($=2^1$), up to column 8 as 128 ($= 2^7$). Thus, the letter R, which is XOXOX.XOX on the tape, shows up in storage as 01010010. The computer displays its storage 8 binary bits (1 byte) at a time as 2 hex digits. The first four bits of the R (0101) become Z5, while the remaining bits (0010) become Z2, resulting in Z52 being displayed. In order to print or punch the character R, the computer must have a ZD9 in storage.[2] The translation requires that each Z52 be replaced by a ZD9, and that a corresponding replacement be made for each of the other printable characters.

This replacement is accomplished by having the original value in storage select the proper element of an array (L) (see program listing in Figure 1) that contains the needed replacement value (see Figure 2). First the original value is read, using FORMAT(1X,79A1), into array NIN, which is a 79-element INTEGER*2 array. This gets rid of the Z00, which is always the first character of card images generated when tape is read, and makes the other 79 characters INTEGER*2 variables. INTEGER*2 variables take up 2 bytes (8 bits/byte), while our original characters took up only 1 byte of storage. The unused bytes are filled by the computer with Z40's. The letter R then becomes Z5240. We

```
C     PROGRAM TO READ PAPERTAPE TO CARD IMAGE FILE
      IMPLICIT INTEGER*2(N,L)
      DIMENSION NIN(79),NOUT(80),L(128)
      DATA LF/Z4040/,NP/Z8000/
      DATA L/31*':',' ','!','"','#','$','%','&',Z7D40,'(',')','*',
     1 '+',',','-','.',Z6140,'0','1','2','3','4','5','6','7','8',
     2 '9',':',';','<','=','>','?','@','A','B','C','D','E','F',
     3 'G','H','I','J','K','L','M','N','O','P','Q','R','S','T','U',
     4 'V','W','X','Y','Z','[','\',']','↑','←',33*':'/
      IFLAG=0
      NI=0
      READ(50,102)LIG1,LIG2,LIG3,LIG4,LDL1,LDL2,LDL3,LDL4,
     1 LSP1,LZP1,LSP2,LZP2,LSP3,LZP3,LCOL,LREC
  102 FORMAT(8(1X,1Z4),8I5)
      L(LSP1)=L(LZP1)
      L(LSP2)=L(LZP2)
      L(LSP3)=L(LZP3)
   10 READ(50,100,END=999) NIN
  100 FORMAT(1X,79A1)
      DO 11 N=1,79
      IF(NIN(N) .LT. 0) NIN(N)=NIN(N)-NP
      IF(NIN(N) .EQ. LDL1) GO TO 200
      IF(NIN(N) .EQ. LDL2) GO TO 200
      IF(NIN(N) .EQ. LDL3) GO TO 200
      IF(NIN(N) .EQ. LDL4) GO TO 200
      IF(NIN(N) .EQ.   64) GO TO 11
      IF(NIN(N) .EQ. LIG1) GO TO 11
      IF(NIN(N) .EQ. LIG2) GO TO 11
      IF(NIN(N) .EQ. LIG3) GO TO 11
      IF(NIN(N) .EQ. LIG4) GO TO 11
      IF(IFLAG .EQ. 1) GO TO 201
   12 NI=NI+1
      NJ=NIN(N)/256
      NOUT(NI)=L(NJ)
      IF(NOUT(NI) .EQ. L(58)) GO TO 206
   13 CONTINUE
      IF(NI .EQ. LREC) GO TO 205
   11 CONTINUE
      GO TO 10
  101 FORMAT(80A1)
  200 IFLAG=1
      GO TO 11
  201 IF(NI .EQ. 0) GO TO 203
      IF(NI .EQ. 80) GO TO 202
      NB=NI+1
      DO 202 I=NB,80
      NOUT(I)=LF
  202 CONTINUE
      WRITE(60,101) NOUT
  203 IFLAG=0
      NI=0
      GO TO 12
  205 WRITE(60,101) NOUT
      NI=0
      GO TO 11
  206 IF(LCOL .EQ. 0) NI=NI-1
      IF(LCOL .EQ. 2) NOUT(NI)=L(32)
      GO TO 13
  999 NB=NI+1
      IF(NI .EQ. 0) GO TO 99
      IF(NI .EQ. 80) GO TO 901
      DO 902 I=NB,80
      NOUT(I)=LF
  902 CONTINUE
  901 WRITE(60,101)NOUT
   99 STOP
      END
```

FIG. 1.--Program listing

IN	NJ	L(NJ)	OUT	IN	NJ	L(NJ)	OUT	IN	NJ	L(NJ)	OUT
0140	01	7A40	:	2C40	44	6B40	,	5740	87	E640	W
0240	02	7A40	:	2D40	45	6040	-	5840	88	E740	X
0340	03	7A40	:	2E40	46	4B40	.	5940	89	E840	Y
0440	04	7A40	:	2F40	47	6140	/	5A40	90	E940	Z
0540	05	7A40	:	3040	48	F040	0	5B40	91	7940	[
0640	06	7A40	:	3140	49	F140	1	5C40	92	CF40	\
0740	07	7A40	:	3240	50	F240	2	5D40	93	4940	]
0840	08	7A40	:	3340	51	F340	3	5E40	94	B040	↑
0940	09	7A40	:	3440	52	F440	4	5F40	95	6D40	←
0A40	10	7A40	: (a)	3540	53	F540	5	6040	96	7A40	:
0B40	11	7A40	:	3640	54	F640	6	6140	97	7A40	:
0C40	12	7A40	:	3740	55	F740	7	6240	98	7A40	:
0D40	13	7A40	: (b)	3840	56	F840	8	6340	99	7A40	:
0E40	14	7A40	:	3940	57	F940	9	6440	100	7A40	:
0F40	15	7A40	:	3A40	58	7A40	:	6540	101	7A40	:
1040	16	7A40	:	3B40	59	5E40	;	6640	102	7A40	:
1140	17	7A40	:	3C40	60	4C40	<	6740	103	7A40	:
1240	18	7A40	:	3D40	61	7E40	=	6840	104	7A40	:
1340	19	7A40	:	3E40	62	6E40	>	6940	105	7A40	:
1440	20	7A40	:	3F40	63	6F40	?	6A40	106	7A40	:
1540	21	7A40	:	4040	64	7C40	@	6B40	107	7A40	:
1640	22	7A40	:	4140	65	C140	A	6C40	108	7A40	:
1740	23	7A40	:	4240	66	C240	B	6D40	109	7A40	:
1840	24	7A40	:	4340	67	C340	C	6E40	110	7A40	:
1940	25	7A40	:	4440	68	C440	D	6F40	111	7A40	:
1A40	26	7A40	:	4540	69	C540	E	7040	112	7A40	:
1B40	27	7A40	:	4640	70	C640	F	7140	113	7A40	:
1C40	28	7A40	:	4740	71	C740	G	7240	114	7A40	:
1D40	29	7A40	:	4840	72	C840	H	7340	115	7A40	:
1E40	30	7A40	:	4940	73	C940	I	7440	116	7A40	:
1F40	31	7A40	:	4A40	74	D140	J	7540	117	7A40	:
2040	32	4040	SP	4B40	75	D240	K	7640	118	7A40	:
2140	33	5A40	!	4C40	76	D340	L	7740	119	7A40	:
2240	34	7F40	"	4D40	77	D440	M	7840	120	7A40	:
2340	35	7B40	#	4E40	78	D540	N	7940	121	7A40	:
2440	36	5B40	$	4F40	79	D640	O	7A40	122	7A40	:
2540	37	6C40	%	5040	80	D740	P	7B40	123	7A40	:
2640	38	5040	&	5140	81	D840	Q	7C40	124	7A40	:
2740	39	7D40	'	5240	82	D940	R	7D40	125	7A40	:
2840	40	4D40	(	5340	83	E240	S	7E40	126	7A40	:
2940	41	5D40	)	5440	84	E340	T	7F40	127	7A40	:
2A40	42	5C40	*	5540	85	E440	U				
2B40	43	4E40	+	5640	86	E540	V				

(a) LINE FEED
(b) CARRIAGE RETURN

FIG. 2.--Translation table

also need Z40 fillers in our output character list. The output R is then ZD940.

Next, the input is checked to see if the parity hole (column 8) was punched. Depending on the tape punching system, this hole may or may not be punched for any given character. Our R with the parity hole punched is ZD240 instead of Z5240. The bit generated by the parity punch makes the value of our input negative when looked at by the computer as an integer. To ignore the parity punch we check our input to see if it is a negative integer, and, if it is, subtract Z8000. If positive, the number is left as is. The value is then divided by 256 (Z100) to get rid of the Z40 filler. Our R is now Z0052, or, as a deciman integer, 82 (= 5 × 16 + 2). We make element 82 of array L contain ZD940 (R) so that each R input on tape will give an R output character. This same procedure is followed in selecting the other elements of array L. The values in array L are initialized by a data statement at the beginning of the program. Note that any value could be put into a particular element of L to cause a different output character to result from a given input character. The program allows for three such nonstandard translations.

After ignoring the parity punch, but before translation, the input characters are searched for special characters which have been designated either as delimiters or as characters to be ignored. If a delimiter is encountered, a flag is set. When the next translatable character or an end of file is read, the remainder of the 80-character record being assembled is filled with blanks, and the record is written to the output device. If a character to be ignored is encountered, the next character is read. Unpunched tape (Z0040) is ignored.

Use

The program reads one card which specifies all the changeable parameters in the program. This card is read according to FORMAT (8(1X,1Z4),8I5)— that is, 16 5-column fields. The first 8 fields are read as hex variables, while the last 8 are read as integer variables. The card is read into variables: L1G1, L1G2, L1G3, L1G4, LDL1, LDL2, LDL3, LDL4, LSP1, LZP1, LSP2, LZP2, LSP3, LZP3, LCOL, LREC. Variables L1G1 to 4 are hex representations of input characters to be ignored. Blank tape (Z0040) is automatically ignored.

If no characters are to be ignored, put b0040 into L1G1 to 4. For example, if all Q's are to be ignored, put b5140 into L1G1 (see Figure 2), where b is a blank.

LDL1 to 4 are hex representations of input characters which are to be used as delimiters. The delimiters trigger the start of a new record when the next translatable character is read. If more than one delimiter is read at one time, only one new record will be started. A delimiter can be any character that can be punched on the tape (parity holes are ignored). Common examples are carriage return, b0D40, line feed, b0A40, and blank tape b0040. If fewer than 4 delimiters are needed, unused positions can be filled with repeats of used delimiters.

LSP1 to 3 are array L element numbers which are to be changed to be the same as a corresponding LZP1 to 3 element number. For example, if all A's (element 65) are to be translated as C's (element 67), LSP1 would be bbb65, and LZP1 would be bbb67. This can be done with any character that can be punched on the tape. For example, line feeds could be translated as L's by entering LSP2 as bbb10 and LZP2 as bbb76. Line feeds, in this case, cannot be also used as a delimiter because delimiters are not translated. Unused pairs of LSP's and LZP's can be filled with any equal numbers.

LCOL determines how a colon (:) is to be handled. In the translation array (L) all unprintable characters are filled with colons. If LCOL is 0, all colons are ignored. If LCOL is 1, all colons are written as colons. If LCOL is 2, all colons are replaced by spaces.

LREC sets the maximum number of characters that will be written on a record before a new record is started. If, for example, data are in groups of 25 characters followed by carriage returns and line feeds, setting LREC to 25 would start a new record every 25 characters, even though the carriage returns and line feeds were sometimes missing.

A standard card for translating a tape from a teletype machine would ignore rubouts (7F40), use carriage returns and line feeds (0D40, 0A40) as delimiters, have no nonstandard translations, print colons as colons, and set a maximum line length of 80. This card would be b7F40b0000b0000b0000

b0D40b0A40b0A40b0A40bbbb1bbbb1bbbb1bbbb1bbbb1bbbb1bbbb1bbb80.

The job control (JCL) cards needed to run this program to make a card image dataset from a standard teletype punched tape using the above described parameter card would look like this:

```
//JOBNAMEbJOBb(FXXXXX,2,0,1),REGION=64K
ACCOUNT CARD
//STEP1bEXECbFGILG,PRELIB='LOADLIBRARYNAME',EP='MAIN'
//GO.SYSLINbDDbDISP=SHR,DSN=LOADLIBRARYNAME(MEMBER)
//GO.FT60F001bDDbDISP=(NEW,CATLG),DCB=(RECFM=FB,LRECL=80,
      BLKSIZE=1680),
//bbbbUNIT=LONGSHRD,SPACE=(TRK,(10,2),RLSE),
//bbbbDSN=DATASETNAME
//GO.FT50F001bDDb*
b7F40b0000b0000b0000b0D40b0A40b0A40b0A40bbbb1bbbb1bbbb1bbbb1
      bbbb1bbbb1bbbb1bbb80
/*SYSINbDDbPT
SPECIAL CARD TO SPECIFY DELETE AND EOT CHARACTERS
/*ENDbOFbFILE
```

Two things in the JCL should be explained. First, the "special card" to designate a teletype RUBOUT CHARACTER as the delete character and CNTL D as the end of the tape mark will have, in column 1, punches 2,3,4,5,6,7,8, and 9, and in column 2, punches 2 and 7. More information on feeding tape into RADS stations can be found in Ref. 1. Second, the //GO.FT60F001 card and the following two cards, which are continuations, designate where the output is going. If these three cards are replaced with the card //GO.FT60F001bDDb SYSOUT=A the result will be a listing on the printer instead of a dataset. If the three cards are replaced with the card //GO.FT60F001bDDbSYSOUT=B the result will be a card deck instead of a dataset.

I would like to thank Dr. J. C. Person and Mr. P. H. Froehle for many helpful suggestions, both while writing the program and while writing this report.

References

1. Amiot, L., R. Barr, C. Harrison, T. Murphy, F. Salter, R. Schwanke, and V. Tantillo, Argonne National Laboratory Applied Mathematics Division Technical Memorandum No. 207, p. 218 (Sept 1, 1971).
2. IBM System/370 Reference Summary, IBM Publication No. BX20-1950-2 (March 1974).

PUBLICATIONS BY THE STAFF OF THE FUNDAMENTAL MOLECULAR PHYSICS AND CHEMISTRY SECTION FOR THE PERIOD JULY 1974–JUNE 1975.

MAJOR PAPERS

T. Åberg and J. L. Dehmer, Comment on Soft X-Ray Absorption by Alakli Halide Crystals, J. Phys. C: Solid State Phys. 7, L278–L281 (1974).

J. Berkowitz, J. L. Dehmer, Y.-K. Kim, and J. P. Desclaux, Valence Shell Excitation Accompanying Photoionization in Hg, J. Chem. Phys. 61, 2556–2559 (1974).

J. L. Dehmer, Potential Barrier Effects in Inner-Shell Photoabsorption Spectra of Atoms, Molecules, and Solids, Physica Fennica 9, 60–67 (1974).

J. L. Dehmer, Joseph Berkowitz, L. C. Cusachs, and H. S. Aldrich, Photoelectron Spectroscopy of High Temperature Vapors. V. He I Spectra of GaX_3 and InX_3 (X=Cl, Br, I), J. Chem. Phys. 61, 594–599 (1974).

J. L. Dehmer and J. Berkowitz, Partial Photoionization Cross Sections for Hg Between 600 and 250 Å. Effect of Spin-Orbit Coupling on the $^2D_{\frac{5}{2}}$:$^2D_{\frac{3}{2}}$ Branching Ratio of Hg, Phys. Rev. A 10, 484–490 (1974).

J. P. Desclaux and Yong-Ki Kim, Relativistic Effects in Outer Shells of Heavy Atoms, J. Phys. B: Atom. Molec. Phys. 8, 1177–1182 (1975).

Dan Dill and J. L. Dehmer, Electron-Molecule Scattering and Molecular Photoionization Using the Multiple-Scattering Method, J. Chem. Phys. 61, 692–699 (1974).

Mitio Inokuti and Tetsushi Noguchi, Why Do You Call the Innermost Atomic Electron a K Electron? Am. J. Phys. 42, 1118–1119 (1974).

Mitio Inokuti, Introduction to the Symposium on the Jesse Effect and Related Phenomena, Radiat. Res. 59, 343–349 (1974).

Mitio Inokuti and M. R. C. McDowell, Elastic Scattering of Fast Electrons by Atoms. I. Helium to Neon, J. Phys. B: Atom. Molec. Phys. 7, 2382–2395 (1974).

Mitio Inokuti, Atomic and Molecular Effects in the Physical Stage. Critique of Cross-Section Data Governing the Physical Stage of Radiation Action, Physical Mechanisms in Radiation Biology, Proc. Conf. held at Airlie, Virginia, Oct. 11–14, 1972, USAEC Report CONF-721001, pp. 51–67

Mitio Inokuti, Roberta P. Saxon, and J. L. Dehmer, Total Cross Sections for Inelastic Scattering of Charged Particles by Atoms and Molecules — VIII. Systematics for Atoms in the First and Second Row, Int. J. Radiat. Phys.

Chem. 7, 109–120 (1975).

Mitio Inokuti, Theory of W Values of Gases, Hoshasen (Ionizing Radiations) 2, 5–18 (1975) (in Japanese).

Yong-Ki Kim and Tetsushi Noguchi, Secondary Electrons Ejected from He by Protons and Electrons, Int. J. Radiat. Phys. Chem. 7, 77–82 (1975).

Yong-Ki Kim, Energy Distribution of Secondary Electrons. I. Consistency of Experimental Data, Radiat. Res. 61, 21–35 (1975).

M. Naon, M. Cornille, and Yong-Ki Kim, Atomic Form Factor and Incoherent Scattering Function of Ar, J. Phys. B: Atom. Molec. Phys. 8, 864–868 (1975).

James C. Person, E. O. Wollan, Roland E. Meyerott, and John J. Spokas, Tributes to William P. Jesse, Radiat. Res. 59, 337–342 (1974).

James C. Person, Photoionization and the Jesse Effect: A Comparison of Yields and Isotope Effects, Radiat. Res. 59, 408–421 (1974).

D. Spence and W. A. Chupka, Measurement of Resonances in Atomic Oxygen by Electron Transmission Spectroscopy, Phys. Rev. A 10, 71-73 (1974).

D. Spence and M. Inokuti, Search for Low-Lying Resonances in Electron Scattering by Atomic Hydrogen, J. Quant, Spectrosc. Radiat. Transfer 14, 953–957 (1974).

David Spence, Systematics of Feshbach Resonances in the Molecular Halogens, Phys. Rev. A 10, 1045–1052 (1974).

David Spence, Electron Correlation Effects near Threshold for Electron-Impact Ionization of Helium, Phys. Rev. A 11, 1539–1542 (1975).

David Spence, Measurements of the $(3p^2)^1D$ State of H^- by Electron Transmission Spectroscopy, J. Phys. B: Atom. Molec. Phys. 8, L42–L45 (1975).

D. Spence and E. T. McHale, The Role of Negative Halogen Ions in Hydrocarbon Flame Inhibition, Combustion and Flame 24, 211–215 (1975).

David Spence and Tetsushi Noguchi, Feshbach Resonances Associated with Rydberg States of the Hydrogen Halides, J. Chem. Phys. 63, 505–515 (1975).

Smio Tani and Mitio Inokuti, Standing-Wave Modification of Regge Trajectories and Its Application to Atom-Atom and Ion-Atom Scattering at Thermal Energies, J. Chem. Phys. 61, 4422–4432 (1974).

ABSTRACTS OF CONFERENCE PAPERS

J. Berkowitz and J. L. Dehmer, Effect of Spin-Orbit Coupling on the Wavelength Dependence of Atomic Branching Ratios, IVth Int. Conf. on Vacuum-Ultraviolet Radiation Physics, Hamburg, Germany, July 22–26, 1974. Extended Abstracts, Abstract No. 10.

J. L. Dehmer, M. Inokuti, and R. P. Saxon, Atomic Periodicity as Manifested in the Oscillator-Strength Sums, 6th Ann. Mtg. of the Division of Electron and Atomic Physics, Dec. 2–4, 1974, Chicago. Bull. Am. Phys. Soc. 19, 1192 (1974).

R. H. Huebner, Dipole Oscillator-Strength Distributions Derived for Several Hydrocarbons from Electron Energy Spectra, 5th Int. Congr. of Radiation Research, Seattle, July 14–20, 1974, Radiat. Res. 59, 228 (1974).

R. H. Huebner, C. H. Fergurson, R. J. Celotta, and S. R. Mielczarek, Apparent Oscillator-Strength Distributions Derived from Electron Energy Loss Measurements: Methane and n-Hexane, Abstracts of IVth Int. Conf. on Vacuum Ultraviolet Radiation Physics, Hamburg, Germany, July 22–26, 1974, Paper No. 111.

R. H. Huebner, R. J. Celotta, S. R. Mielczarek, and C. E. Kuyatt, Apparent Oscillator Strengths for Molecular Oxygen, 6th Ann. Mtg. of the Division of Electron and Atomic Physics, Dec. 2–4, 1974, Chicago, Bull. Am. Phys. Soc. 19, 1194 (1974).

Mitio Inokuti, Introduction to the Symposium on the Basic Physics of Interactions of Radiation with Matter, 5th Int. Congr. of Radiation Research, Seattle, July 14–20, 1974, Radiat. Res. 59, 88 (1974).

Mitio Inokuti and M. Matsuzawa, Electron Densities of Atoms and Cross Sections for Scattering of Fast Charged Particles, 6th Ann. Mtg. of the Division of Electron and Atomic Physics, Dec. 2–4, 1974, Chicago, Bull. Am. Phys. Soc. 19, 1192 (1974).

Mitio Inokuti, Electron-Collision Cross Sections for the Energy Deposition, 23rd Ann. Mtg. of the Radiation Research Society, Miami Beach, Florida, May 11–15, 1975, Radiat. Res. 62, 546 (1975).

Yong-Ki Kim, Secondary Electron Spectra, 5th Int. Congr. of Radiation Research, Seattle, July 14–20, 1974, Radiat. Res. 59, 89 (1974).

Yong-Ki Kim, Relativistic Effects in Outer Shells of Atoms, 6th Ann. Mtg. of the Division of Electron and Atomic Physics, Dec. 2–4, 1974, Chicago, Bull. Am. Phys. Soc. 19, 1193 (1974).

James C. Person and Paul P. Nicole, New Determinations of the Oscillator-Strength Distribution and the Photoionization Yields for Methane and n-Hexane, IVth Int. Conf. on Vacuum Ultraviolet Radiation Physics, Hamburg, Germany, July 22–26, 1974, Book of Abstracts, Abstract No. 112.

Roberta P. Saxon, Mitio Inokuti, and J. L. Dehmer, An Elementary Approach to the Systematics of W for Monatomic Gases, 5th Int. Congr. of Radiation Research, Seattle, July 14–20, 1974, Radiat. Res. 59, 230 (1974).

David Spence, Total Cross Sections for Double Excitations in He by Electron Impact, 6th Ann. Mtg. of the Division of Electron and Atomic Physics, Dec. 2–4, 1974, Chicago, Bull. Am. Phys. Soc. 19, 1194 (1974).

David Spence, Electron Correlation Effects near Threshold for Electron Ionization of He, 6th Ann. Mtg. of the Division of Electron and Atomic Physics, Dec. 2–4, 1974, Chicago, Bull. Am. Phys. Soc. 19, 1195 (1974).

David Spence and T. Noguchi, Electron Transmission Spectroscopy in the Acid Halides, 6th Ann. Mtg. of the Division of Electron and Atomic Physics, Dec. 2–4, 1974, Chicago, Bull. Am. Phys. Soc. 19, 1195 (1974).

C. E. Theodosiou, U. Fano, and J. L. Dehmer, Electron Optics of Atomic Fields, 6th Ann. Mtg. of the Division of Electron and Atomic Physics, Dec. 2–4, 1974, Chicago, Bull. Am. Phys. Soc. 19, 1187 (1974).